

Development of Battery Thermal Management System for Valve Regulated Lead Acid Battery

A Thesis submitted to Gujarat Technological University

for the Award of

Doctor of Philosophy

In

Mechanical Engineering

By

Mr. Jaydeep Manojkumar Bhatt

[Enrolment No.: 159997119011]

under supervision of

Dr. P. V. Ramana

(Professor)

Department of Mechanical Engineering

Sardar Vallabhbhai Patel Institute of Technology, Vasad (Gujarat).

&

Under co-supervision of

Dr. J. R. Mehta

(Assistant Professor)

Department of Mechanical Engineering

Maharaja Sayajirao University of Baroda, Vadodara (Gujarat).



GUJARAT TECHNOLOGICAL UNIVERSITY

AHMEDABAD

January - 2023

Development of Battery Thermal Management System for Valve Regulated Lead Acid Battery

A Thesis submitted to Gujarat Technological University

for the Award of

Doctor of Philosophy

In

Mechanical Engineering

By

Mr. Jaydeep Manojkumar Bhatt

[Enrolment No.: 159997119011]

under supervision of

Dr. P. V. Ramana

(Professor)

Department of Mechanical Engineering

Sardar Vallabhbhai Patel Institute of Technology, Vasad (Gujarat).

&

Under co-supervision of

Dr. J. R. Mehta

(Assistant Professor)

Department of Mechanical Engineering

Maharaja Sayajirao University of Baroda, Vadodara (Gujarat).



GUJARAT TECHNOLOGICAL UNIVERSITY

AHMEDABAD

January - 2023

© Mr. Jaydeep Manojkumar Bhatt

DECLARATION

I declare that the thesis entitled “**Development of Battery Thermal Management System for Valve Regulated Lead Acid Battery**” submitted by me for the degree of Doctor of Philosophy is the record of research work carried out by me during the period from **20-10-2016** to **17-03-2022** under the supervision of **Dr. P. V. Ramana** and under the co-supervision **Dr. J. R. Mehta** of and this has not formed the basis for the award of any degree, diploma, associateship, fellowship, titles in this or any other University or other institution of higher learning.

I further declare that the material obtained from other sources has been duly acknowledged in the thesis. I shall be solely responsible for any plagiarism or other irregularities if noticed in the thesis.

Signature of the Research Scholar:  Date: 10/01/2023

Name of Research Scholar: **Mr. Jaydeep Manojkumar Bhatt**

Place: GTU, Chandkheda, Ahmedabad.

CERTIFICATE

I certify that the work incorporated in the thesis Development of Battery Thermal Management System for Valve Regulated Lead Acid Battery submitted by Shri Jaydeep Manojkumar Bhatt was carried out by the candidate under my supervision/guidance. To the best of my knowledge: (i) the candidate has not submitted the same research work to any other institution for any degree/diploma, Associateship, Fellowship, or other similar titles (ii) the thesis submitted is a record of original research work done by the Research Scholar during the period of study under my supervision, and (iii) the thesis represents independent research work on the part of the Research Scholar.

Signature of Supervisor:  Date: 10/01/2023

Name of Supervisor: **Dr. P. V. Ramana**

Place: GTU, Chandkheda, Ahmedabad.

Signature of Co-supervisor:  Date: 10/01/2023

Name of Co-supervisor: **Dr. J. R. Mehta**

Place: GTU, Chandkheda, Ahmedabad.

Course-work Completion Certificate

This is to certify that **Mr. Jaydeep Manojkumar Bhatt** enrolment no. **159997119011** is a Ph.D. scholar enrolled in a Ph.D. program in the branch **Mechanical Engineering** of Gujarat Technological University, Ahmedabad.

(Please tick the relevant option(s))

He/She has been exempted from the course-work (successfully completed during M.Phil Course)

He/She has been exempted from Research Methodology Course only (successfully completed during M.Phil Course)

He/She has successfully completed the Ph.D. coursework for the partial requirement for the Ph.D. degree award. His/ Her performance in the course work is as follows:

Grade Obtained in Research Methodology (PH001)	Grade Obtained in Self Study Course (Core Subject) (PH002)
BC	BB

Supervisor's Sign



(Dr. P. V. Ramana)

Co - supervisor's Sign

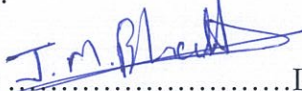


(Dr. J. R. Mehta)

Originality Report Certificate

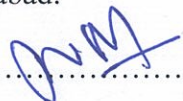
It is certified that the Ph.D. thesis titled "**Development of Battery Thermal Management System for Valve Regulated Lead Acid Battery**" by **Mr. Jaydeep Manojkumar Bhatt** has been examined by us. We undertake the following:

- a. Thesis has significant new work/knowledge as compared already published or are under consideration to be published elsewhere. No sentence, equation, diagram, table, paragraph, or section has been copied from previous work unless it is placed under quotation marks and duly referenced.
- b. The work presented is original and the own work of the author (i.e., there is no plagiarism). No ideas, processes, results, or words of others have been presented as the Author's own work.
- c. There is no fabrication of data or results which have been compiled/analyzed.
- d. There is no falsification by manipulating research materials, equipment or processes, or changing or omitting data or results such that the research is not accurately represented in the research record.
- e. The thesis has been checked using **Urkund** (copy of originality report attached) and found within limits as per GTU Plagiarism Policy and instructions issued from time to time (i.e., permitted similarity index $\leq 10\%$).

Signature of the Research Scholar: Date: 10/01/2023

Name of Research Scholar: **Mr. Jaydeep Manojkumar Bhatt**

Place: GTU, Chandkheda, Ahmedabad.

Signature of Supervisor: Date: 10/01/2023

Name of Supervisor: **Dr. P. V. Ramana**

Place: GTU, Chandkheda, Ahmedabad.

Signature of Co-supervisor: Date: 10/01/2023

Name of Co - supervisor: **Dr. J. R. Mehta**

Place: GTU, Chandkheda, Ahmedabad.

Document Information

Analyzed document	Final Thesis_Jaydeep Bhatt_159997119011.docx (D143596222)
Submitted	9/7/2022 7:26:00 AM
Submitted by	JAYDEEP
Submitter email	jaydeepbhatt54@gmail.com
Similarity	0%
Analysis address	jaydeepbhatt54.gtuni@analysis.urkund.com

Sources included in the report

- W** URL: https://www.reportlinker.com/p05796719/?utm_source=PRN
Fetched: 9/7/2022 7:27:00 AM
- W** URL: <https://www.popsi.com/this-is-what-happens-inside-battery-before-it-explodes>
Fetched: 9/7/2022 7:27:00 AM
- W** URL: http://rave.ohiolink.edu/etdc/view?acc_num=osu1371144911
Fetched: 9/7/2022 7:27:00 AM
- W** URL: <https://www.linkedin.com/pulse/china-does-want-become-lead-acid-battery-manufacturer-lorenzo-mancini>
Fetched: 9/7/2022 7:27:00 AM

Entire Document

CHAPTER 1. INTRODUCTION

Motivation

The transportation system is vital to the global economy, society, and environmental development, particularly in developing countries [1] [2]. The global transportation sector, followed by the industrial sector, is one of the most energy sectors [3]. The global transportation sector consumed approximately 225 quadrillion British thermal units (Btu) of total energy in 2019[4] [5]. On the other hand, this sector accounts for 23% of total energy-related CO2 emissions and is nearly double by 2050 [6]. So, there is a global demand to significantly reduce the negative impact of transportation on humans and the environment [7] [8]. Automobile manufacturers are engaged in era of competition to develop the new vehicles, and electrification is the most promising and sustainable solution. In the midst of rising global CO2 emissions, electric vehicles (EVs) are regarded as emission-free modes of transportation[9] [10]. Electric bikes (E-Bikes) are no mobility devices in urban areas because they are emission-free, make no noise, and use less energy than conventional automobiles [11] [12] [13]. The global E-bike market currently accounts for more than 2.5 percent of total two-wheeler and it is expected to reach 8% by 2023[14]. Because of government support and various subsidies, the E-bike market in India is expanding at an exponential rate. The Indian e-bike market is estimated to be 150 thousand units in 2019, to increase to 633.9 thousand units by 2024 [15]. E-bike uses various battery chemistries like VRLA, Nickel-metal hydride (NiMH) or Lithium-ion (Li-ion) as an energy storage system[16] [17]. Among all available battery technology, the VRLA preferable based on its benefits like robustness, maintenance-free, less expensive, fully recyclable and mature & reliable battery technology [18], [19].

However, the VRLA battery must be precisely managed (electrically and thermally) for better performance and battery life. Almost VRLA battery-based E-bikes have a critical issue related to the unsatisfactory performance of the energy [20] [21]. The operation has a significant effect on life and performance of the battery. Although low temperature also reduces the battery performance, high temperature increases the rate of corrosive reaction, limiting the battery life. In addition, temperature variations within a cell lead to nonuniform battery discharge rates, meaning that available energy cannot readily be accessed, thereby reducing the driving range. So, a thermal management system in the battery pack to reject the heat generated from the battery to the environment in order to avoid overheating during its operation and maintain uniform temperature among the batteries inside the pack.

Overview of VRLA battery

The VRLA battery is an upgraded version of a flooded Lead - Acid battery. McClelland and Davitt invented the VRLA battery with immobilization of electrolyte in Adsorbent Glass Mat (AGM) at the Gates Rubber Company, Denver [23].The

Ph.D. THESIS Non-Exclusive License to
GUJARAT TECHNOLOGICAL UNIVERSITY


In consideration of being a Research Scholar at Gujarat Technological University, and in the interests of the facilitation of research at the University and elsewhere, I, **Mr. Jaydeep Manojkumar Bhatt** having (Enrollment No.) **159997119011** hereby grant a non- exclusive, royalty free and perpetual license to the University on the following terms:

- a. The University is permitted to archive, reproduce and distribute my thesis, in whole or in part, and/or my abstract, in whole or in part (referred to collectively as the “Work”) anywhere in the world, for non-commercial purposes, in all forms of media;
- b. The University is permitted to authorize, sub-lease, sub-contract or procure any of the acts mentioned in paragraph (a);
- c. The University is authorized to submit the Work at any National / International Library, under the authority of their “Thesis Non-Exclusive License”;
- d. The Universal Copyright Notice (©) shall appear on all copies made under the authority of this license;
- e. I undertake to submit my thesis, through my University, to any Library and Archives. Any abstract submitted with the thesis will be considered to form part of the thesis.
- f. I represent that my thesis is my original work, does not infringe any rights of others, including privacy rights, and that I have the right to make the grant conferred by this non-exclusive license.
- g. If third party copyrighted material was included in my thesis for which, under the terms of the Copyright Act, written permission from the copyright owners is required, I have obtained such permission from the copyright owners to do the acts mentioned in paragraph (a) above for the full term of copyright protection.
- h. I understand that the responsibility for the matter as mentioned in the paragraph (g) rests with the authors / me solely. In no case shall GTU have any liability for any acts/ omissions / errors / copyright infringement from the publication of the said thesis or otherwise.

- i. I retain copyright ownership and moral rights in my thesis, and may deal with the copyright in my thesis, in any way consistent with rights granted by me to my University in this non-exclusive license.
- j. GTU logo shall not be used /printed in the book (in any manner whatsoever) being published or any promotional or marketing materials or any such similar documents.
- k. The following statement shall be included appropriately and displayed prominently in the book or any material being published anywhere: “The content of the published work is part of the thesis submitted in partial fulfilment for the award of the degree of Ph.D. in Mechanical Engineering of the Gujarat Technological University”.
- l. I further promise to inform any person to whom I may hereafter assign or license my copyright in my thesis of the rights granted by me to my University in this nonexclusive license. I shall keep GTU indemnified from any and all claims from the Publisher(s) or any third parties at all times resulting or arising from the publishing or use or intended use of the book / such similar document or its contents.
- m. I am aware of and agree to accept the conditions and regulations of Ph.D. including all policy matters related to authorship and plagiarism.

Date: 10/01/2023

Place: GTU, Chandkheda, Ahmedabad


Signature of the Research Scholar

Recommendation of the Supervisor: Agreed

Recommendation of the Co-Supervisor (if any): Recommended


Signature of Supervisor


Signature of Co-Supervisor

Thesis Approval Form

The viva-voce of the Ph.D. Thesis submitted by Shri **Jaydeep Manojkumar Bhatt** (Enrollment No. **159997119011**) entitled "**Development of Battery Thermal Management System for Valve Regulated Lead Acid Battery**" was conducted on 10/01/2023 (Tuesday) at Gujarat Technological University.

(Please tick any one of the following options)

The performance of the candidate was satisfactory. We recommend that he/she be awarded the Ph.D. degree.

Any further modifications in research work recommended by the panel after three months from the date of first viva-voce upon request of the Supervisor or request of Independent Research Scholar after which viva-voce can be re-conducted by the same panel again.

(briefly specify the modifications suggested by the panel)

The performance of the candidate was unsatisfactory. We recommend that he/she should not be awarded a Ph.D. degree.

(The panel must give justifications for rejecting the research work)


Dr. P. V. Ramana

Name and Signature of Supervisor with Seal


Dr. J. R. Mehta

Name and Signature of Cosupervisor with Seal


Dr. Santosh D. Sancheti

1) (External Examiner 1) Name and Signature


Dr. Milind Siddhpura

2) (External Examiner 2) Name and Signature

ABSTRACT

The VRLA battery is an improved Lead-Acid battery. The VRLA battery uses the same base materials and chemical reaction as a traditional battery; the main difference is that the electrolytes are immobilised. Typically, VRLA batteries are preferred as a power source in electric motorcycles (E-bikes) because of advantages such as robustness, maintenance-free operation, lower costs, full recycling, and mature and reliable battery technology. However, for greater better performance and battery life, VRLA batteries must be precisely regulated (electrically and thermally). VRLA battery-powered E-bikes have serious concerns with short battery life and poor performance. The Battery Thermal Management System (BTMS) in a battery pack is required to reject heat generated by the battery to the surrounding environment in order to avoid overheating during operation and to keep the temperature nearly constant among the batteries in the pack.

A systematic approach to developing a BTMS is established on the basis of a review of the relevant literature. The first step towards developing BTMS is to conduct experiments to determine how temperature of battery affects various performance parameters metrics of VRLA batteries. Experimental data indicate that higher temperatures improve capacity and discharge recovery, however battery operation at a higher temperature for an extended duration leads in acid evaporation from the Adsorbent Glass Mat (AGM) separator, reducing battery life. On the other hand, internal resistance increases with decreasing temperature, and a high internal resistance results in a start-up problem with the VRLA battery. As a result, either too low or too high temperatures are detrimental to VRLA batteries.

The following phase in the development of BTMS is to determine the real temperature obtained by VRLA batteries on an E-bike, when running in summer settings (most adverse conditions). Thus, field testing using several routes were conducted in accordance with the geography and climatic conditions circumstances of the region. According to the results of the field testing, ambient temperature plays an important effect in increasing the battery temperature. During afternoon field tests, the battery temperature rapidly rises, reaching up to 45.4°C when the ambient temperature is 39.7°C. An evaporative cooling-based BTMS is designed and constructed based on the peak temperature obtained by VRLA batteries of the E-bike during field testing. Finally, in a field test, the performance of the battery pack integrated with the newly created BTMS is compared to that of a regular battery pack. The thermal behaviour of valve-regulated lead-acid batteries during field testing and charging is

investigated using three alternative cooling strategies: evaporative cooling-based BTMS, pre-cooling + BTMS, and without BTMS. The results show that using the pre-cooling + BTMS cooling mode on a VRLA battery resulted in much lower temperatures and temperature variations. During the road testing with pre-cooled + BTMS cooling mode, the average temperature of the batteries remained 5°C below ambient. In addition to that, a minimal temperature fluctuation of 1.6°C was observed during field testing and charging with pre-cooling + BTMS cooling mode. As a result of this study, it is shown that a battery thermal management system based on evaporative cooling is very effective in cooling down the batteries and maintaining uniform temperature distribution amongst batteries.

Acknowledgment

I am deeply thanking God for one more reason- for providing me an opportunity to work with my supervisor , **Dr. P. V. Ramana**, Professor, Department of Mechanical Engineering Sardar Vallabhbhai Patel Institute of Technology, Vasad (Gujarat) and Co-supervisor **Dr. J. R. Mehta**, Assistant Professor, Department of Mechanical Engineering, Maharaja Sayajirao University of Baroda, Vadodara (Gujarat) whose invaluable guidance and constant encouragement at all stages of the research work provided me with valuable insight without which this research work would not have been possible.

Beside my guide, I would like to appreciate Doctoral Progress Committee **Dr. R. G. Kapadiya**, Professor, L. D. College of Engineering, Ahmedabad & **Dr. V. N. Singh** , Professor & I/C Principal , A. D. Patel Institute of Technology, New Vallabh Vidyanagar for their rigorous examinations and constructive suggestions in my entire journey of research.

I would like to thank **Mr. Bharat Ramanuj**, Owner of Anjaney Thermocontrols and **Mr. Chirag Vaghasiya**, Owner of Vedant E-bikes for helping me for experimental setup preparation.

I would like to mention special thanks to **Dr. Rakesh Buntariya**, Lecturer, Government Polytechnic, Porbandar for helping me in Thesis writing & **Mr. Amit Patel** for patent drafting and filling support.

I am thankful to the authorities of Government Polytechnic, Junagadh, especially to **Mr. Bharat D. Parmar**, Head of Mechanical Engineering Department for providing me all kind of support and encouragement during my doctorate work.

I would also like to acknowledge the support and motivation provided by my colleagues especially **Mr. M. R. Zala**, **Mr. M. R. Buntariya** & **Mr. D. R. Bhatu** , who is always there with me during fabrication work. **Mr. V. M. Parmar** who help me to prepare electric circuit of battery thermal management system. **Mr. A. M. Girach** who helped me for the understanding Microsoft excel and Autodesk Inventor.

I owe my most sincere gratitude to my parents **Dr. Manojkumar J. Bhatt** and **Mrs. Parulben M. Bhatt**, for all their efforts and encouragement they have given throughout my life. Whose blessing and honest support has given me energy to start my work successfully. I admire my parents determination and sacrifice helped me during the difficult moments of my life. my wife, **Gayatri** and my sister, **Dishita**, who always tried to come up with the solution to any problem I faced throughout this tenure. Special love to my beloved daughter **Kavyanshi** for all the maturity they both have demonstrated through the tenure. Thank is a very small word for this. Last but not the least thanks to almighty for giving me such a platform.

“यत भावो - तत भवति”
(“You become what you believe”)

-Jaydeep Manojkumar Bhatt

Table of Content

CHAPTER 1. INTRODUCTION	1
1.1 Motivation.....	1
1.2 Overview of VRLA battery.....	2
1.3 Technical terms of VRLA battery.....	3
1.4 Effect of temperature on VRLA battery.....	5
1.5 Battery Thermal Management System (BTMS)	6
1.5.1 Purpose of BTMS in E-bike.....	7
1.6 Thesis outline.....	8
CHAPTER 2. Literature Review	11
2.1 Comparison of different battery technologies used in Electric vehicles	11
2.2 Effect of temperature on VRLA battery.....	15
2.3 Evaluation of different technologies of BTMS	17
2.4 Statistical analysis.....	22
2.5 Research gap	26
2.6 Problem definition.....	27
2.7 Research objectives.....	27
2.8 Research Methodology.....	28
CHAPTER 3. Thermal analysis of VRLA battery	29
3.1 Thermal analysis for heat generation from the VRLA battery.....	29
3.2 Thermal analysis for heat dissipation through surface of battery	31
CHAPTER 4. Experimental Studies – 1: Effect of Temperature on Different Parameters of Battery Performance	37
4.1 Introduction.....	37
4.2 Description of different experimental tests	37
4.3 Experimental setups and procedures for various test	40
4.3.1 Capacity Test.....	40
4.3.2 Charging test	42
4.3.3 Measurement of gassing rate.....	44
4.3.4 Self discharging test	46
4.4 Results and discussions	48
4.4.1 Comparison of discharging time in 1C – capacity tests with different temperatures.....	48
4.4.2 Comparison of battery capacities with different temperatures.....	49
4.4.3 Comparison of charging process in charging tests with different temperatures	50

4.4.4 Comparison of gassing at different temperature.....	52
4.4.5 Self-discharge test.....	53
4.4.6 Measurement of Internal resistance	54
4.5 Conclusions	56
CHAPTER 5. Experimental Studies – 2: Performance assessment of VRLA battery of E-bike in field test	57
5.1 Introduction	57
5.2 Experimental setup & Instrumentation.....	59
5.2.1 Location of sensors.....	60
5.2.2 Steps for attachment of temperature sensor.....	61
5.2.3 Data logger	62
5.3 Experimentation	63
5.3.1 Development of the driving cycle.....	64
5.3.2 Description of Routes	65
5.3.3 Detail of field test	68
5.3.4 Flow chart of field test experiment.....	70
5.3.5 Assessment of field test	71
5.4 Results and analysis.....	73
5.4.1 Battery Temperature	73
5.4.2 Comparison of battery temperatures.....	77
5.4.3 Influence of ambient temperature and speed on power consumption	79
5.4.4 Influence of route pattern and ambient temperature on energy consumption	80
5.4.5 A mathematical relationship between ambient temperature and energy consumption....	81
5.5 Conclusions	83
CHAPTER 6. Development of Evaporative cooling based BTMS	85
6.1 Design calculations.....	86
6.2 Uncertainty Analysis	87
6.3 Design criteria	88
6.4 Working principle of BTMS.....	88
6.5 Detail of individual components.....	91
6.5.1 Battery pack.....	91
6.5.2 Mid supported box.....	92
6.5.3 Cooling Unit	93
6.5.4 Control Unit.....	96
6.6 Complete prototype of evaporative cooling based BTMS for E-bike	98

CHAPTER 7. Experimental Studies – III: Performance assessment of evaporative cooling based BTMS in field test	101
7.1 Experimental setup & Instrumentation	101
7.2 Design of Experiment using full factorial method	103
7.3 Experimentation	105
7.3.1 Detail of field test.....	105
7.3.2 Vehicle speed	107
7.4 Flow chart of field test-based experiment.....	108
CHAPTER 8. Results and Discussion	109
8.1 Battery temperature profile with BTMS cooling mode	109
8.2 Battery temperature profile with precooling+BTMS cooling mode	111
8.3 Battery temperature profile with natural convection cooling mode.....	112
8.4 Comparison of individual battery temperature ranges	113
8.5 Comparison of individual battery temperature difference from ambient condition	114
8.6 Total energy consumption in field test with different cooling mode	114
8.7 Analysis of full factorial design	115
CHAPTER 9. Conclusions and Future scope.....	119
9.1 Conclusions.....	119
9.2 Future scope	120
List of References	121

List of abbreviation

BTMS	Battery Thermal Management System
VRLA	Valve Regulated Lead Acid
Li-ion	Lithium ion
NiMH	Nickel Metal Hydride
Ni-Cd	Nickel–cadmium
LiFePO ₄	Lithium iron phosphate
E – Bike	Electric Bike
EV	Electric Vehicle
HEV	Hybrid Electric Vehicles
BEV	Battery Electric Vehicle
EREV	Extended Range Electric Vehicle
BTU	British thermal units
AGV	Automated Guided Vehicles
SOC	State of Charge
SOH	State of Health
AGM	Adsorbent Glass Mat
UPS	Uninterruptible Power Supply
OCV	Open Circuit Voltage
SOC	State of Charge
DOD	Depth of Discharge
PCM	Phase Change Material
JC08	Japanese Chassis dynamometer emission test cycle
FTP-75	Federal Test Procedure
NEDC	New European Driving Cycle
CFD	Computational fluid dynamics
BLAST – V	Battery Life time Analysis and Simulation Tool for Vehicles
ANN	Artificial Neural Network
DAS	Data Acquisition System
DAQ	Data Acquisition
SOH	State of Health
GPS	Global Positioning System

GPX	GPS (Global Positioning System) Exchange Format
NREL	National Renewable Energy Laboratory
BMS	Battery Management System
BLDC	Brushless Direct Current
CFM	Cubic Feet per Minute
PVC	Polyvinyl Chloride
AC	Alternating Current
DC	Direct Current
LED	Light Emitting Diode
DBT	Dry Bulb Temperature
WBT	Wet Bulb Temperature
ANOVA	Analysis Of Variance
VIF	Variance Inflation Factor
SiO ₂	Silicone Oxide
H ₂ SO ₄	Sulphuric acid
Pb	Lead
PbO ₂	Lead Oxide
TiO ₂	Titanium dioxide

List of Symbols

Symbol	Description	Unit
Q	Heat generation rate	W/cell
I	Current	A
V	Voltage	V
P	Power	W
Ah	Ampere – Hour	Ah
T	Cell temperature	°C
dE/ dT	Temperature coefficient	V/K
E	Open-circuit voltage of cell	V
v	Cell voltage	V
M _b	Mass of battery module	Kg
K	Thermal conductivity	W/m°C
h	Overall heat transfer coefficient	W/m ² °C
A _s	Surface area of container wall	m ²
I.R.	Internal Resistance	mΩ
P _{drag}	Drag force	W
P _{rc}	Rolling resistance	W
C _d	Drag coefficient	
ρ	Density	kg/m ³
g	Gravitational force	m/s ²
ω	Rotational speed	rad/s
T	Torque	Nm
C _p	Specific heat	J/kgK
q	Volumetric flow rate	m ³ /s
T ₁ , T ₂ , T ₃ , T ₄	Thermocouple temperatures of battery surface	°C
T ₅ & T ₆	Inlet & outlet air temperature	°C
Greek Letters		
ΔQ	Uncertainty in Heat generation rate	W
Δm _a	Uncertainty in Volumetric Flow rate of Air	kg/s
ΔG	Change in Gibbs free energy	J
ΔH	Change in the enthalpy	J/kg
ΔT	Temperature Difference	°C

List of Figures

Figure 1.1 Construction of VRLA battery	3
Figure 1.2 Effect of temperature on battery life[28]	6
Figure 1.3 Active Type Battery Thermal Management System [30]	7
Figure 1.4 Passive Type Battery Thermal Management System [30].....	7
Figure 2.1 Comparison of energy densities and specific energy of different rechargeable batteries [33].....	12
Figure 2.2 Life time and cost comparison of VRLA and Li-ion battery [39]	13
2.3 Article published with different battery technology	24
Figure 2.4 Articles published with different battery application	24
Figure 2.5 Article published with Various Battery Thermal management strategy.....	25
Figure 2.6 Nos. Of articles published from 2011-2021.....	25
Figure 2.7 Country wise published articles.....	26
Figure 3.1 Various mechanisms of heat exchange.....	32
Figure 4.1 Schematic diagram of capacity test experimental setup	41
Figure 4.2 Experimental Setup for capacity test	41
Figure 4.3 Schematic diagram of charging test experimental setup.....	43
Figure 4.4 Experimental Setup for charging test.....	43
Figure 4.5 Schematic diagram of experimental setup for measurement of gassing.....	44
Figure 4.6 Experimental setup for measurement of gassing at different temperatures	45
Figure 4.7 (a)Collecting of gas from battery through vents (b) Gas measuring setup .	45
Figure 4.8 Schematic diagram of experimental setup for self discharge test.....	46
Figure 4.9 Experimental setup for measurement for self discharge test	47
Figure 4.10 Comparison of discharging time in 1C capacity tests.....	48
Figure 4.11 Comparison of battery capacity with different temperatures.....	49
Figure 4.12 Comparison of charging process with different temperatures	50
Figure 4.13 Comparison of charging time with different temperatures	51
Figure 4.14 Comparison of amount of gas released from battery at different temperatures.....	52
Figure 4.15 Comparison of voltage drop with different temperature.....	53
Figure 4.16 Comparison of Self discharge rate with different temperature	53
Figure 4.17 Internal resistance of battery at different temperature	55
Figure 5.1 OREVA ALISH E-Bike [148].....	58
Figure 5.2 Arrangement of different components of experimental Setup in E-bike	59
Figure 5.3 Location of temperature sensors and direction of flow of current in E-Bike	60
Figure 5.4 Arrangement of temperature sensors in E-Bike battery pack.....	60
Figure 5.5 Tip of J – type thermocouple	61
Figure 5.6 Temperature sensor pasted on foam tape.....	61
Figure 5.7 Backside of temperature sensor pasted on Vinyl adhesive tape	62
Figure 5.8 Temperature sensor pasted on the battery surface	62
Figure 5.9 Khoat KH – 208 paperless data recorder	62
Figure 5.10 OREVA ALISH E-bike battery sets	63
Figure 5.11 Typical route of a traveled area on the urban road with GPS data. Image provided by Google map, map data ©2020	65
Figure 5.12 Photographs of Urban Road.....	65
Figure 5.13 Typical route of the traveled area on gradient road with GPS data. Image provided by Google map, map data ©2020	66
Figure 5.14 Photographs of Gradient road.....	66

Figure 5.15 Typical route of a traveled area on highway road with GPS data, Image provided by Google map, map data ©2020.....	67
Figure 5.16 Photographs of highway road.....	67
Figure 5.17 Typical route of a traveled area on a rural road with GPS data, Image provided by Google map, map data ©2020.....	67
Figure 5.18 Photographs of rural road.....	68
Figure 5.19 Speed – time profile of E – bike on various routes	72
Figure 5.20 power – time profile of E – bike on various routes.....	72
Figure 5.21 Battery temperature profiles for new and old batteries during the morning field tests.	74
Figure 5.22 Battery surface temperature profiles for new and old batteries during the afternoon field tests.....	76
Figure 5.23 Battery surface temperature profiles for new and old batteries during the evening field tests.....	77
Figure 5.24 Comparison of battery surface temperature during different routes with the new battery set.....	78
Figure 5.25 Comparison of battery surface temperature during different routes with old battery set	78
Figure 5.26 Wireframe plot showing the influence of ambient temperature and vehicle speed on power consumption	79
Figure 5.27 Battery temperature as a function of power consumption and ambient temperature	80
Figure 5.28 Influence of ambient temperature on total energy consumption during a field test.	81
Figure 5.29 Comparison of actual results of energy consumption with mathematically predicted results.....	82
Figure 6.1 Conceptual design of the developed evaporative cooling based Battery Thermal Management System (BTMS).....	90
Figure 6.2 Detail drawing of battery pack.....	91
Figure 6.3 Snapshot of battery pack	92
Figure 6.4 Detail drawing of mid supported box.....	92
Figure 6.5 Snapshot of mid supported box.....	93
Figure 6.6 Schematic diagram of cooling unit	93
Figure 6.7 Assembly drawing of cooling unit	95
Figure 6.8 Snapshot of cooling unit.....	95
Figure 6.9 Circuit diagram of control unit.....	97
Figure 6.10 Snapshot of Control unit	97
Figure 6.11 Assembly drawing of complete prototype of evaporative cooling based BTMS.....	98
Figure 6.12 Complete prototype of evaporative cooling based BTMS	99
Figure 7.1 Experimental setup.....	102
Figure 7.2 Location of measuring elements and current flow direction in VRLA battery pack of E-bike	102
Figure 7.3 Multilevel full factorial design in Minitab with experimental matrix.....	104
Figure 7.4 Typical route of the travelled area for road test with GPS data	106
Figure 7.5 Speed Profile for (a) Eco mode & (b) Power mode	107
Figure 8.1 Battery temperature profiles during field test with BTMS cooling mode.....	110
Figure 8.2 Battery temperature profiles during field test with precooling + BTMS cooling mode	112
Figure 8.3 Battery temperature profiles during field test with natural convection cooling mode ..	113
Figure 8.4 Comparison of temperature ranges for individual batteries during field tests with different cooling modes	113

Figure 8.5 Comparison of average temperature difference from ambient condition during charging process with different cooling modes	114
Figure 8.6 Total energy consumption by E-bike with different cooling modes.....	115
Figure 8.7 General Linear Model: ΔT versus Cooling strategy, Speed mode & load condition in MINITAB18.....	116
Figure 8.8 Residual plots for temperature difference.....	117

List of Tables

Table 1.1 Table of C-rate with example	4
Table 2.1 Summary of Theoretical work and experimental work related to different BTMS techniques	20
Table 4.1 Values of performance parameters of a VRLA battery at different temperatures	56
Table 5.1 Specification of OREVA ALISH E- BIKE	58
Table 5.2 Data logger channels description.....	63
Table 5.3 Estimated values of regression coefficient for battery temperature by MINITAB	82
Table 6.1 Possible error in measurement devices.....	87
Table 7.1 Details of instrumentation	102
Table 7.2 Assessment criteria for field test	103
Table 7.3 Details of design factors with levels.....	103
Table 7.4 Design summary of full factorial method.....	103
Table 7.5 Simplified Experimental matrix	105
Table 7.6 Detail of route for field test	105

List of Appendices

Appendix A Calibration Certificates	135
Appendix B Design Calculations	137
Appendix C Uncertainty Analysis.....	145
Appendix D Comparison of results of typical field test with new and old battery set	148
Appendix E : Field test data (Experimental study – 3).....	149

CHAPTER 1. INTRODUCTION

1.1 Motivation

The transportation system is vital to the global economy, society, and environmental development, particularly in developing countries [1] [2]. The global transportation sector, followed by the industrial sector, is one of the most energy-demanding sectors [3]. The global transportation sector consumed approximately 225 quadrillion British thermal units (Btu) of total energy in 2019[4] [5]. On the other hand, this sector accounts for 23% of total energy-related CO₂ emissions and is expected to nearly double by 2050 [6]. So , there is a global demand to significantly reduce the negative impact of transpiration on humans and the environment [7] [8]. Automobile manufacturers are engaged in era of competition to develop the next generation of vehicles, and electrification is the most promising and sustainable solution. In the midst of rising global CO₂ emissions, electric vehicles (EVs) are regarded as emission-free modes of transportation[9] [10] . Electric bikes (E-Bikes) are popular as personal mobility devices in urban areas because they are emission-free, make no noise, and use less energy than conventional automobiles [11] [12] [13]. The global E-bike market currently accounts for more than 2.5 percent of total two-wheelers on the road, and it is expected to reach 8% by 2023[14]. Because of government support and various subsidies, the E-bike market in India is expanding at an exponential rate. The Indian e-bike market is estimated to be 150 thousand units in 2019, with a projected increase to 633.9 thousand units by 2024 [15]. E-bike uses various battery chemistries like VRLA, Nickel-metal hydride (NiMH) or Lithium-ion (Li-ion) as an energy storage system[16] [17]. Among all available battery technology, the VRLA battery is preferable based on its benefits like robustness, maintenance-free, less expensive, fully recyclable and mature & reliable battery technology [18], [19].

However, the VRLA battery must be precisely managed (electrically and thermally) for better performance and battery life. Almost VRLA battery-based E-bikes have a critical issue related to the unsatisfactory performance of the energy storage system [20] [21]. The operation has a significant effect on life and performance of the battery. Although low temperature also reduces the battery performance, high temperature increases the rate of corrosive reaction, limiting the battery lifetime [22]. In addition, temperature variations

Overview of VRLA battery

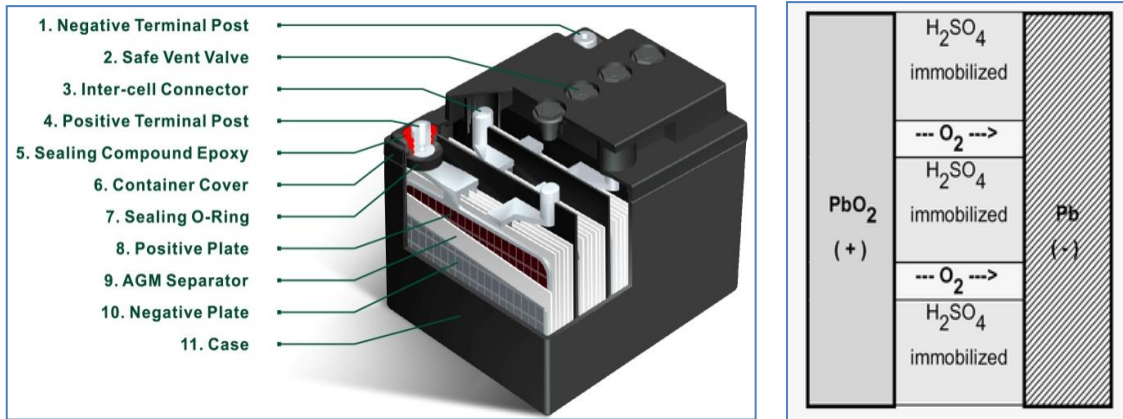
within a cell lead to nonuniform battery discharge rates, meaning that available energy cannot readily be accessed, thereby reducing the driving range. So, A thermal management system in the battery pack is essential to reject the heat generated from the battery to the environment in order to avoid overheating during its operation and maintain uniform temperature among the batteries inside the pack.

1.2 Overview of VRLA battery

The VRLA battery is an upgraded version of a flooded Lead - Acid battery. McClelland and Davitt invented the VRLA battery with immobilization of electrolyte in Adsorbent Glass Mat (AGM) at the Gates Rubber Company, Denver [23]The VRLA battery works with the same base materials and chemical reaction as the conventional version; the only difference is the electrolyte's immobilization. Immobilization means electrolyte moisten into AGM separator or clotted by addition of SiO_2 [24]. AGM is a highly porous and absorbent mat fabricated from micro-glass fibres, is partially filled with electrolytes, and acts as the separator/electrolyte reservoir. Due to the immobilized design, the VRLA batteries will not leak if inverted or if the container is broken. They can mount in any orientation and position, even immersed in water.

An AGM separator is placed between the positive and negative plates of the VRLA battery. Figure 1.1 shows that Positive and negative plates react chemically through the AGM separator, which is wetted with sulphuric acid (H_2SO_4). Positive and negative electrodes create oxygen and hydrogen, respectively. Oxygen and hydrogen are recombined and dissolved in H_2SO_4 to create H_2O under normal conditions. Therefore, there is never a need to add water to a VRLA battery.

VRLA batteries are used in power storage battery packs in a variety of applications such as Electric Vehicles (EVs), Automated Guided Vehicles (AGVs), various UPS systems, photovoltaic solar power, and so on. Furthermore, due to its low cost and compactness, it is one of the most popular E-bike batteries in the Indian market. However, there are several disadvantages to using VRLA batteries. VRLA batteries are more expensive and have a lower specific energy density than flooded batteries. A VRLA battery requires precise charging control, especially when charging in high-temperature conditions.



(a) Different components of VRLA battery [25]

(b) Chemical reaction [26]

Figure 1.1 Construction of VRLA battery

1.3 Technical terms of VRLA battery

These various electrochemical terms have been defined for VRLA batteries to characterize battery performance. The following terms are under IS 1885 (part 15): 2008 (Indian Standard for Electrotechnical vocabulary - Part 15 primary and secondary cells and batteries) [27].

1) Cell

The assembly of electrode, electrolyte, container, terminal and separator is used as a source of electric energy obtained by directly converting chemical energy.

2) Battery

One or more cells fitted with devices necessary for use is known as a battery.

3) Ampere Hour Capacity (Ah)

Electric charge, which cell can deliver under specified discharge conditions.

The S.I. unit of electric charge is the coulomb (1C = 1 As). But in practice, battery capacity is expressed in terms of Ah.

4) Rated Capacity (C_n)

The value of capacity declared by the manufacturer is known as rated capacity.

Technical terms of VRLA battery

5) Discharge rate:

It is an electric current at which the battery is discharged. The discharge rate can be calculated as the rated capacity divided by the corresponding discharge time which results in electric current.

6) C – rate

It is a method for expressing the rate of discharge current. It is used to represent a charge or discharge rate equal to the capacity of a battery at a specific time.

Its expressed as $I = M C_n$

Where I = Current, M = fraction of multiple and C_n = Rated capacity in ampere-hours. For example, A 1C – rate means discharge current will discharge the entire battery in 1 hour. 1C – rate for a battery of 100 Ah. Capacity equal to removing current 100 A.

Table 1.1 Table of C-rate with example

C – rate	Discharging Time (T)	Example: Discharging current for 100 Ah battery ($I = M C_n$)
1C	1 Hour	$I = 1 \times 100 \text{ Ah.} = 100 \text{ A}$
1.5C	45 min.	$I = 1.5 \times 100 \text{ Ah.} = 150 \text{ A}$
2C	30 min.	$I = 2 \times 100 \text{ Ah.} = 200 \text{ A}$
C2	2 Hrs.	$I = \frac{1}{2} \times 100 \text{ Ah.} = 50 \text{ A}$
C3	3 Hrs.	$I = \frac{1}{3} \times 100 \text{ Ah.} = 33.3 \text{ A}$
C5	5 Hrs.	$I = \frac{1}{5} \times 100 \text{ Ah.} = 20 \text{ A}$
C8	8 Hrs.	$I = \frac{1}{8} \times 100 \text{ Ah.} = 12.5 \text{ A}$
C10	10 Hrs.	$I = \frac{1}{10} \times 100 \text{ Ah.} = 10 \text{ A}$
C20	20 Hrs.	$I = \frac{1}{20} \times 100 \text{ Ah.} = 5 \text{ A}$

7) Open Circuit Voltage (OCV)

It is a battery voltage under no-load conditions.

8) Cut-off voltage

It is a specified battery voltage at which a discharge of the battery is considered as a finish.

9) Float voltage

It is the voltage at which a battery is maintained after being fully charged to maintain that capacity.

10) Overcharging

Continued charging after a full charge of the battery is known as overcharging.

11) Self-discharge

Loss of chemical energy due to spontaneous reaction within the battery when not connected to external circuit.

12) Internal resistance

It is the overall equivalent resistance within the battery. It is different for charging and discharging and may vary as the operating condition changes.

13) State of Charge (SOC)

The remaining capacity expressed as a percentage of the full charge capacity is known as the state of charge.

$$\text{SOC} = \frac{\text{Actual Capacity}}{\text{Fully Charged Capacity}} \times 100\%$$

14) Depth of Discharge (DOD):

The depth of discharge is the capacity taken from the battery after a full charge.

Basically, $\text{DOD} = 1 - \text{SOC}$

1.4 Effect of temperature on VRLA battery

The lifespan of the VRLA battery is the most crucial parameter. Operating conditions of the battery and climatic changes are mainly affecting the lifespan of the VRLA battery. Battery temperature is one of the significant parameters influencing a battery's lifespan. Temperature directly affects the chemical reaction and is responsible for ions mobility between the positive and negative electrodes of the cell. Figure 1.2 shows the plot of temperature versus rated life of battery. It was clearly observed that the life of battery is reduced with increase in operating temperature.

The VRLA battery provides with an AGM (Absorbent Glass Mat) separator between the positive and negative electrodes. AGM separator is made to fill with sulfuric acid (H_2SO_4) until it becomes completely wet. During a chemical reaction, ions transfer from the positive electrode to the negative electrode through a wet AGM separator. According to the Arrhenius equation, the chemical rate will increase when the temperature of the battery rises, which will ultimately lead to an increase in the capacity of the battery.

Battery Thermal Management System (BTMS)

When the battery operates at a high temperature for a long period, it affects the AGM separator of a cell. The temperature of the wet AGM separator rises as the temperature of the battery rises. So acid from the AGM separator gradually evaporates and becomes dry after a particular period. Once AGM becomes dry then the capacity of AGM for chemical reaction drastically reduces and reduces the battery life. Thus, proper thermal management of batteries is essential to keep the temperature within the manufacturer's recommended range (25°C to 30°C) for optimal performance and long battery life.

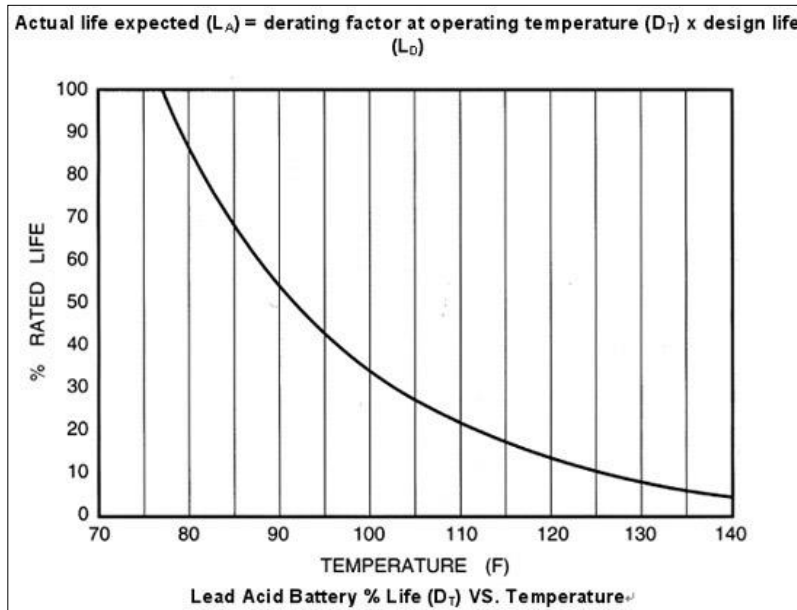


Figure 1.2 Effect of temperature on battery life[28]

1.5 Battery Thermal Management System (BTMS)

The scheme and method that maintains the battery pack at its optimum temperature range are known as Battery Thermal Management System (BTMS). According to the Arrhenius law of battery electrochemistry, the battery reaction increases exponentially with the battery's temperature [29]. As a result, hotter cells degrade more quickly than colder cells. Those few overheated cells shorten the lifetime of a whole battery pack. Due to overheating, the cell capacity decreases quickly. Thus, proper thermal management of batteries is essential to keep the temperature within the manufacturer's recommended range (25°C to 30°C) for optimal performance and long battery life.

There are mainly two types of BTMS used for battery packs, active thermal management system (heat transfer to air by forced convection).

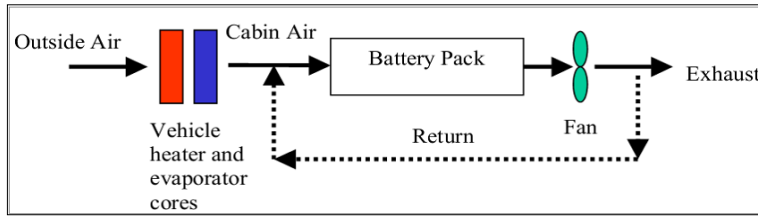


Figure 1.3 and passive thermal management system (heat transfer to liquid or PCM by natural convection, [30])

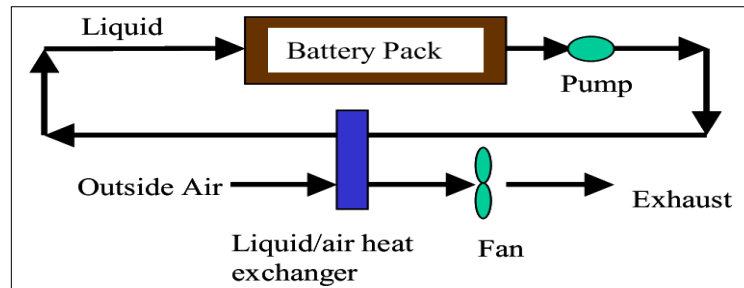


Figure 1.4 The passive thermal management system can absorb a large amount of latent heat, so it's more effective than the active thermal management system [30]. The proper thermal management can be achieved by using air cooling, evaporative cooling, liquid cooling, refrigeration system, phase change material, insulating material etc.

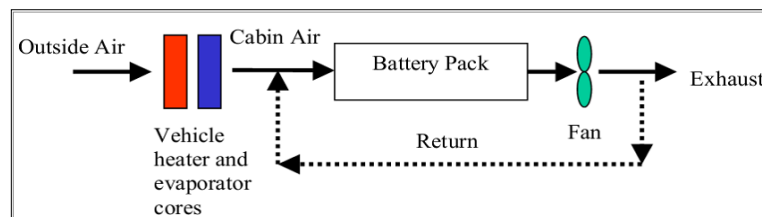


Figure 1.3 Active Type Battery Thermal Management System [30]

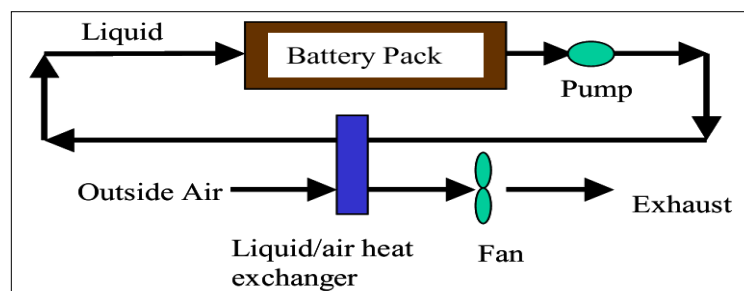


Figure 1.4 Passive Type Battery Thermal Management System [30]

1.5.1 Purpose of BTMS in E-bike

Battery thermal management systems (BTMS) based on air or liquid cooling are commonly utilised in EVs. Deciding which type of battery management system to use in a vehicle depends on specific factors like power consumption, the number of battery cells, space

Thesis outline

availability and cost. The energy consumption of various components used in air or liquid cooling, such as pumps, blowers, and so on, directly affects the range of E-bikes. The ideal thermal management system would be small, light, and inexpensive. The liquid cooling system has been considered an effective cooling system for substantial battery packs, but it increases the operating cost, weight and volume of the battery.

The primarily liquid cooling system is used for Li-ion battery packs in electric cars and hybrid vehicles. The air-cooling system has preferred due to its simplification. The air-cooling system used the forced cooling draft technique to maintain the uniform temperature in the battery pack. Moreover, Because of the fans, pumps, tubing and other equipment, forced air and liquid cooling systems are massive, complicated, and costly. Also, an air or liquid-cooled thermal management system cannot keep the battery temperature below ambient. Evaporative cooling can keep battery temperatures below ambient[31]. Thus, in this research work, an evaporative cooling-based thermal management system was developed and investigated its effect on VRLA batteries for E-bikes.

1.6 Thesis outline

The thesis is composed of eight chapters. The overview of each chapter is briefly described below,

- **Chapter 1** is a brief collection of the general information related to a research project. It also signifies how battery life is essential in modern electric vehicles. It also provides information on how temperature affects battery life. This chapter also provides a brief description of the battery thermal management system and discusses the function of the BTMS in an e-bike.
- **Chapter 2** on "literature review" contains an extensive review of the literature on the effect of temperature on battery life and thermal management systems in electric vehicles, as well as statistical analysis, the scope of the research, research gap, problem definition, the research objectives and stages of development of battery thermal management system for E-bike.

The following chapters are organized chronologically in accordance with the stages of development of the battery thermal management system.

- The thermal study of a VRLA battery under operational conditions is covered in **Chapter 3**. This chapter provides a detailed explanation of the thermal analysis of heat generation from VRLA batteries and heat dissipation from the battery surface.
- **Chapter 4** represents the first step in the development of BTMS. This chapter describes multiple studies that were conducted to study the effect of temperature on various performance aspects of VRLA batteries. In addition, the results are graphically shown and thoroughly described.
- **Chapter 5** is the second step toward the development of BTMS. This chapter is entitled "Experimental study – 2: Performance assessment of VRLA battery of E-bike in field test". The details of field experiments conducted to ascertain the actual temperature obtained by E-bike VRLA batteries are discussed in depth in this chapter. Also, the performance characteristics, such as battery temperature and energy usage, are graphically illustrated and discussed.
- **Chapter 6** is the third step towards the development of BTMS. This chapter includes conceptual design, working principle and fabrication details of the evaporative cooling-based BTMS.
- **Chapter – 7** is the fourth step toward the development of BTMS. This chapter is entitled "Experimental study – 3: comparison of the performance of BTMS-based battery pack and conventional battery pack in field test". The discussion under the heading is about evaluating the thermal behaviour of VRLA batteries in a field test with an evaporative cooling-based BTMS and an E-bike charging test.
- **Chapter 8** is about the results and discussion of experiments carried out during the experimentation related to E-bike performance in the presence and absence of BTMS. Results are graphically analyzed and validated using regression analysis. The conclusion of the whole research and future work are discussed at the end of the thesis.

CHAPTER 2. Literature Review

This chapter presents an extensive literature review on the effect of ambient temperature on valve regulated lead acid (VRLA) batteries, a comparison of different types of BTMS, the current scenario of different thermal control strategies used in electric vehicles, and the scope of a newly developed evaporative cooling based thermal management system for batteries. In newly developed battery applications, battery life and performance face major challenges. For many years, several thermal management approaches and tactics for decreasing the effect of temperature on batteries have been investigated. The goal of the literature review is to look at and study past research papers and articles about ways to deal with heat, how to make batteries last longer, and what kind of cooling system a battery pack needs.

The review of the literature has been divided into four distinct sections in accordance with the steps for creating a successful thermal control system, namely: (1) A comparison of the various battery technologies used in electric vehicles; (2) The effect of temperature on VRLA batteries; (3) A comparison of the various technologies used in battery thermal management systems; and (4) Battery thermal management systems used in various electric vehicles.

2.1 Comparison of different battery technologies used in Electric vehicles

Batteries are essential energy-storage components in transportation and energy conversion systems. In most electric vehicles, valve-regulated lead acid (VRLA) and lithium-ion (Li-ion) batteries are employed. Both battery technologies have advantages and disadvantages in terms of performance, battery life, cost, safety, recyclable nature, and so on. The following sections compare VRLA with Li-ion batteries based on various factors.

Energy Density

Energy density of the Li-ion battery is 2.5 times than that of VRLA battery. So, it can store more amount of energy compared to VRLA battery in same volume [32].

Comparison of different battery technologies used in Electric vehicles

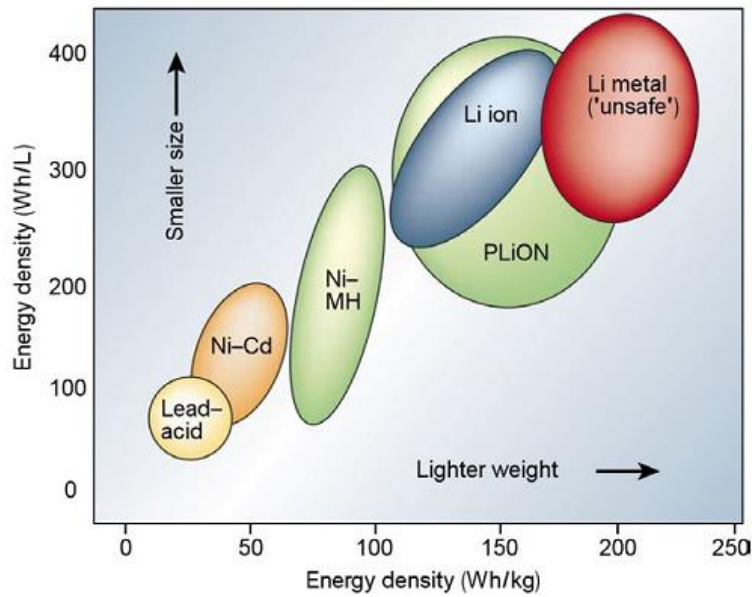


Figure 2.1 Comparison of energy densities and specific energy of different rechargeable batteries [33]

Figure 2.1 shows the comparison of energy densities and specific energy of different rechargeable batteries. It is evident that Li-ion batteries have a higher energy density than other batteries. The high energy density of the Li-ion battery can sometimes cause the battery to explode [33]. Because of its high energy density, the Li-ion battery can store a large amount of charge. As a result, the battery bursts in the event of a short circuit or a minor flaw in the battery.

Safety

Overcharging and rapid charging are not advised for VRLA or Li-ion batteries. During overcharging, excess energy transferred to the battery is converted to heat. During overcharging, the temperature of the battery cell rises, resulting in gassing from the battery cell as sulphuric acid evaporates. Vents in a VRLA battery allow gases created by the battery during overcharging to escape. As a result, there is no risk of an explosion due to overcharging of the battery.

When a Li-ion battery is overcharged or charged too quickly, an explosion might occur. An oxygen and carbon dioxide bubble is formed when the lithium ion batteries are overcharged because of the breakdown of the battery's composition. As a result, the battery bursts due to the build-up of pressure inside of it [34]. A protective circuit is required in every Li-ion battery for this reason. In the presence of oxygen, lithium metal is extremely combustible. Manufacturers are required to pack more material into the electrode and compress it in a

smaller volume to boost the energy density of the battery [35]. As a result, inadvertently puncturing a battery can result in an internal short and explosion. Since 1991, three significant aviation accidents and 160 aircraft accidents have been reported as a result of Li-ion battery explosions [36].

Cost

Li-ion batteries are more expensive than VRLA batteries because the primary metals used in Li-ion batteries, such as lithium and cobalt, are more expensive than the lead used in VRLA batteries. Lead resources are more than lithium metal resources in the earth's upper crust. Reserved lead and lithium resources are estimated to be around 2 billion tones and 53 million tones, respectively[37], [38]. As a result, the cost of a lead-based battery is lower than that of a lithium-based battery. Because lithium-ion chemistry is more complicated than VRLA chemistry, the manufacturing cost is likewise higher. According to the cost analysis as shown in Figure 2.2 , the battery cost of the Li-ion battery is three times higher than the VRLA battery, and the lifetime cost of the Li-ion battery is 18% higher than the VRLA battery for moderate climate.

	VRLA (moderate climate: 25°C)	→ VRLA (hot climate: 33°C)	Lithium-ion
System size	100 kWh	100 kWh	62.5 kWh
Battery Cost	\$12,000 (\$120/kWh)	\$12,000 (\$120/kWh)	\$37,500 (\$600/kWh)
Cycle Life	1,000 @ 50% DoD	→ 500 @ 50% DoD	1,900 @ 80% DoD
Installation	\$20/kWh	\$20/kWh	\$3.6/kWh
Transportation	\$28/kWh	\$28/kWh	\$5/kWh
Lifetime cost	\$0.34/kWh throughput	\$0.67/kWh throughput	\$0.40/kWh throughput

Figure 2.2 Life time and cost comparison of VRLA and Li-ion battery [39]

Recycling nature

VRLA batteries are totally recyclable; an internal component includes up to 60% of the battery mass. As a result, no separating procedure is necessary. The VRLA battery recycling procedure is basic. To begin, the battery case is opened and the electrolyte is drained from the battery. Electrodes and connectors are extracted from the battery case and recovered in their entirety. The recovered lead is melted and refined before being used to create new components. One of the main reasons for the success of VRLA battery recycling is that all

Comparison of different battery technologies used in Electric vehicles

VRLA battery manufacturers use the same raw material as an electrolyte: lead, lead oxide, and sulfuric acid. Recycling a Li-ion battery is harder than recycling other types of batteries because each cell in a Li-ion battery has a wider range of materials. The Li-ion battery, along with the slag-forming chemical, is fed into a high-temperature furnace. Lithium, aluminium, silica, calcium, iron, and manganese are all present in the slag. The extraction of lithium from slag is an expensive procedure[40]. The manufacturing cost of a Li-ion battery is lower than the raw material cost. Recycling lithium is widely used in a variety of applications, including lubricating greases (WD-40) and other items [41].

Discharge rate

The ratio of vehicle mass to passenger mass is high for electric bikes. Therefore, it requires a powerful electric motor. The E-bike's motor required a substantial quantity of current. The fact that a VRLA battery is a deep cycle battery indicates that it has a high specific power [42]. Therefore, a VRLA battery can have a high discharge current to power an electric motor. When a lot of current drains from a lithium-ion battery, it quickly warms up. Li-ion batteries are therefore inappropriate for an electric bike.

Charging Flexibility

In comparison to Li-ion batteries, charging for VRLA batteries is more flexible and tolerable to improper recharging. This reduces the risk of personal injury and property damage[42]. Li-ion cannot withstand overcharging circumstances. A special arrangement of protection circuits is required to control overcharging and overvoltage in Li-ion batteries. It makes things even more expensive. On the other hand, lead-acid batteries work just fine when they are overcharged. When a VRLA battery is overcharged, hydrogen gas is emitted from the battery.

According to the comparison above, Li-ion batteries have a higher energy density and a longer life term than VRLA batteries. However, VRLA batteries are being replaced by Li-ion batteries. While VRLA batteries are non-explosive, Li-ion batteries are very explosive. The price of a VRLA battery is nearly half that of a Li-ion battery. Deep discharge batteries include VRLA batteries. Therefore, it can give an electric motor in an EV high specific power for beginning torque. While Li-ion batteries are rapidly heated up when a large current is drawn from the battery for an electric vehicle's starting torque.

Moreover, VRLA batteries are a well-established and recyclable battery technology. Thus, VRLA batteries are the preferred battery technology in developing countries such as India. The Bluewave E-bike market research [43] shows that VRLA battery leads the Electric vehicle market in India due to its benefits like robustness, low cost and better safety. Because India is in a tropical location, the average atmospheric temperature in practically all sections of the country ranges from 30°C to 40°C[44] . Such high temperatures have a significant impact on the performance and longevity of the VRLA battery. Due to this reason, a proper battery thermal management system is essential to maintain battery temperature within its optimum operating temperature range.

2.2 Effect of temperature on VRLA battery

A battery is a chemical device that functions on the basis of thermoelectric chemistry. A chemical reaction happens between the positive and negative plates. Temperature is a crucial factor in every form of chemical reaction. The literature review indicates that temperature and heat generation during the charging-discharging process impact the performance and lifespan of valve-regulated lead-acid batteries. Changes in battery temperature affect the battery's performance. Temperatures that are too low or too high have an impact on battery performance and life.

D. Valkovska[45] studies the thermal behaviour of a Valve Regulated Lead Acid (VRLA) cell when it is overcharged and has a saturation level of roughly 90%. Only the charging current determines the thermal behaviour of a 2V, 4 Ah. VRLA battery in experiments. The experimental results reveal that the temperature of the cell is linearly related to the charging current of the VRLA battery.

C. Michael Hoff [46] finds the thermal runaway zone in VRLA batteries and proposes various techniques for preventing thermal runaway. Thermal runaway is a condition that occurs in a VRLA battery when the temperature rises to the point where the battery fails. The experimental results reveal that the thermal runaway zone varies with ambient temperature and battery float voltage. Additionally, older batteries have lower thermal runaway zone limits.

D. Pavlov [47] investigates the heat phenomena that occur throughout the chemical and electrochemical phases of the oxygen cycle in a 2V, 4.5 A VRLA battery. The effect of

Effect of temperature on VRLA battery

temperature on the current flowing through the battery, the velocity of gas leaving the battery, and the thickness of the AGM separator is tested experimentally. Results indicate that during the discharging phase, the temperature rise in an electrochemical reaction is greater than in a chemical reaction. The rate of gas release increases with temperature, and thermal runaway occurs at higher voltages when the AGM separator is thicker.

R. Hutchinson [48] conducts an experiment to assess the influence of temperature on the life and capacity of VRLA batteries. The Sigma Systems C4 temperature chamber is used to examine the performance of VRLA batteries at various temperatures. The battery has an 80 percent capacity at 0 degrees Celsius, a 100 percent capacity at 25 degrees Celsius, and a 120 percent capacity at 55 degrees Celsius, according to the results of an experiment, and every 8 degrees Celsius (15 degrees Fahrenheit) increase in temperature halves the battery's lifespan. This means that the VRLA battery's capacity grows with temperature, but excessive temperatures shorten its lifespan.

B. Culpin [49] investigates the causes of unstable chemical processes in VRLA batteries at high operating temperatures and the causes of thermal runaway in a 6V, 100 Ah. VRLA battery. The battery is overcharged to 2.65V potential per cell and the battery temperature, gas evaluation rate, and current are all measured. The conclusion was reached that the applied voltage is the primary cause of thermal runaway. Temperature is just an accelerating factor.

A. Kirchev [47] investigates the effect of heat generation owing to temperature change and electrolyte saturation on the rate and efficiency of the oxygen cycle at various negative plate potentials in a VRLA battery. For the experiment, a 1.5 Ah VRLA battery with a 2.5 mm thick AGM separator is used. The AGM separator is built with 15% compression. The heat generated by the battery has an impact on the efficiency of the oxygen cycle. As the temperature increases, the efficiency decreases as the constant negative plate potential falls. At greater temperatures, hydrogen production is elevated, lowering the efficiency of the oxygen cycle.

E.meissner [50] examined the thermal behaviour of VRLA batteries under abnormal operating conditions experimentally. The studies were carried out using a 6V, 85 Ah VRLA battery. During charging of a 6V, 85Ah VRLA battery, total heat generation and heat dissipation rates were measured. It has been discovered that heat generation is closely related

to electrochemical reactions, which are strictly related to the amount of react material. 6 volts, 85 amp-hours. VRLA battery is overloaded with a constant current of 10A, resulting in undesired heat creation. Overcharging with constant current means constantly adding energy, which results in unwanted heat generation. Therefore, the distribution of charge, water decomposition, and oxygen cycles can be used to estimate heat generation.

The thermal performance of electric car battery modules is evaluated by A. Pesaran [51]. The temperature distribution of the VRLA battery cell is predicted using finite element analysis. In addition, utilising infrared photography and liquid crystal thermography, obtain thermal images of the battery surface during charge-discharge conditions. For the analysis, a 12V, 24Ah. VRLA battery was employed. For all battery surfaces, a temperature of 25°C and a power density of 35 W/m²K are chosen for finite element analysis. Observation demonstrates that high motor power and an aggressive charging-discharging process are too responsible for battery thermal issues in electric vehicles. Finally, conclude that the heat produced by the battery cell is dependent on the entropy change caused by chemical reactions and the joule effect caused by the battery's internal resistance. In addition, data reveals that adding ventilation holes to the battery module enhanced the battery's thermal performance.

It reveals that temperature has a significant impact on the performance and lifespan of VRLA batteries. Consequently, an effective thermal management system is required for a battery pack to disperse the generated heat to the environment, prevent the battery from overheating during operation, and maintain a consistent temperature across the pack's batteries.

2.3 Evaluation of different technologies of BTMS

For many years, researchers have studied various thermal management strategies and techniques to reduce the impact of temperature on batteries. Cosley et al. developed a BTMS for VRLA batteries used in telecommunication applications [52]. The cold plate-based BTMS was designed with the battery resting perfectly on the cold plate and a warming pad put below the cold plate. It also uses Fourier's law of conduction to measure thermal conductivity for VRLA in all three directions. Finally, determine whether the VRLA battery is temperature-sensitive. The difference in ambient temperature and the heat generated due to the chemical reaction rate significantly impact battery life. In an outdoor environment, the life of a VRLA battery has been found to range from 1.5 to 7 years, depending on location, temperature, charging, and maintenance. As a result, hotter cells degrade more rapidly

Evaluation of different technologies of BTMS

decayed than colder cells. These few hot cells reduce an entire battery pack's lifetime. Thus, proper thermal management of batteries is essential to keep the temperature within the optimum temperature range (25°C to 30°C) for optimal performance and long battery life. According to the Arrhenius equation for battery electrochemistry, the battery reaction increases exponentially with battery cell temperature.

The Thermal Management System uses different cooling technologies, such as air cooling, liquid cooling, evaporative cooling, PCM, and heat pipe. Yu et al. [53] compared the charging/discharging process of Li-ion batteries used in electric vehicles (EVs) using two different cooling systems, natural cooling and forced air cooling. Forced air cooling at a flow rate of 0.8 m/s improves the transient thermal properties of a battery pack at a high discharging rate (1C) and the battery pack's life cycle.

Bao et al. [54] examined and compared the energy performance of active air cooling BTMSs with exterior and internal air circulation during fast charging of the Li-ion battery pack. The results show that compared with the external air circulation system, the active air-cooling BTMS with internal air circulation can save up to 69.4% and 83.6% of the total energy consumption at 30°C and 40°C surrounding temperatures, respectively. It's indicated that interior air circulation was more effective than external air circulation.

Zhen et al. [55] examined the performance of a Li-ion battery with a liquid-cooled cold plate equipped with a variable number of mini-channels. The effects of number of channels, inlet mass flow rate, flow direction and width of channels on the thermal behaviours of the battery pack were analysed. The results showed that the mini-channel cold-plate thermal management system provided better cooling efficiency and maintained a uniform battery temperature at higher discharge. The number of mini-channels and inlet mass flow rate strongly affect the cooling efficiency. It proved that a 5-channel cold plate was enough and could be reduced the temperature by increasing the inlet mass flow rate.

Zhang et al. [56] developed an efficient BTMS on ultrathin flat heat pipes combined with liquid cooling. The performance of a heat pipe-based cooling system is compared with natural air convection and aluminium plate cooling. It found the highest temperature reached with ultrathin flat heat pipe-liquid cooling to be 73.7% lower than with natural convection and aluminium plates. It showed that heat pipe-based BTMS effectively decreases the

maximum temperature reached by the battery and effectively maintains the uniform temperature distribution at a low cost.

Ataur Rahman [57] proposed a BTMS based on evaporative cooling for LiFePO₄ battery packs used in electric vehicles (EV). The EV performance of an evaporative cooling-based BTMS was compared to an air cooling-based BTMS. BTMS based on evaporative cooling can save 17.69% more energy than air cooling.

Behi et al. [58] also presented a Li-ion battery-based BTMS based on evaporative cooling. The temperature of the cell and module is evaluated experimentally and numerically by the absence of natural convection, natural convection, forced convection, and evaporative cooling. The evaporative cooling approach was found to reduce the maximum temperature of the cell and module by up to 35.8% and 23.8%, respectively.

Samimi et al. [59] assessed the performance of a PCM-based battery thermal management system for a lithium-ion battery pack. The computational and experimental performance of carbon fiber-based composite PCM-based BTMS was compared to air cooling and natural PCM-based BTMS. It was found that the presence of carbon fibres has a significant impact on temperature distribution within the thermal management system. Because of the fast-melting rate, the presence of carbon fibres in PCM improves temperature uniformity and boosts thermal conductivity.

Ling et al. [60] created a hybrid system that incorporated PCM with forced air convection to increase thermal management performance. Experimental findings validated the numerical analysis. The results indicate that the ambient temperature of passive TMS was approximately 7°C higher than that of forced air convection.

Said Al-Hallaj et al. [61] conducted an experiment on the Li-Ion battery of an electric scooter using four distinct types of cooling media: natural convection cooling, aluminium foam, phase change material (PCM), and a combination of aluminium foam and PCM. The rise in temperature during the C1 rate discharge test was as follows: Without PCM and Al foam = 40 °C, with Al foam = a temperature drop of 8°C, and with PCM alone a temperature reduction of around 45 percent.

Evaluation of different technologies of BTMS

Table 2.1 Summary of Theoretical work and experimental work related to different BTMS techniques

Literature & Year	BTMS Strategy	Type of application	Description	Critique outcome
Mohammadian et al. (2015) [62]	liquid cooling	*	The operating fluids used for both internal and exterior cooling were liquid electrolyte and water.	improved internal cooling and temperature consistency
Zhen et al. (2016) [63]	Liquid cooling with mini-channel cold plate	*	Battery performance was assessed using a variety of micro channels.	superior cooling up to five channels
Bai et al. (2017) [64]	PCM and cold plate	*	battery performance examined at various cold plate heights.	5cm height is best for cooling.
Yu et al. (2019) [65]	PCM and cold plate	EV	Battery performance was examined using various numbers of water cooling tubes.	Three water cooling tubes provide superior cooling.
Bao et al. (2019) [66]	air cooling with external and internal air circulation	EV	The energy efficiency of active air cooling BTMSs with exterior and internal air circulation was investigated.	It was discovered that internal air circulation was more efficient.
Zhang et al. (2020) [56]	heat pipe	*	It was proposed to develop an efficient BTMS based on an ultrathin flat heat pipe-liquid cooling approach.	In comparison to natural convection and aluminium plates, the highest temp. measured was 73.7 % lower.
Klenier et al. (2020) [67]	heat pipe	*	The heat pipes are attached to the battery's terminals.	The temperature at terminals is 19°C lower.
Chen et al. (2020) [68]	pulsating heat pipes	EV	It uses the water-based TiO ₂ nanofluid as working medium.	The heat dissipation performance of TiO ₂ -based nanofluid is good.

Literature & Year	BTMS Strategy	Type of application	Description	Critique outcome
El-Ladan et al. (2015) [69]	Evaporative cooling	Hybrid Electric Vehicle	Various European drive cycles were employed to compare the performance of the new technique to traditional air-cooling technologies.	The fan-pad evaporative cooling system performs better than the air-cooling system.
Ataur Rahman (2014) [57]	Evaporative cooling	Electric Vehicle	Developed evaporative cooling-based BTMS performance compared to air-cooling-based BTMS performance.	BTMS based on evaporative cooling can save 17.69% more energy than BTMS based on air cooling.
Rao et al. (2011) [70]	PCM based cooling	*	Thermal conductivity between the PCM and the cell is explored in terms of thermal behaviour.	PCM with a melting temperature less than 45°C is more effective.
Yu et al. [71]	Natural and forced air cooling	EV	Charging/discharging process was compared using two cooling strategies, natural cooling and forced air cooling.	Forced air cooling with a flow velocity of 0.8 m/s is found to improve transient thermal properties at a high discharging rate (1C).
Fan et al. (2019) [72]	air cooling	EV	Battery performance was examined using aligned, staggered, and cross aligned battery configurations.	The aligned configuration offers the best cooling performance, whereas the cross layout offers the worst.
Wang et al. (2015) [73]	Paraffin/Al foam composite as PCM	EV	Compare the performance of the battery with only paraffin and with a Paraffin/Al foam composite as the PCM.	The presence of Al foam increases the melting of paraffin, resulting in greater temperature uniformity in the cells.
Darcovich et al. (2019) [74]	liquid cooling with cooling plate	EV	Compare the effectiveness of two types of pack liquid channel configure with cooling plates & ice plates in the EV battery pack.	Better cooling, highly complex system.

Statistical analysis

Literature & Year	BTMS Strategy	Type of application	Description	Critique outcome
Behi et.al. (2021) [75]	Evaporative cooling	*	The temperature of the cell/module is determined experimentally and numerically by the absence of natural convection, natural convection, forced convection, and evaporative cooling.	The evaporative cooling method decreased the maximum cell and module temperatures by 35.7% and 23.8% respectively.
Rui Zhao (2020) [76]	Evaporative cooling	*	Experiments were conducted on both single batteries and battery packs in cooling tunnels capable of producing both unidirectional and bidirectional air flows under the three cooling conditions of natural convection cooling, forced air cooling, and direct evaporative cooling.	The direct evaporative cooling equipped battery offers superior long-term performance, with less capacity loss than batteries cycled under baseline and air-cooling conditions.

2.4 Statistical analysis

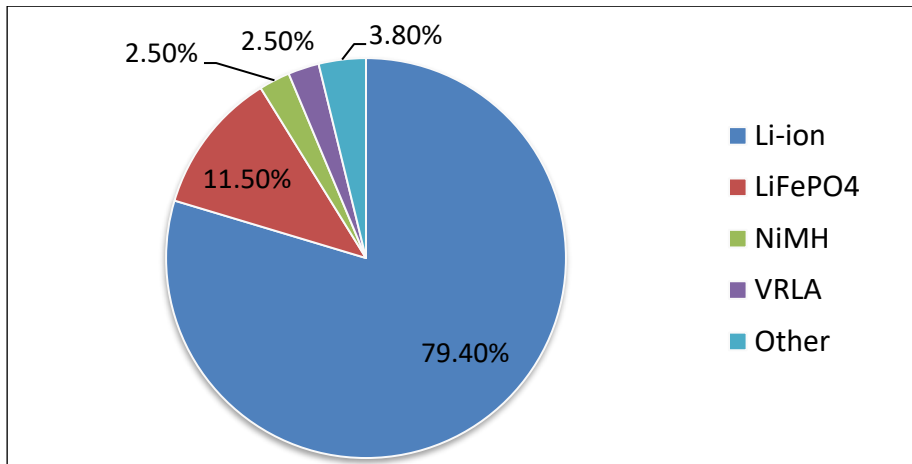
This literature review examines the impact of ambient temperature on valve-regulated lead acid (VRLA) batteries, compares various BTMS types, examines the current state of various thermal control strategies used in electric vehicles, and discusses the potential of a newly developed evaporative cooling based thermal management system for batteries. In previous studies, battery performance has been evaluated using a variety of methods, including an Artificial Neural Network (ANN), experimental study, and simulation software. In this section, we analyse current research efforts using statistical analysis and attempt to show the position of our study in relation to the relevant literature review. Over a ten-year period, 67 articles from Elsevier, Springer, Taylor & Francis, and other reputable journals were referred for the literature review.

Type of battery	Application	BTMS Strategy									
		Air cooling	Liquid cooling	Refrigeration	Evaporative	PCM	Heat pipe	Thermoelectric	Hydrogel	Other	Total
Li-ion	EV	[77] [78] [79] [80] [81] [82] [83]	[84] [85] [86] [87] [88] [89] [90]	[91]	[92]	[93] [94] [65]	[95] [68]	[96] [97]			23
	HEV	[98] [99] [100]	[101] [102]								5
	E-Bike		[103]	[104]		[105]					3
	Other	[106] [107] [108] [109] [110] [111] [112] [113]	[114] [63]		[76]	[115] [116] [117] [118] [60]	[119] [120]		[97], [121]	[122] [123] [124]	23
VRLA	EV										
	HEV										
	E-Bike										
	Other					[125] [126]					2
NiMH	EV										
	HEV		[127]								1
	E-Bike										
	Other		[128]								1
LiFePO ₄	EV						[129]				1
	HEV	[130]				[57]					2
	E-Bike										
	Other	[131] [132]				[133]	[134] [135] [64]				6
	Total	21	14	2	2	13	8	2	2	3	67

Figure 2.3 Article published with different battery technology

displays the total number of studies using various battery technologies that have been published. It was noted that more studies that included evaluations of the performance of Li-ion batteries were published. There is a fairly limited amount of published research available on the performance evaluation of VRLA batteries.

Statistical analysis



2.3 Article published with different battery technology

Batteries are used as a power source in various application like electric vehicles (EVs), Hybrid Electric Vehicles (HEVs), Electric bikes (E-bikes), Uninterruptible Power Supply (UPS), laptops etc. Figure 2.4 illustrate the classification of research articles based on various battery application. It was observed that batteries are more demanded in field of transportation. Electric Vehicle (EV) and Hybrid Electric Vehicle (HEV) are considering environmentally free transportation in the mid of rising oil prices and global climates due to greenhouse emissions.

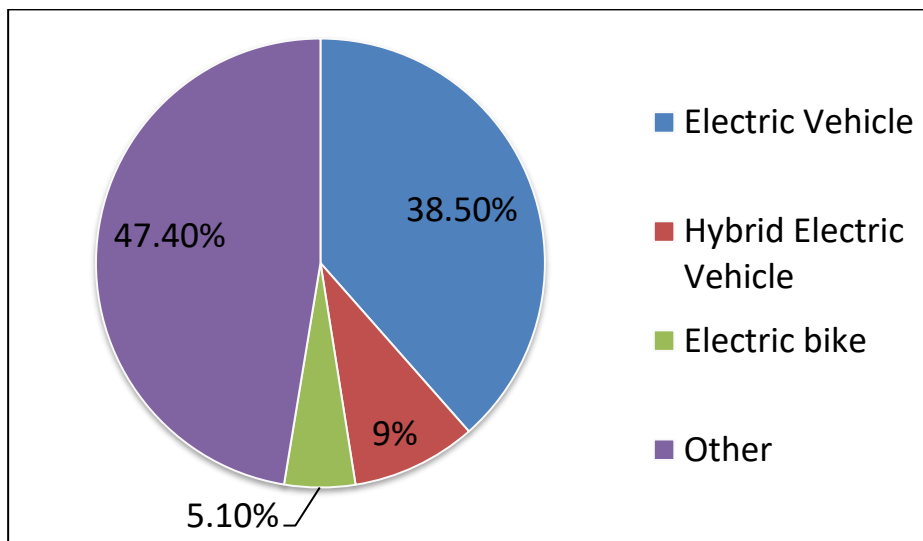


Figure 2.4 Articles published with different battery application

Figure 2.5 depicts the total number of publications published on battery thermal management systems employing various approaches. It was found that more research articles on battery thermal management systems employing air cooling have been published.

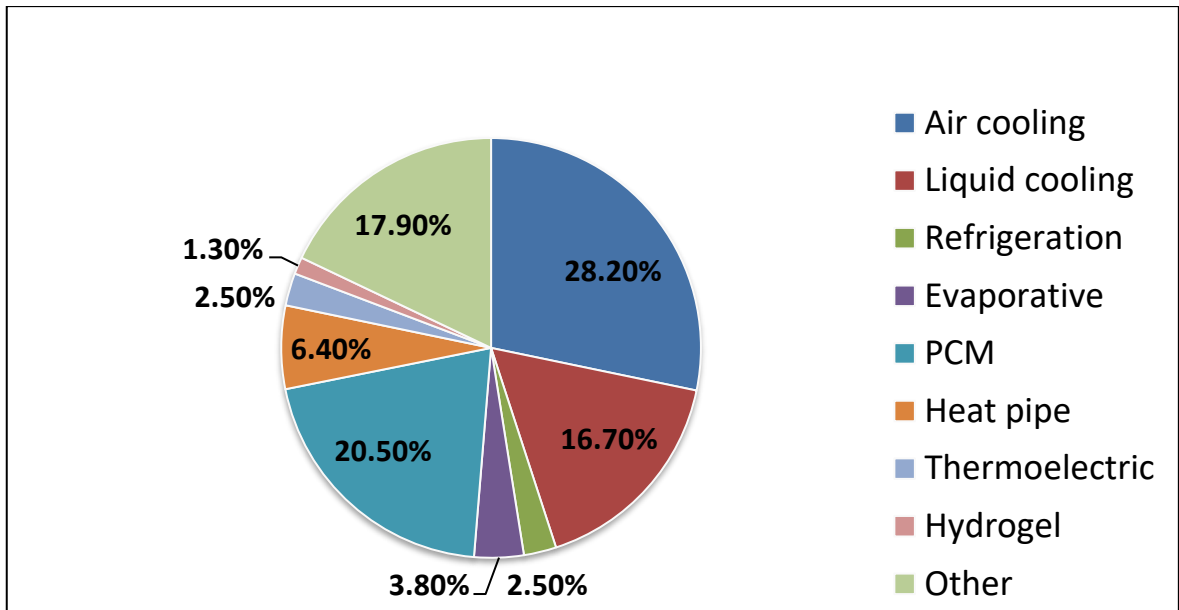


Figure 2.5 Article published with Various Battery Thermal management strategy

Figure 2.6 displays the total number of publications that will have been published between the years 2011 and 2021. It was found that more articles were published in 2014.

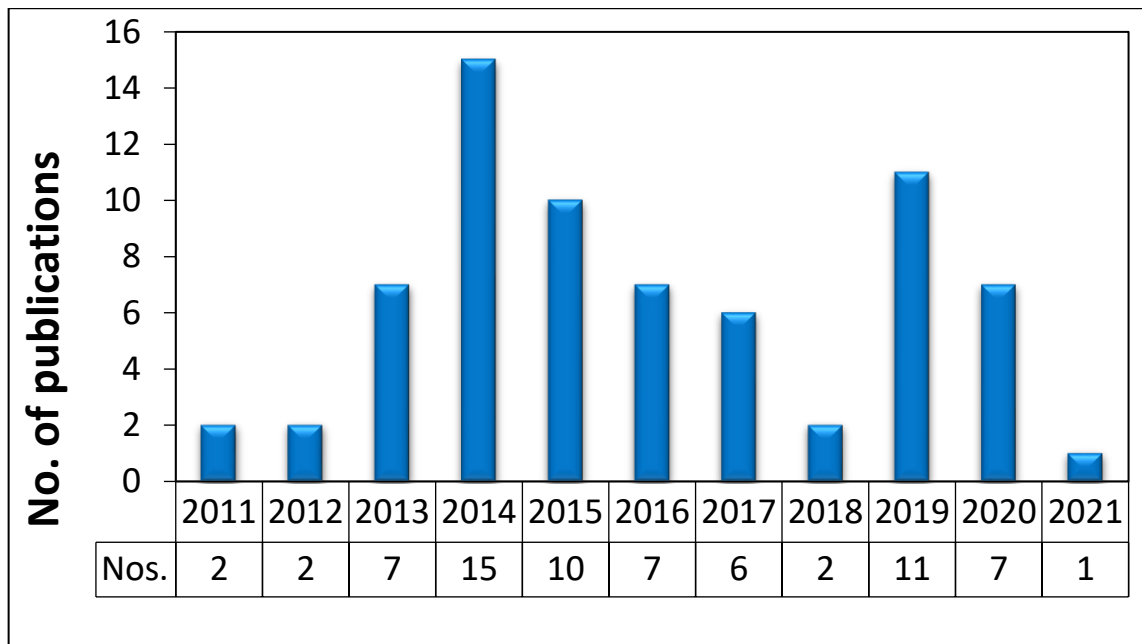


Figure 2.6 Nos. Of articles published from 2011-2021

Figure 2.7 depicts the county-level categorisation of published papers between 2011 and 2021. It noted that China published the most research publications. It was also observed that there was insufficient research on battery temperature management solutions in India.

Research gap

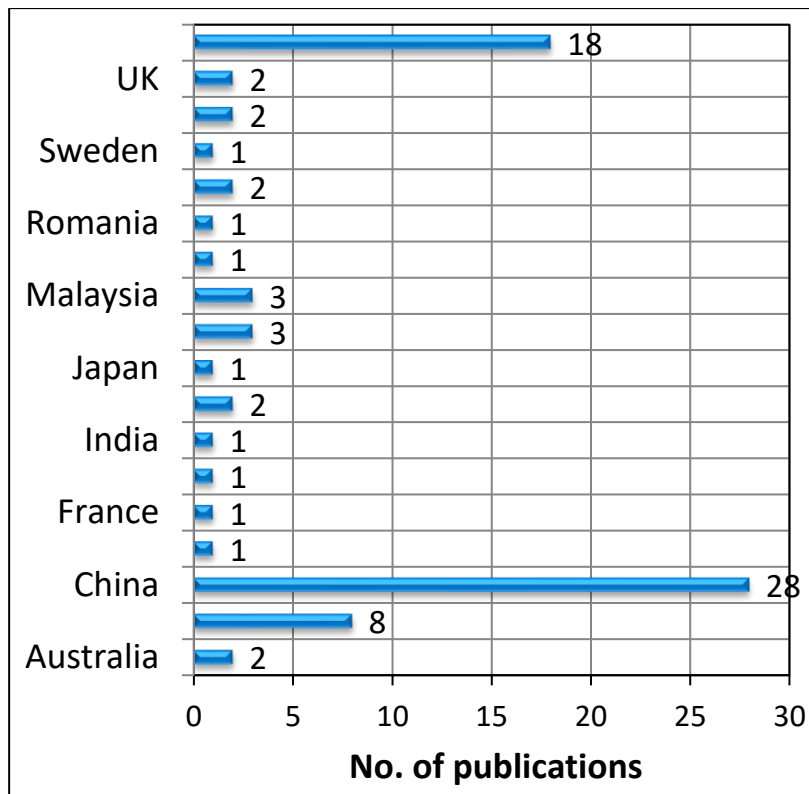


Figure 2.7 Country wise published articles

2.5 Research gap

The literature shows that temperature is a significant parameter that negatively impacts the performance and life of VRLA and Li-ion batteries. Major research was conducted on Li-ion batteries, which are extensively used in electric vehicles. Li-Ion batteries are more successful in electric vehicles in various countries, but due to their low cost, VRLA batteries are preferable in developing countries like India. Typically, the battery thermal management system has been implemented in electric vehicles (EVs) and Hybrid Electric Vehicles (HEVs) to reject the heat from a battery pack. There is no arrangement to reject the generated heat during the operation of the VRLA battery in an electric bike.

Air or liquid-based temperature management systems are often employed in electric car battery packs. Still, it has been noticed that a high amount of power is consumed by the air blower or pump during operation. Additionally, many researchers avoid to use the liquid-based thermal management systems due to the problem of leakage and corrosion. While the PCM-based thermal management technology is more effective than air or liquid-based thermal control. It has a problem with the PCM overheating during periods of excessive

battery heat generation. Thus, a PCM-based thermal management system is insufficient during periods of excessive heat generation.

Additionally, a thermal management system that is air-cooled, liquid-cooled, or based on a PCM cannot keep the battery temperature below ambient. Refrigeration or evaporative cooling are the only methods for lowering battery temperatures below ambient [10].

2.6 Problem definition

According to the literature review, the operational temperature significantly impacts the life and performance of VRLA batteries. Every 15°F (8.3°C) above 77°F (25°C) reduces battery life by half [28]. Thus, a more effective Battery Thermal Management System (BTMS) is necessary to control the temperature of the batteries within their optimal range while also protecting them from the impacts of seasonal climate variations.

2.7 Research objectives

Prime objective of the present research work is,

“To develop a battery thermal management system for valve-regulated lead-acid battery, which can maintain the battery temperature within the preferred temperature range, resulting in enhanced battery life and improvement in the battery performance”

Sub-objectives

1. Experimentally understanding the effect of temperature on performance of VRLA battery.
2. To identify the highest temperature reached in VRLA batteries during the adverse operating condition of E-bike.
3. To design & fabricate an evaporative cooling based battery thermal management system for the VRLA battery pack used in E-bike.
4. Experimentally evaluate the performance of VRLA battery with BTMS and compare it with a conventional battery pack.

2.8 Research Methodology

This research aims to develop a thermal management system for valve-regulated lead-acid batteries. Numerous techniques for designing a battery temperature management system are possible, depending on the sophistication and accessible data. Based on the knowledge gained from the literature study, the following systematic approach to developing BTMS is proposed,

1. Experimentally understanding the effect of temperature on VRLA battery.

- Development and experimentation of test setups to determine the effect of temperature on various performance parameters of a VRLA battery, including the charging - discharging process, battery capacity, internal resistance, self discharge rate, and gassing rate.

2. To Measure the actual operating temperature of VRLA battery in summer condition (most adverse condition) for E-bike during the working condition.

- To conduct a field test to determine the effect of real-world driving and climatic conditions on the thermal behaviour of VRLA batteries in an e-bike.
- To develop a transportable experiment setup that arranged within the available space of the E- bike.

3. Design & fabrication of Evaporative cooling based battery thermal management system.

- To determine the rate of heat generation by VRLA batteries in an E-bike based on the actual temperature reached during field testing.
- To determine the volumetric flow rate required to reject the heat. Additionally, choose the type of fan, cooling pad and other equipment for evaporative cooling-based BTMS.

4. Experimentally compare the performance of battery pack integrated with new BTMS & conventional battery pack.

- To conduct field tests to evaluate the performance of a VRLA battery pack integrated with a novel BTMS.
- Using the full factorial method, create sets of experimental trials with different assessment criteria. Also, analyze and validate the experimental results using Analysis of Variance (ANOVA).

CHAPTER 3. Thermal analysis of VRLA battery

3.1 Thermal analysis for heat generation from the VRLA battery

The VRLA battery is a type of electrochemical system. The heat effect is usually associated with the electrochemical reaction between electrodes in a battery. There are two heat-generating sources in VRLA batteries [136], [137]

(1) Heat generation due to reactions between active materials. [138]

(2) The joule effect causes by current flow through the battery.[138]

Summation of heat generation due to reaction and the Joule effect gives the total heat generated in cell or battery. [137]

$$Q_{total} = Q_{Rec.} + Q_{Joule} \quad \dots\dots (1)$$

VRLA battery is an electrochemical system. So, heat release during a chemical reaction is describe by the Gibbs Helmholtz equation, [136]

$$\Delta H = -T^2 \frac{d\Delta G}{dT} \quad \dots\dots (2)$$

Now, according to Michael faraday statement,

“The maximum amount of work that can be produce by electrochemical cell (W_{max}) is equal to product of the cell potential (E_{cell}) and total charge transferred during the reaction (q).” [139]

$$W_{max} = - q E_{cell}$$

$$W_{max} = - nF E_{cell} \quad \therefore q = nF$$

Here, n = No. of moles of Electrons

F = faraday Constant = 9.64855×10^4 C/mol. e^-

Work is expressed negative because it's done on surrounding.

The change in free energy (ΔG) is a measurement of maximum amount of work to be performed during chemical process. [139]

$$\text{So, } \Delta G = W_{max}$$

$$\Delta G = - nF E_{cell}$$

Thermal analysis for heat generation from the VRLA battery

Put the value of ΔG in eq. (2),

$$\Delta H = nFT^2 \frac{dE}{dT}$$

$$\frac{\Delta H}{nFT} = T \frac{dE}{dT}$$

$\frac{\Delta H}{nFT}$ is a heat generated due to charge transfer reaction.

Now, Heat generation due to chemical reaction (Q_{rev}) equal to the product of current flux and heat generated due to charge transfer reaction.

$$\text{So, } Q_{rev} = I \left[\frac{\Delta H}{nFT} \right]$$

$$\boxed{Q_{rev} = I \left[T \frac{dE}{dT} \right]} \quad \dots\dots (3)$$

Now, the rate of change in electric potential energy between a cell's positive and negative electrodes can be used to compute the heat produced by the Joule effect. Electric potential energy is the energy a charge possesses because of its position relative to another charge.

When charge moves from positive to negative electrode or negative to positive electrode that time change in electric potential energy (Δu) describe as,

$$(\Delta u) = \Delta Q \cdot \Delta V$$

Here, ΔQ = Quantity of charge transferred between positive and negative electrodes in cell.

ΔV = Potential difference between electrodes.

The heat generation rate due joule effect can be found by calculate the rate at which charge (ΔQ) loses the electric potential energy between electrodes [140].

$$\frac{du}{dt} = \frac{dQ}{dt} \Delta V$$

$$\frac{du}{dt} = I \Delta V \quad \left(\because \frac{dQ}{dt} = I \right)$$

The rate at which charge loses the electric potential energy is equal to the power (P) delivered to cell. ^[20]

$$\text{So, } P = I \Delta V$$

But $\Delta V = IR$ (Ohm's law)

$$P = I^2R$$

Also $Q_{joule} = I^2R$

We can say that $P = Q$ according to above equations,

$$P = Q_{joule} = I \Delta V \quad \dots\dots (4)$$

Now, Potential difference between electrodes (ΔV) is a difference of open circuit voltage (E) and cell voltage (V). So, $\Delta V = E - V$.

Put the value of ΔV in eq. (4),

$$Q_{joule} = I (E - V) \quad \dots\dots (5)$$

Put the value of eq. (3) and (5) in eq. (1),

$$Q_{total} = Q_{Rec.} + Q_{Joule}$$

$$Q_{total} = I \left[T \frac{dE}{dT} \right] + I (E - V) \quad \dots\dots (6)$$

The heat generation rate in a cell can be calculated from eq. (6). [51] [141] [142]

Where,

- Q_{total} = Heat generation rate (W/cell)
- I = Current (A); $I > 0$ for discharging and $I < 0$ for charging
- T = Cell temperature (K)
- dE/dT = Temperature coefficient (V/K)
- dE = Cell voltage difference
- dT = Temperature difference
- E = Open-circuit voltage of cell (V)
- V = Cell voltage (V)

3.2 Thermal analysis for heat dissipation through surface of battery

When the battery surface temperature rises above the ambient temperature, heat begins to escape from the battery. The battery's side walls effectively dissipate the heat created by the battery cell. Heat dissipated through side walls is directed through two obstacles [137],

- (i) The side walls itself
- (ii) The phase boundary between side walls and surrounding fluid.

Thermal analysis for heat dissipation through surface of battery

The heat flow through the container wall is determined by the thermal conductivity and wall thickness of the container material. The heat exchange between side walls and the environment occurs in several ways. The following Figure 3.1 depicts the numerous heat exchange processes.

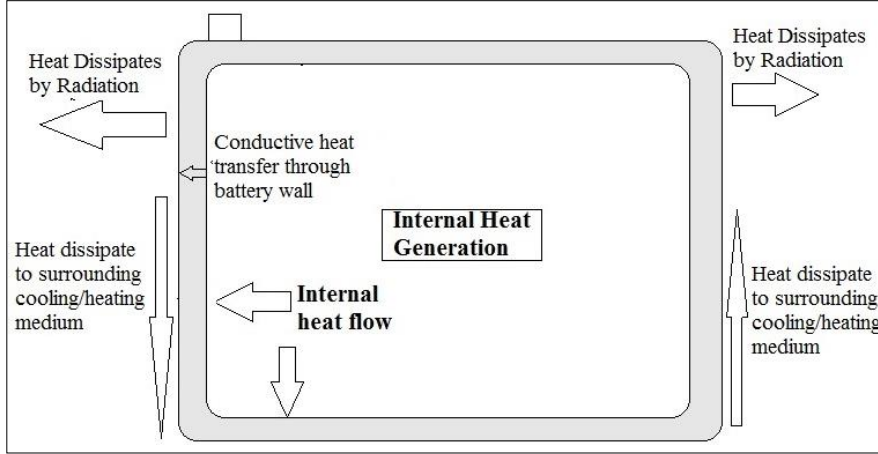


Figure 3.1 Various mechanisms of heat exchange

According to the first law of thermodynamics, the quantity of energy stored within the control volume is equal to the sum of the energy that enters the control volume, the energy that is produced within the battery cell, and the energy that leaves the control volume. So, an overall energy balance equation is [57].

$$Q_{st} = Q_{in} + Q_{gen} - Q_{out}$$

Now, assume that there is no heat transfer from cell to cell so $Q_{in} = 0$

$$Q_{st} = Q_{gen} - Q_{out} \quad (1)$$

Heat stored inside the battery is given by [143],

$$Q_{st} = M_b C_b \left[\frac{dT_b}{dt} \right]$$

Where,

M_b = Mass of battery module (kg.)

C_b = Specific heat of battery (J/kg.K)

dT_b = Average battery temperature (K)

There are mainly three mechanisms considered for Heat dissipate (Q_{out}) from container wall,^{[1][5]}

- (i) Conductive heat transfer within container wall.
- (ii) Heat carried by cooling or heating medium surrounding the container wall. (Convective heat transfer between container wall and fluid.)
- (iii) Heat loss by radiation.

So, Heat dissipates (Q_{out}) is a summation of conductive heat transfer (Q_{cond}), convective heat transfer between container wall and cooling or heating medium (Q_{conv}) and heat loss due to radiation (Q_{rad}).

$$Q_{out} = Q_{cond} + Q_{conv} + Q_{rad} \quad (2)$$

Heat transfer due to conduction through container wall

The battery cell is directly in contact with the container side walls and bottom surface. As a result, the majority of the heat created by the battery cell is released into the atmosphere via the side walls and bottom surface of the battery. There is no direct contact of upper surface with the battery cells, hence the upper surface is less critical for heat dissipation. The heat drop across the container wall is minor in comparison to the heat transmission between the container wall and the surrounding environment. The temperature distribution decreases from the interior of the battery to the surrounding [144].

$$T_{(interior)} > T_{(wall)} > T_{(surrounding)}$$

Heat flow through container wall can be determined by thermal conductivity of wall material and thickness of container. Conductive heat transfer is expressed as follow,

$$Q_{cond} = \frac{K A_s}{d} (T_i - T_a) \quad (3)$$

Here, K = Thermal conductivity of battery container material,

Container material = Acrylonitrile Butadiene Styrene (ABS)

Thermal conductivity of ABS (K) = 0.25 W/m·K

A_s = Surface area of container wall (W/m·K)

T_i = Average internal temperature of battery

T_s = Average surface temperature container wall

Heat dissipation by convection

Convective heat transfer occurs at the phase boundary between container surface and coolant fluid. The estimated calculation for convective heat transfer at a phase boundary with surrounding fluid depends on the thermodynamic parameters of the surrounding fluid. There are two distinct probable convective heat transfer modes.

(i) Natural convection

(ii) Forced convection

Thermal analysis for heat dissipation through surface of battery

Heat transfer due to natural convection

Natural convection of air at the phase boundary of the container wall is the most basic method of heat transmission. Natural cooling is sufficient under similar thermal circumstances with some battery thermal control approaches. Heat transfer to air by natural convection is normally determined by the temperature difference between the battery wall and the surrounding air, thermal conductivity, and the thickness of the battery container's wall. The heat transfer is calculated at the battery container's phase boundary with air. This heat exchange can be estimated using the Nusselt number (Nu), Grashof number (Gr), and Prandtl number (Pr), which are dependent on the temperature difference at the phase boundary and other characteristics such as surface area, thermal conductivity, and so on [145].

$$Q = \frac{A_s}{h} k Nu$$

Where,

A = Surface area (m²)

h = Height of battery (m)

K = Thermal conductivity (K)

Nu = C (Gr Pr)ⁿ

Convective heat transfer rate calculated for side walls of battery container.

$$Nu = C (Gr Pr)^n$$

$$Gr = \frac{\beta g L^3 \Delta T}{\nu^2}$$

Where,

Volumetric coefficient (β) = $\frac{1}{T_f + 273}$ K⁻¹ (Film temperature (T_f) = $\frac{T_s + T_a}{2}$)

Temperature difference between surface and air

$$\Delta T = T_s - T_a$$

ν = Kinematic viscosity of air

g = Standard gravity (9.81 m/s²)

Pr = Value of Prandtl number for air can be taken from data book

Now,

C = 0.56 & n = 0.25 for $10^4 < Gr Pr < 10^8$

C = 0.13 & n = 1/3 for $10^8 < Gr Pr < 10^{12}$

Heat transfer due to forced convection

VRLA batteries are utilised as a power source in a variety of applications, including solar PV and electric vehicles. Under operating conditions, these batteries produce heat. Occasionally, an external thermal control device is necessary to prevent the battery from becoming overheated. The most common method of forced cooling is forced air flow or circulation of liquid coolant. Convective heat transfer at phase boundary of container wall can be expressed by,

$$Q_{conv} = h A_s (T_s - T_a) \quad (4)$$

Heat dissipation by radiation

The part of the heat generation dissipates by radiation is expressed by using Stefan Boltzmann law. According to Stefan Boltzmann law,

$$Q_{rad} = \varepsilon \sigma T^4$$

Rate at which heat transported by radiation is proportional to fourth power of absolute temperature. Heat always flows from warmer body to colder body. So, radiative heat transfer between container wall and surrounding is given by,

$$Q_{rad} = \varepsilon \sigma (T_s^4 - T_a^4) \quad (5)$$

Where,

ε = emissivity of container material

σ = Stefan Boltzmann constant = $5.67 \times 10^{-8} \text{ W/m}^2\text{k}^4$

T_s = Surface temperature

T_a = Surrounding temperature

As previously stated, heat created in a battery is partially rejected to the surrounding environment and partially accumulated in the battery module. It is also feasible that if the surrounding temperature is higher than the temperature of the battery, heat will be transferred in reverse from the surrounding to the battery.

Now, put the value of eq. (3), (4) and (5) in eq. (2).

$$Q_{out} = Q_{cond} + Q_{conv} + Q_{rad}$$

$$Q_{out} = \left[\frac{K A_s}{d} (T_i - T_a) \right] + [h A_s (T_s - T_a)] + [\varepsilon \sigma (T_s^4 - T_a^4)] \quad (6)$$

Put the value of Q_{st} and Q_{out} in eq. (1),

$$Q_{gen} - Q_{st} = Q_{out}$$

Thermal analysis for heat dissipation through surface of battery

$$Q_{gen} - \left[M_b C_b \left(\frac{dT_b}{dt} \right) \right] = \left[\frac{K A_s}{d} (T_i - T_a) \right] + [h A_s (T_s - T_a)] + [\varepsilon \sigma (T_s^4 - T_a^4)] \quad (7)$$

Eq. (7) describes an overall energy balance equation for battery module.

Radiative heat transmission from the container surface is the fourth term. If the battery surface temperature is less than 100°C, radiative heat transmission is usually minor compared to convective heat transfer. Under normal operating circumstances, the surface temperature of a VRLA battery is less than 100°C. As a result, in the case of a VRLA battery, this term can be ignored [51].

$$Q_{gen} - \left[M_b C_b \left(\frac{dT_b}{dt} \right) \right] = \left[\frac{k A_s}{d} (T_i - T_a) \right] + [h A_s (T_s - T_a)] \quad (8)$$

Overall energy balance equation can be used for obtain the uniform temperature distribution in VRLA battery pack. If certain amount of fluid is circulating around the battery pack, change in fluid temperature can be obtained from,

$$[h A_s (T_s - T_a)] + \left[M_f C_f \left(\frac{dT_f}{dt} \right) \right]_{pack} = [m_f C_f (T_{out} - T_{in})]_{pack}$$

Second term in above equation $\left[M_f C_f \left(\frac{dT_f}{dt} \right) \right]_{pack}$ is shows the thermal inertia of the whole battery pack. This means the degree of slowness of surface temperature reaching to the surrounding temperature of circulating fluid can be expressed by that relation. To analyse the thermal behaviour of a battery pack, this term must be added to convective heat transfer. Where M_f is the mass of fluid in a battery pack and C_f is the fluid's specific heat. Rearrange the equation above,

$$[h A_s (T_s - T_a)] + = \left[m_f C_f (T_{out} - T_{in}) - M_f C_f \left(\frac{dT_f}{dt} \right) \right]_{pack} \quad (9)$$

Put the value of eq. (9) in eq. (8)

$$N \left[Q_{gen} - \left[M_b C_b \left(\frac{dT_b}{dt} \right) \right] \right] = \left[\frac{K A_s}{d} (T_i - T_a) \right] + \left[m_f C_f (T_{out} - T_{in}) - M_f C_f \left(\frac{dT_f}{dt} \right) \right]_{pack} \quad (10)$$

Equation (10) is an overall energy balance equation for the thermal behaviour of a VRLA battery when a certain volume of fluid surrounds the battery pack, where N is the number of batteries in the battery pack. Using the above equations and thermal method, one can compute the heat dissipation rate.

CHAPTER 4. Experimental Studies – 1: Effect of Temperature on Different Parameters of Battery Performance

4.1 Introduction

A battery is a chemical device that uses the thermoelectric chemistry concept to power itself. A chemical reaction happens between the positive and negative plates. Temperature is an important factor in any form of chemical reaction. According to the previous chapter's literature review, it should be demonstrated that temperature and heat generation influence the performance and life of a valve-regulated lead-acid battery. Temperatures that are relatively low or high affect the battery's performance and lifespan.

The first stage in building a battery thermal management system is to investigate the behaviour of VRLA batteries at various temperatures and determine the optimal temperature range for a battery. According to Indian climatic conditions, the battery is typically operated between 10 °C and 45 °C temperature throughout the year. So, in this experimental investigation, various experiments were performed at five different temperatures, namely 10 °C, 20 °C, 30 °C, 40 °C, and 45 °C. In this section, assess the battery's performance parameters at various temperatures.

- | | |
|----------------------------------|-------------------------------|
| (1) Battery capacity | (2) Charging-discharging time |
| (3) Rate of gassing from battery | (4) Internal resistance |
| (5) Self-discharging rate | |

4.2 Description of different experimental tests

The major goal of the experimental study is to identify the different performance parameters of batteries that are impacted by temperature, as well as the temperature range at which VRLA batteries function best and have the longest life span. Various performance factors, such as battery capacity, charging-discharging time, self-discharge rate, battery life, and internal resistance, are affected by operating temperature. Several tests provide information

Description of different experimental tests

regarding the effect of temperature on certain battery performance parameters. The battery chosen for the research has a capacity of 12V/7Ah. IS - 15549: 2005 (Indian standard for stationary valve-regulated lead-acid battery - specification) was used to design all of the experiments [27]. The VRLA battery performed seven performance tests to assess the effect of temperature on various parameters. The following is a description of each test:

Capacity Test

The batteries are rated in terms of voltage and capacity. The capacity [Ampere - Hour (Ah.)] of the VRLA battery was determined using this test. A prior study found that temperature had an effect on the rated capacity of the battery. The battery is discharged at a constant current in this test. C - rate was used to determine the discharging current. The capacity test was carried out at various temperatures, namely 10°C, 20°C, 30°C, 40°C, and 45°C, with a discharging rate of 1C. The battery is placed in a constant temperature water bath for this test. The temperature of the water in the bath is adjusted externally by a heater and cooler. During this test, battery capacity and discharge time at various temperatures were measured.

Charging test

The charging test demonstrates how temperature affects charging time. According to a review of the literature on VRLA batteries, charging time varied with temperature. Following that, the charging procedure involves forcing a charge in the form of direct current into the battery in the opposite direction. The chemical process during charging is the reverse of the process while discharging. Lead sulphate reacts with water in the electrolyte to produce metallic lead, hydrogen, and sulphate ions. After charging, sulfuric acid returns to its original chemical state. The rate of a chemical reaction between positive and negative plates is directly influenced by the ambient temperature and current rate. The charging time and behaviour are affected by temperature and charging current rate. So, a charging test needs to be done to find out how temperature affects the charging process.

In this experiment, the battery is charged at various temperatures using a 1A constant direct current supply. There are three types of charging methods: (1) constant voltage charging, (2) constant current charging, and (3) trickle charging. This experiment use the constant current charging approach. The constant current charging method charges the battery with a constant current until it is fully charged. The amount of charge that enters the battery while charging is referred to as the State of Charge (SOC). During the charging process, the battery voltage rises. The battery voltage increases during the charging process . In this experiment, as per

Experimental Studies – 1: Effect of Temperature on Different Parameters of Battery Performance

the manufacturer's specifications, 12V, 7Ah. The Chloride Exide Safepower (EXIDE) Valve Regulated Lead Acid (VRLA) battery is fully charged at 14.5 V. There is a Testronix DC power supply variable single output (92B) model used as a battery charger.

Measurement of gassing rate

This experiment is performed under the overcharging circumstance. In an overcharging state, hydrogen gas will be released through the gas vents of a VRLA battery. Normally, throughout the charging and discharging processes, as well as under typical circumstances, hydrogen and oxygen are produced on the negative and positive plates. They come back together and create water, which is then dissolved in H_2SO_4 . However, during overcharging, additional hydrogen accumulates in the gas phase, which increases pressure and is released by vents [146]. During operation, the oxygen produced at the positive plate travels to the negative plate via the AGM separator, where it subsequently reacts chemically to produce the water. At higher temperatures, the temperature has an impact on the oxygen cycle's effectiveness. High hydrogen production lowers the oxygen cycle's effectiveness [147].

This experiment examines the gassing of the battery during overcharging at various temperatures. During the overcharged condition, an electric charge enters the battery at a low current (5% of battery capacity, i.e. 0.3A). Otherwise, there is a risk of VRLA battery thermal runaway during the experiment. This experiment is hazardous to the battery because more overcharging has the potential to damage it. Thus, safety is more important during this investigation. During the investigation, the battery is overcharged with a low current and the gassing from the battery is measured.

Self discharging test

Self-discharge is the energy loss of a battery caused by an internal chemical reaction when it is disconnected from an external circuit. The rate of self-discharge depends on the chemistry and temperature of the cell. The rate of a chemical reaction is temperature-dependent. The rate of chemical reactions goes up with temperature, so the rate of self-discharge also goes up with temperature.

A VRLA battery's self-discharge rate at room temperature (25°C) is typically between 4 and 6 percent per month. A high rate of self-discharge reduces the battery's storage life. also known as "shelf life." Thus, the rate of self-discharge should be as low as possible. This test determines the self-discharge rate at different temperatures. In this test, the battery is placed

Experimental setups and procedures for various test

in a water bath at a constant temperature for up to 28 days to determine the rate of self-discharge.

Internal resistance test

Internal resistance is the total resistance within the battery. Internal resistance might change depending on the outside temperature. This test determines the internal resistance of the VRLA battery at various temperatures. An internal resistance meter can be used to measure the battery's internal resistance.

4.3 Experimental setups and procedures for various test

IS - 15549: 2005 (Indian standard for stationary valve-regulated lead-acid battery-specification). Each battery test requires a particular test process and instrumentation. Thus, the individual setup has been built to run various tests.

4.3.1 Capacity Test

The Figure 4.1 illustrates the schematic diagram of the experimental setup for the capacity test. The capacity test was carried out at various temperatures, namely 10°C, 20°C, 30°C, 40°C, and 45°C, with a discharging rate of 1C. 12V, 7Ah. The VRLA battery was placed in the water bath. Inside the water bath are other components such as the water heater, motorised stirrer, and temperature sensors. The temperature inside the water bath is controlled by the temperature controller. A temperature controller is a device that regulates the temperature of a water heater by turning it on and off. To keep the temperature constant around the battery, the motorised stirrer continuously stirs the water inside the water bath. The battery eliminator provides the necessary DC power source to drive the stirrer. The stirrer's spinning speed can be adjusted by adjusting the supplied voltage in the battery eliminator.

As a Data Acquisition System (DAQ), a KH-208 paperless data recorder is provided, which measures the value and logs it with a computer in data analysis software. DAQ is made up of sensors, measuring devices, and a computer that runs data analysis software. The data recorder includes 8 channels. Temperature sensors, voltage measurement pins, and current measurement pins are linked to the various channels in the data recorder. Each channel measures a different quantity.

Experimental Studies – 1: Effect of Temperature on Different Parameters of Battery Performance

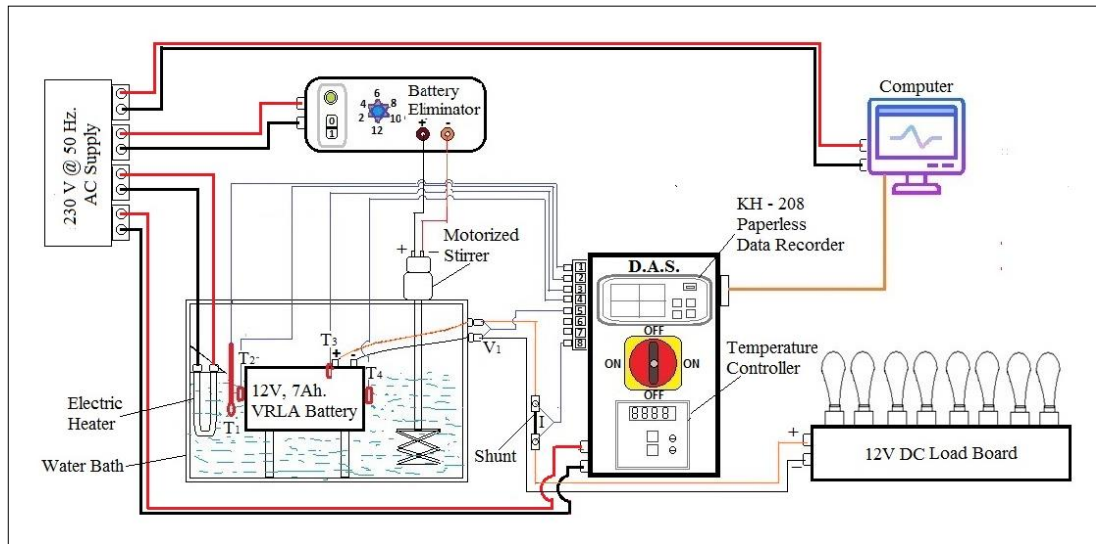


Figure 4.1 Schematic diagram of capacity test experimental setup

Ch. – 1	Water temperature (T_1)	Ch. – 5	Battery voltage (V)
Ch. – 2	Battery surface temperature (T_2)	Ch. – 6	-
Ch. – 3	Battery internal temperature (T_3)	Ch. – 7	-
Ch. – 4	Battery surface temperature (T_4)	Ch. – 8	Battery current (A)

The ATC-820 Interface converter (RS-485) is used to transport data from the data recorder to the computer. As illustrated in figure, a 12V DC load board is used to discharge the battery at a preset current. The load board is made up of eight 12V DC bulbs of varying capacity. The image of detailed components of experimental setup for capacity test is shown in Figure 4.2. The figure shows the connection between all the components in experimental setup.

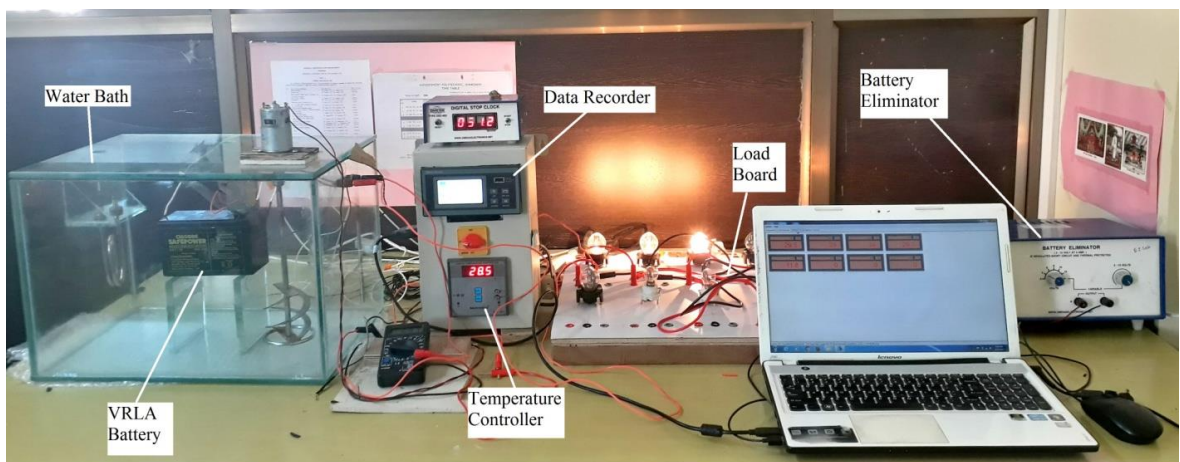


Figure 4.2 Experimental Setup for capacity test

Experimental setups and procedures for various test

Test Procedure

1. First place the 12V, 7Ah. VRLA battery inside the water bath. Than hold the battery until temperature of the battery is maintain as per requirement (minimum 2 hours).
2. Now battery is connected properly with the other equipment, also check status of other equipment before starting the experiment.
3. Record the initial temperature of the battery, initial voltage and starting time of the experiment.
4. Start the stop watch and turn the load board switch ON.
5. Measure the battery voltage, discharging current, water temperature, battery surface temperature and battery internal temperature at interval of 1 min. until OCV reach up to 9.6 V.
6. Turn the load board switch OFF; when voltmeter indicate the 9.6 V.
7. At last, record battery voltage, final discharge current and final temperature of battery.
8. Calculate the capacity:

$$\text{Capacity} = \text{final time duration (in hours)} \times \text{final discharge current.}$$

4.3.2 Charging test

The Figure 4.3 shows a schematic diagram of an experimental setup for the charging test. This experimental setup is set up to conduct charging tests on a 12V, 7Ah VRLA battery at various temperatures. The experimental setup is extremely similar to the last experimental arrangement. The only difference is that the load board has been replaced with a constant current charger. As a constant current charger, the testronix DC power supply is used. The output voltages and currents of this device are continually adjustable via coarse and fine knobs on the front control panel. The set value and measured value of voltage and current are displayed on the front panel of the constant current charger in a seven-segment display.

Experimental Studies – 1: Effect of Temperature on Different Parameters of Battery Performance

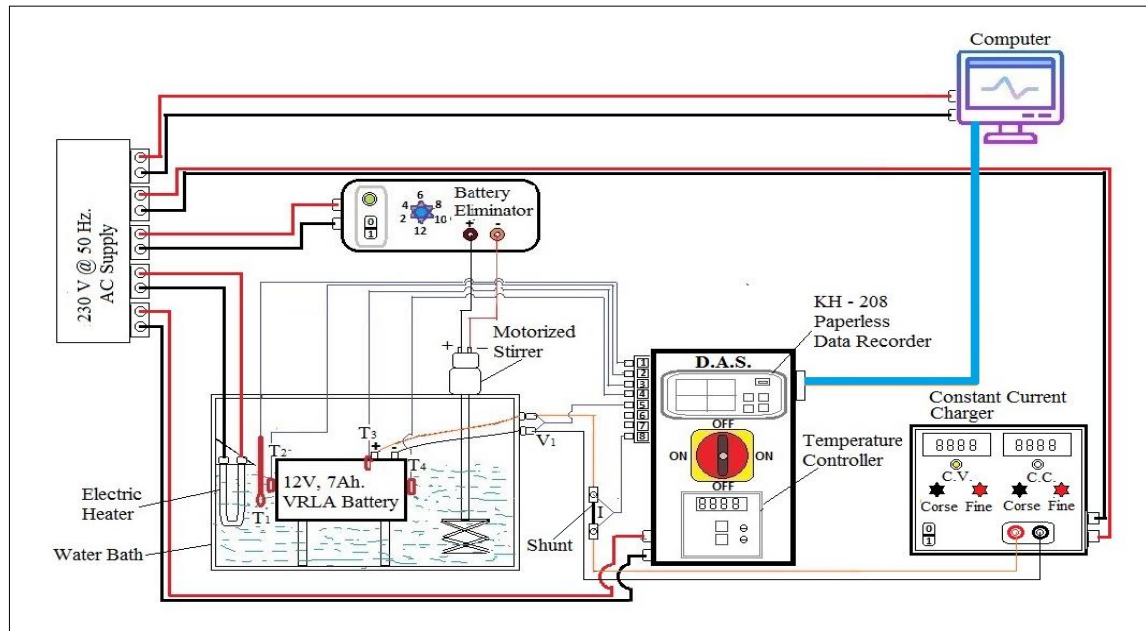


Figure 4.3 Schematic diagram of charging test experimental setup

Temperature sensors, voltage and current measurement probes are all linked to the data recorder. Every ten minutes, the data recorder records the measured value. Other component connections are the same as in the prior experimental arrangement. The Figure 4.4 illustrates the detailed features of the experimental setup for the charging test. The diagram shows the connection between all of the components in the experimental setup.

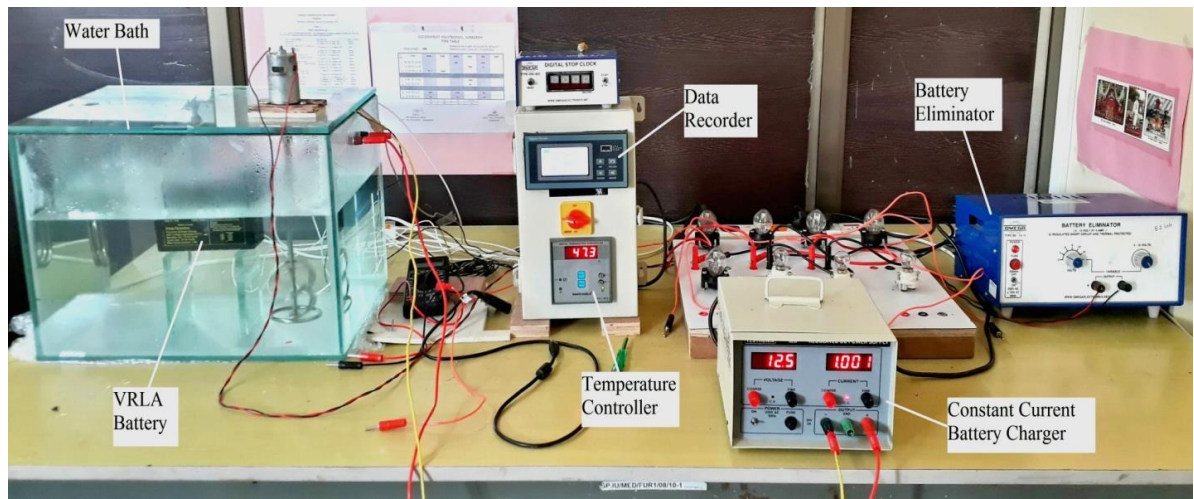


Figure 4.4 Experimental Setup for charging test

Test Procedure

First place the VRLA battery inside the water bath. Then hold the battery until temperature of the battery is maintained as per requirement (minimum 2 hours).

Experimental setups and procedures for various test

1. Now connect battery properly with the constant current battery charger and other equipment. Also check the external power supply to charging unit (230 V@ 50 Hz.)
2. Set the charging current = 1A in constant current battery charger.
3. Record the initial temperature of the battery, initial voltage and starting time of the experiment.
4. Start the digital stop clock and turn the charging unit switch ON.
5. Record the battery voltage, charging current and battery temperature at every interval of an 10 minutes until battery voltage reaches 14.5 V.
6. Turn the Charging unit switch OFF; when voltmeter indicates the 14.5 V.
7. At last, record the battery voltage and final temperature of battery.

4.3.3 Measurement of gassing rate

The Figure 4.5 is a schematic design of an experimental setup for the gassing test. This experimental setup is set up to measure gassing from a 12V, 7Ah VRLA battery under overcharged conditions at various temperatures. The experimental setup is nearly identical to the last experimental arrangement. A constant current battery charger is linked to a VLRA battery to overcharge the battery. Throughout the experiment, the VRLA battery is charged with a steady current of 0.5A. Voltage is one sort of electric pressure; hence, a reduced electric current also results in a lower charging voltage.

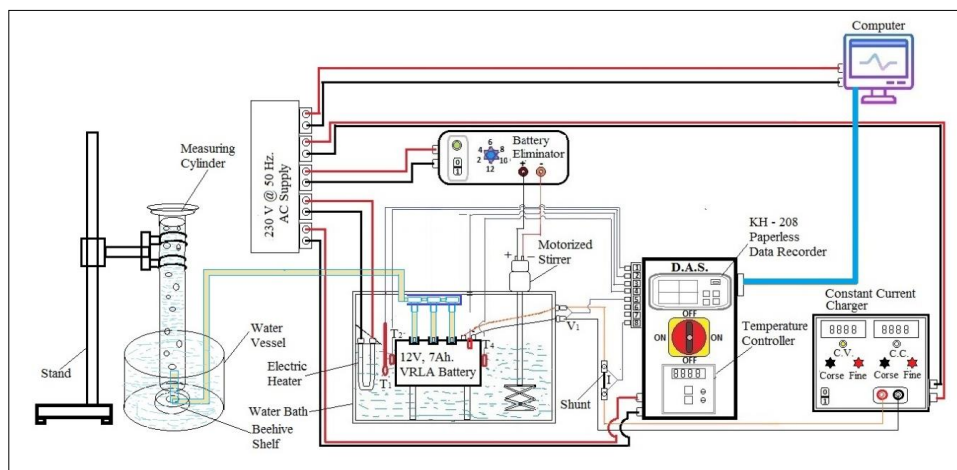


Figure 4.5 Schematic diagram of experimental setup for measurement of gassing

The Figure 4.6 represents the detailed components of an experimental setup for the gassing test. The diagram shows the connection between all of the elements in an experimental setup. The VRLA battery is inserted into the water bath. The water bath is used to keep the battery at the appropriate temperature. The temperature controller maintains the predetermined

Experimental Studies – 1: Effect of Temperature on Different Parameters of Battery Performance

temperature of the water at all times. Other component connections are the same as in the prior experimental arrangement.

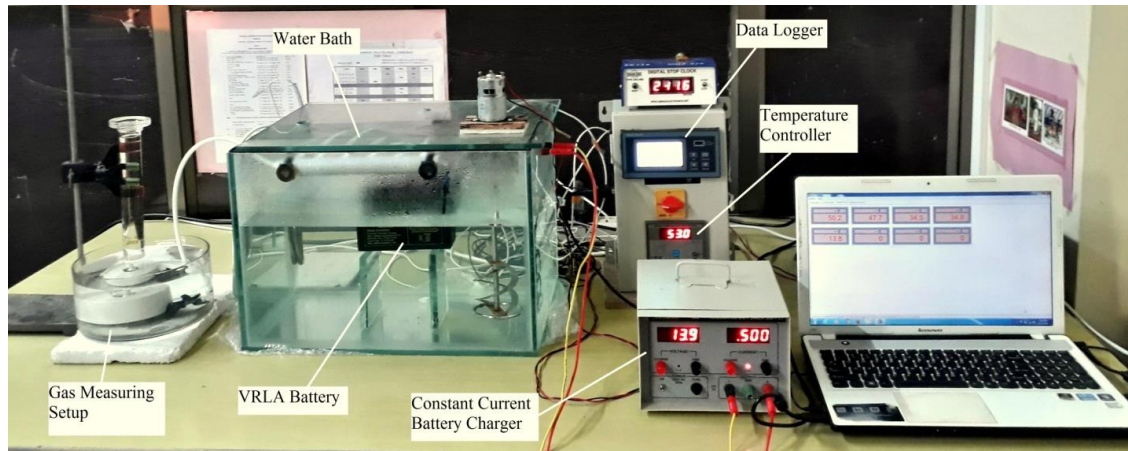


Figure 4.6 Experimental setup for measurement of gassing at different temperatures

On top of the battery, there are gassing vents. During the overcharged condition, hydrogen gas is emitted from the gassing outlet. To collect the hydrogen gas, a separate gas measuring apparatus is externally attached to the battery (as shown in Figure 4.7) Through connection tubes, gas released from the battery is delivered to the gas measuring equipment. The tubes are connected to the gassing vent through flexible connections. There are six vents provided on the top of battery. The tubes are connected between vents and the central tube through T – type air tight joints. All the connections of tubes are leakage-proof. Another end of the central tube is connected with a gas measuring cylinder in the gas measuring setup. The gas measuring setup consists of a gas measuring cylinder, water vessel, beehive shelf and stand.

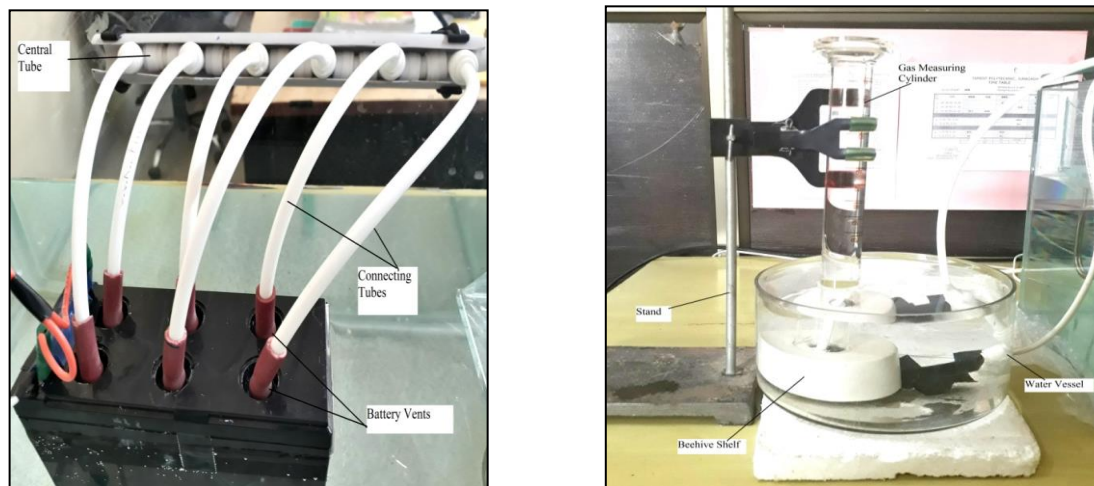


Figure 4.7 (a)Collecting of gas from battery through vents

(b) Gas measuring setup

A gas measuring cylinder is utilised to collect the gas released by an overcharged battery. The collected gas within the measuring cylinder is measured using a scale set on the measuring cylinder's surface. The calibration of the measuring scale is in millilitres.

Experimental setups and procedures for various test

Test Procedure

1. First place the fully charged VRLA battery inside the water bath. Then hold the battery until temperature of the battery is maintained as per requirement (minimum 2 hours).
2. Now connect battery with the constant current battery charger and other equipment. Also check the external power supply to charging unit (230 V @ 50 Hz.)
3. Set the charging current = 0.5A in constant current battery charger.
4. Record the initial temp. of the battery, voltage and starting time of the experiment.
5. Start the digital stop clock and turn the charging unit switch ON.
6. Record the battery voltage, charging current and battery temperature at every interval of an 1 minute until battery voltage reaches 14.5 V.
7. Turn the Charging unit switch OFF; when voltmeter indicates the 14.5 V.
8. At last, record the battery voltage and final temperature of battery.

4.3.4 Self discharging test

The Figure 4.8 is showing a schematic diagram of an experimental setup for the self-discharge test. This experimental setup is built up to determine the self-discharge rate of a 12V, 7Ah VRLA battery at various temperatures. The self-discharge test was carried out at three distinct temperatures: 20°C, 30°C, and 40°C. The experimental configuration is nearly identical to the last experimental arrangement. The experiment includes three distinct water baths. Each water bath is kept at different battery temperatures (20°C, 30°C, and 40 °C). Each water bath has one battery placed inside it.

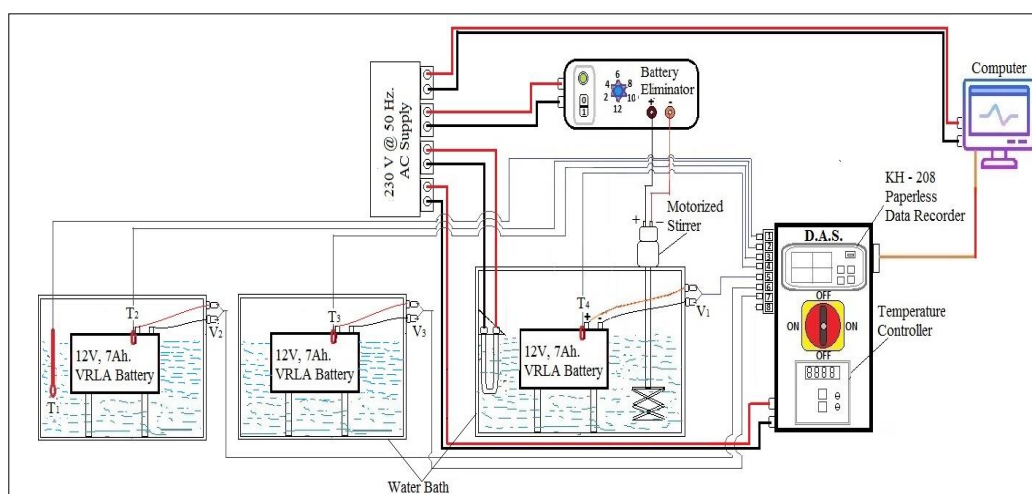


Figure 4.8 Schematic diagram of experimental setup for self discharge test

The Figure 4.9 below shows the detailed components of an experimental setup for the self-discharge test. The diagram displays the connection between all of the elements in an

Experimental Studies – 1: Effect of Temperature on Different Parameters of Battery Performance

experimental setup. Inside the various water baths are three separate VRLA batteries. The first water bath was used to keep the VRLA battery at a low temperature (20°C). Chilled water is used to keep the battery inside the water bath at a low temperature. The auto-controlled water cooler chills the water. The temperature controller is installed in a water cooler, which keeps the water at the desired temperature all of the time. The VRLA battery's temperature is kept at 30°C by a second water bath. An aquarium heater maintains the required temperature within the water bath. The aquarium heater's temperature controller keeps the water at the desired temperature. A third water bath maintains the water's temperature inside the water bath at 40°C. An external U-shaped 1000W, AC powered water heater is used to maintain the proper temperature inside the water bath. The temperature controller regulates the water temperature. The temperature controller is connected to the water heater through an external connection.

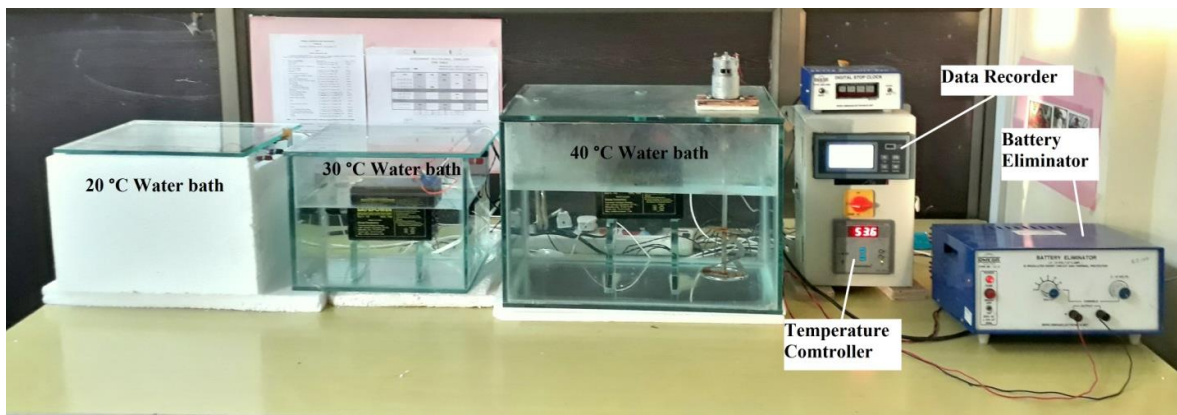


Figure 4.9 Experimental setup for measurement for self discharge test

Test Procedure

1. Perform the C1 capacity test for VRLA battery at 20 °C, 30°C and 40 °C temperature and note down the capacity (C).
2. Store the battery at 20 °C, 30°C and 40 °C (constant temp.) for 28 days.
3. Record the battery voltage and battery temperature at an interval of 24 hours.
4. Again Perform the C1 capacity test for battery at 20 °C, 30°C and 40 °C temperature after 28 days. Note down the capacity (C1)
5. Calculate self discharge rate = $\frac{C-C1}{C} \times 100$

Results and discussions

4.4 Results and discussions

4.4.1 Comparison of discharging time in 1C – capacity tests with different temperatures

Temperature (°C)	10	20	30	40	45
Discharging Time (sec.)	1260	1752	1872	2064	2502

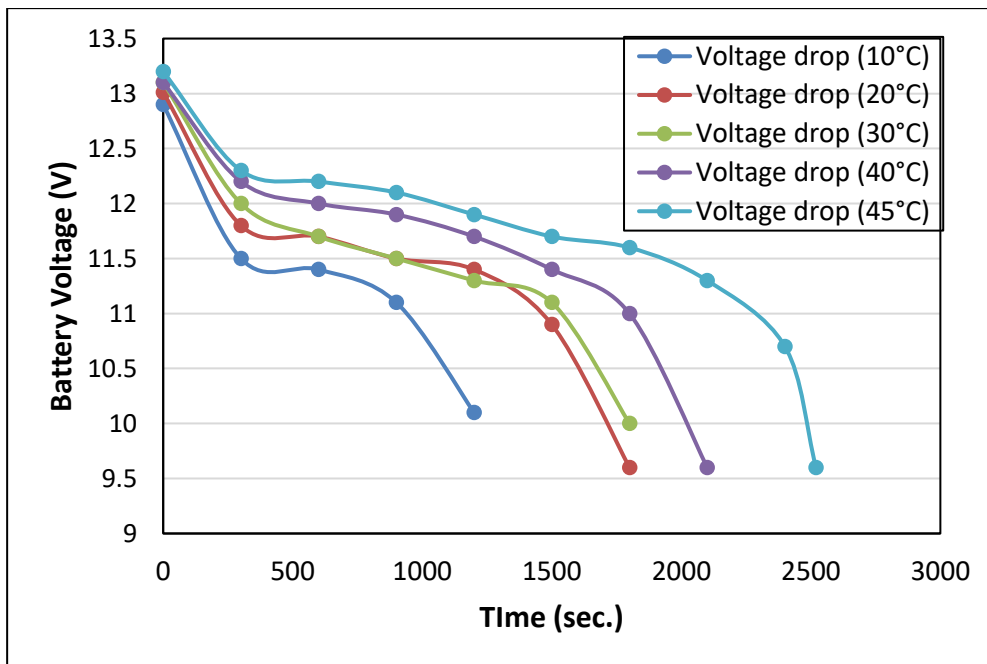


Figure 4.10 Comparison of discharging time in 1C capacity tests

Observation

The graphical study compares discharge periods and voltage drop behaviour during the 1C capacity test at various temperatures. The lowest discharging time was recorded with a 1C capacity test at 10°C and the highest discharging time was recorded with a 1C capacity test at 45°C. It is evident that when battery temperature rises, discharging time increases.

The voltage drop results indicate that it is more uniform at higher temperatures. The rate of chemical reactions increased as the temperature rises. Consequently, voltage drop is steadier at higher temperatures. Extreme temperatures accelerate the rate of acid evaporation from a battery, which reduces its lifespan. Compared to high temperatures, the voltage decreases quickly at low temperatures. Because of the low internal resistance at low temperatures, the rate of a chemical reaction is slower. As a result, the battery performs quietly at low temperatures.

Experimental Studies – 1: Effect of Temperature on Different Parameters of Battery Performance

4.4.2 Comparison of battery capacities with different temperatures

Temperature (°C)	10	20	30	40	45
Capacity (Ah.)	2.45	3.40	3.64	4.01	4.86

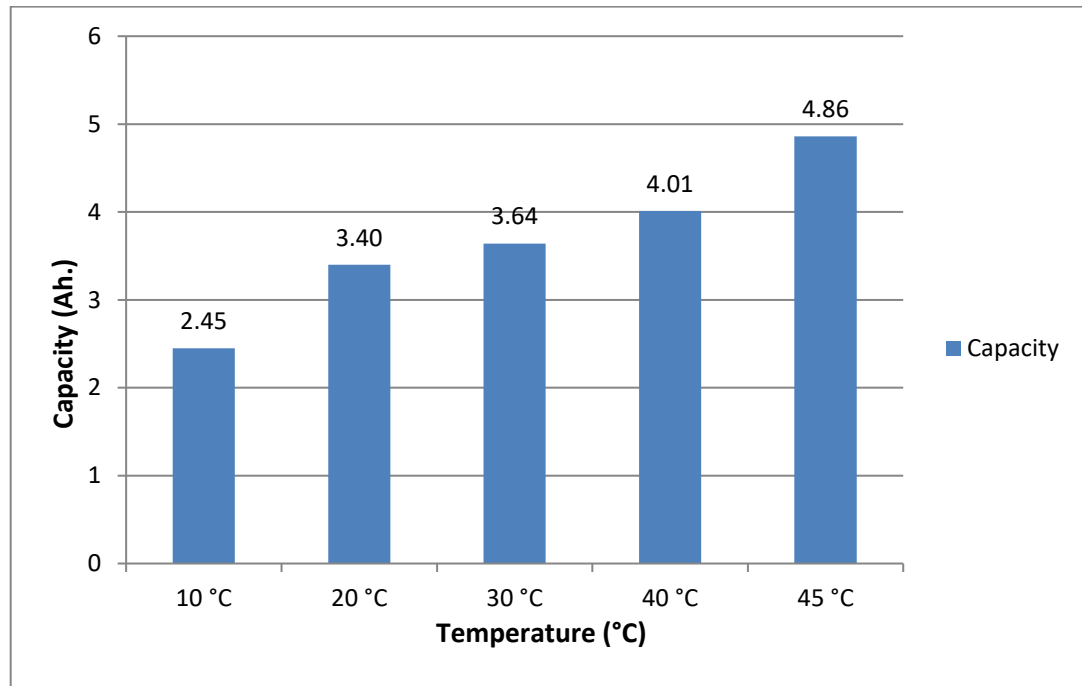


Figure 4.11 Comparison of battery capacity with different temperatures

Observation

It was noticed in Figure 4.11 that battery capacity increases as temperature rises. At 45°C, the highest capacity of the battery was seen. According to manufacturer data, the rated battery capacity for a VRLA battery tested using a 1C capacity test under the stated climatic conditions is approximately 4 Ah. It was observed that the battery had a capacity of 4.01 Ah at 40°C, which is close to the manufacturer's rated capacity. However, at higher temperatures, the rate of acid evaporation from the battery increases, resulting in a shorter battery life.

Results and discussions

4.4.3 Comparison of charging process in charging tests with different temperatures

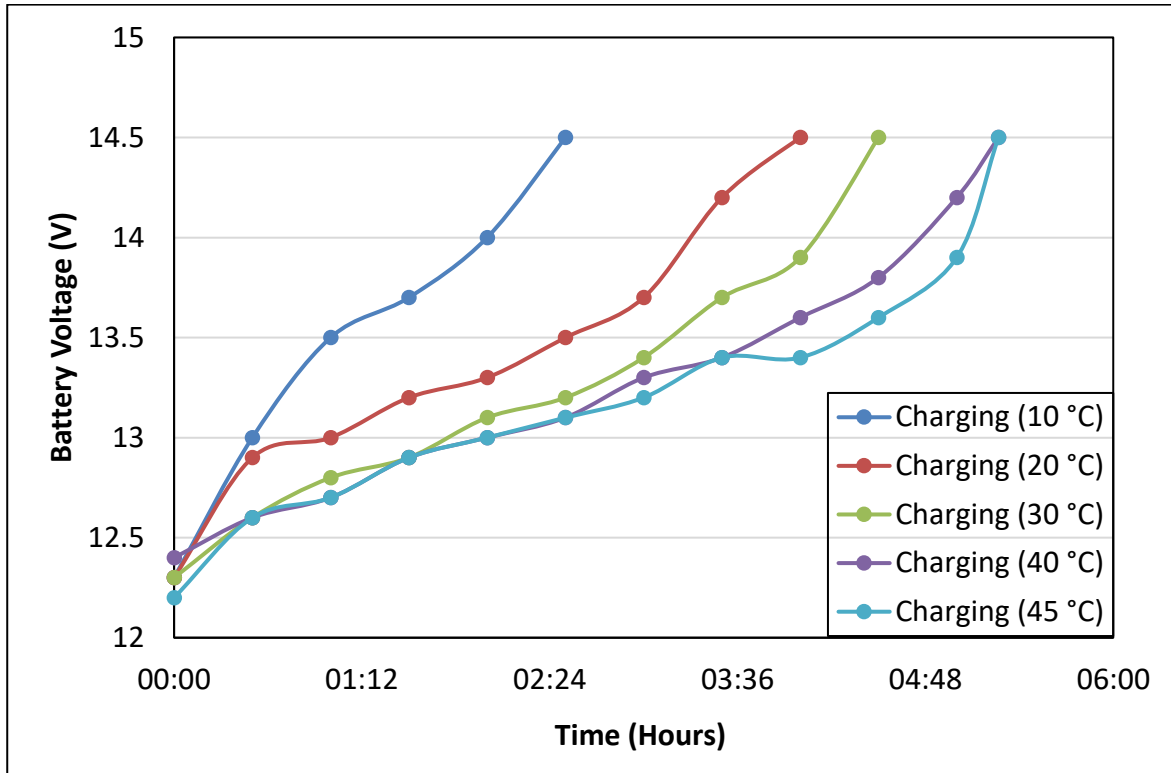


Figure 4.12 Comparison of charging process with different temperatures

Observation

The graphical analysis in Figure 4.12 shows the comparison of the charging process at various temperatures. The maximum limit of the battery voltage is set at 14.5V according to manufacturer's guidelines. The battery voltage increases during the charging process and it is fully charged when it achieves 14.5. In graphical analysis, it's observed that charging time increases with temperature increases. The battery is fully charged within 2 hours and 24 minutes at 10°C temperature, whereas the battery is fully charged in 5 hours and 20 minutes at 45°C temperature. It's clearly shown that lowest charging time was observed in the charging test at 10°C temperature and the highest charging time was observed in the charging test at 45°C temperature.

Experimental Studies – 1: Effect of Temperature on Different Parameters of Battery Performance

(1) Comparison of charging time with different temperatures

Temperature (°C)	10	20	30	40	45
Charging Time (Hours)	2:24	3:56	4:50	5:16	5:20

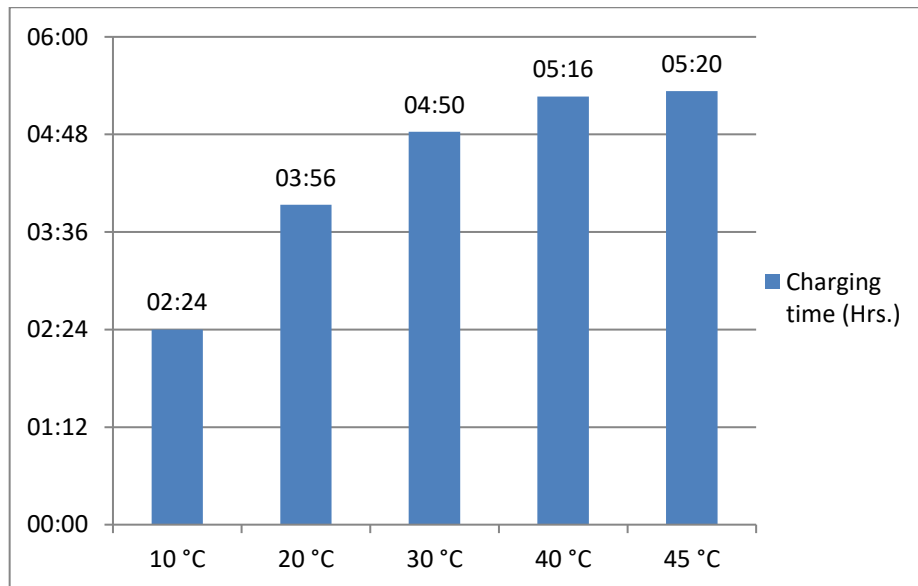


Figure 4.13 Comparison of charging time with different temperatures

Observation

The graphical analysis compares the charging process at different temperatures (Shown in Figure 4.13). According to the manufacturer's recommendations, the battery is fully charged when it exceeds 14.5V. The battery voltage rises during charging, and it is fully charged when it reaches 14.5. A graphical analysis shows that charging time increases as the surrounding temperature rises. At 10°C, it takes 2 hours and 24 minutes to fully charge the battery; at 45°C, it takes 5 hours and 20 minutes. Charging at lower temperatures needed the least amount of time, whereas charging at higher temperatures required the most time. Due to greater internal resistance at low temperatures, the charging time is accelerated. Due to increased internal resistance, the rate of a chemical reaction slows down at low temperatures. At lower temperatures, the battery is not completely discharged or charged, hence charging and discharging times are shortened. At higher temperatures, the charging time is seen to be longer. At higher temperatures, the internal resistance is too low, so the chemical reaction rate is faster. As a result, charging and discharging times are longer at higher temperatures.

Results and discussions

4.4.4 Comparison of gassing at different temperature

Temperature (°C)	10	20	30	40	45
amount of gas released (ml.)	1.4	5	12.5	15.2	29

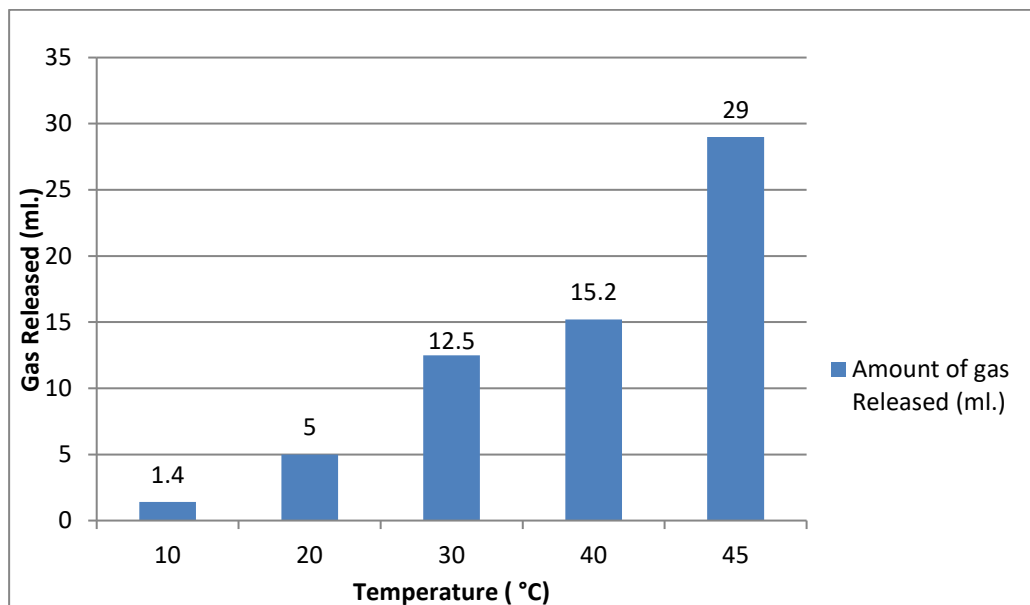


Figure 4.14 Comparison of amount of gas released from battery at different temperatures

Observation

This test determines the amount of gas released from the battery during overcharging. The gassing test is carried out at a variety of temperatures (10°C, 20°C, 30°C, 40°C, and 45°C). The plots above in Figure 4.14 compare gas emission from the battery at various temperatures during overcharging conditions. It was discovered that the least amount of gas was released from a battery during a gassing test at 10°C and the highest amount of gas was released during a gassing test at 45 °C. As the temperature rises, so does the rate of gas emissions. Consequently, the rate of gas emission increases as the temperature rises.

There are two primary causes for the increased rate of gas release at elevated temperatures. A higher temperature accelerates the rate of a chemical reaction between positive and negative electrodes, which increases the rate of gassing under overcharged conditions. In addition, electrolytes begin to evaporate at higher temperatures, resulting in an excessive gassing rate at higher temperatures. Due to the increased gassing rate, battery cells gradually become dry.

Experimental Studies – 1: Effect of Temperature on Different Parameters of Battery Performance

4.4.5 Self-discharge test

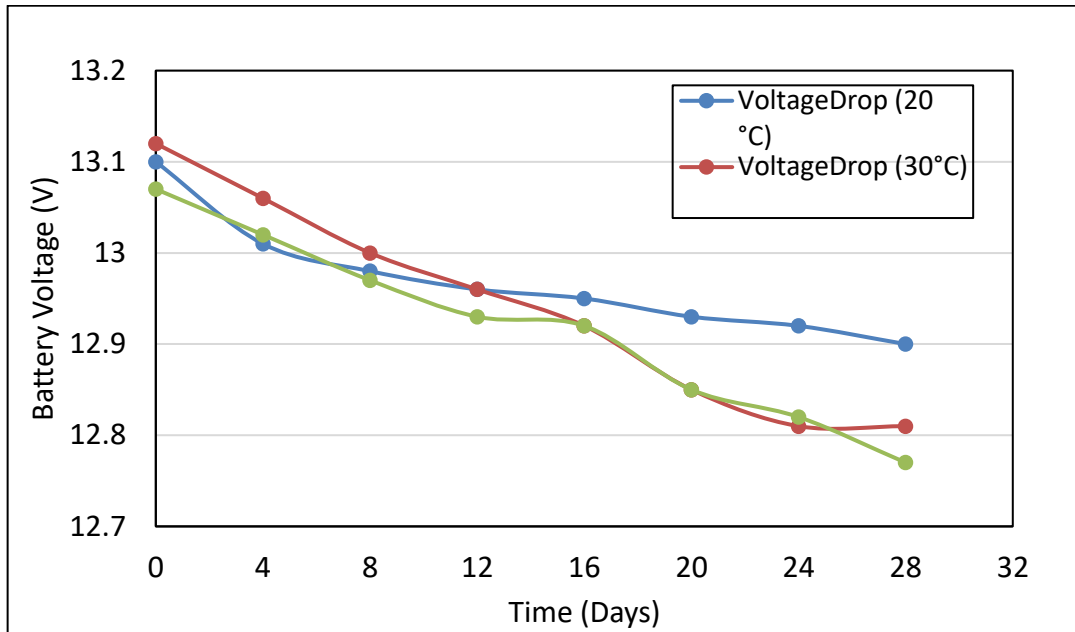


Figure 4.15 Comparison of voltage drop with different temperature

The graph as shown in Figure 4.15 examines the battery voltage loss over 28 days at three different temperatures. The lowest voltage drop is seen during the self-discharge test at 20°C, while the greatest voltage loss is observed at 40°C. It has been noticed that a higher battery temperature results in a greater voltage drop. The battery's response to voltage loss at 30°C and 40°C temperatures is fairly similar. A larger voltage drop gap was noticed between self-discharge tests performed at 20°C and 30°C temperatures.

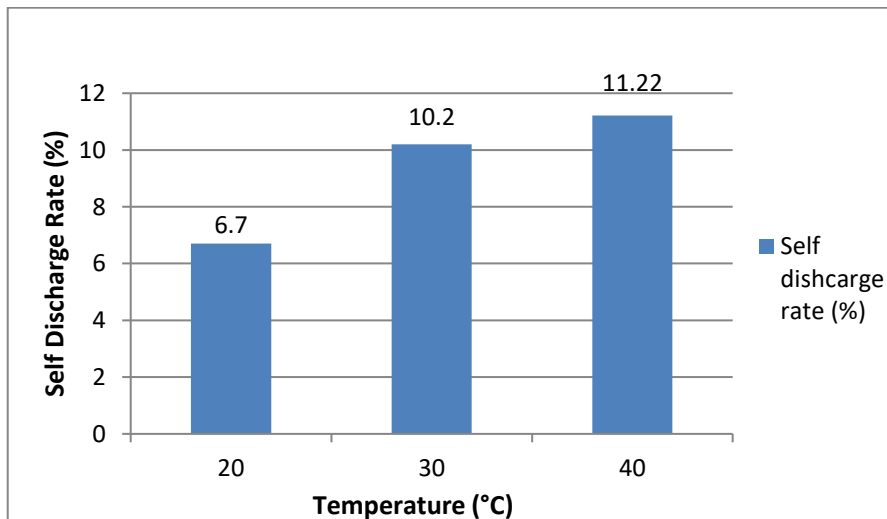


Figure 4.16 Comparison of Self discharge rate with different temperature

The battery self-discharging is a loss of energy caused by an undesired chemical process. The plot above illustrates the rate of self-discharge at three distinct temperatures (20°C, 30°C, and 40°C). The lowest rate of self-discharge was observed at 20°C, whereas the

Results and discussions

highest rate was observed at 40°C. Observations indicate that the rate of self-discharge increases as the temperature rises. According to the Arrhenius equation, the rate of chemical reaction accelerates as the temperature rises, resulting in energy loss due to undesired chemical reactions. Consequently, a higher rate of chemical reaction is responsible for a higher rate of self-discharge at higher temperatures. Because of this, the battery manufacturer recommends storing the battery at a lower temperature when it is not in use.

4.4.6 Measurement of Internal resistance

Internal resistance is the overall equivalent resistance within the battery. Internal resistance refers to the obstruction to current flow within a battery. The battery's internal resistance is dependent on its size, chemical composition, age, temperature, charge-discharge current, and other operational factors.

There are mainly two components of the internal resistance:

- (1) Electronic resistance
- (2) Ionic resistance

- Electronic resistance: It is a resistivity of the actual material, such as metal cover and internal components.
- Ionic resistance: It is a resistance to current flow caused by electrochemical parameters such as electrode area, electrolyte conductivity, electrolyte temperature, and so on.

Temperature is the most important factor influencing the electrochemical characteristics of the battery. Electrochemical properties have a direct relationship with internal resistance. Thus, temperature is indirectly responsible for battery internal resistance. As a result, internal resistance measurement is essential to determine the influence of temperature on internal resistance. The internal resistance of a battery is measured in mΩ (milliohms). An internal resistance meter is used to test the internal resistance of a battery.

Experimental Studies – 1: Effect of Temperature on Different Parameters of Battery Performance

Measurement data:

Temperature (°C)	10	20	30	40	45
Internal Resistance (mΩ)	23.54	20.45	19.16	17.21	16.12

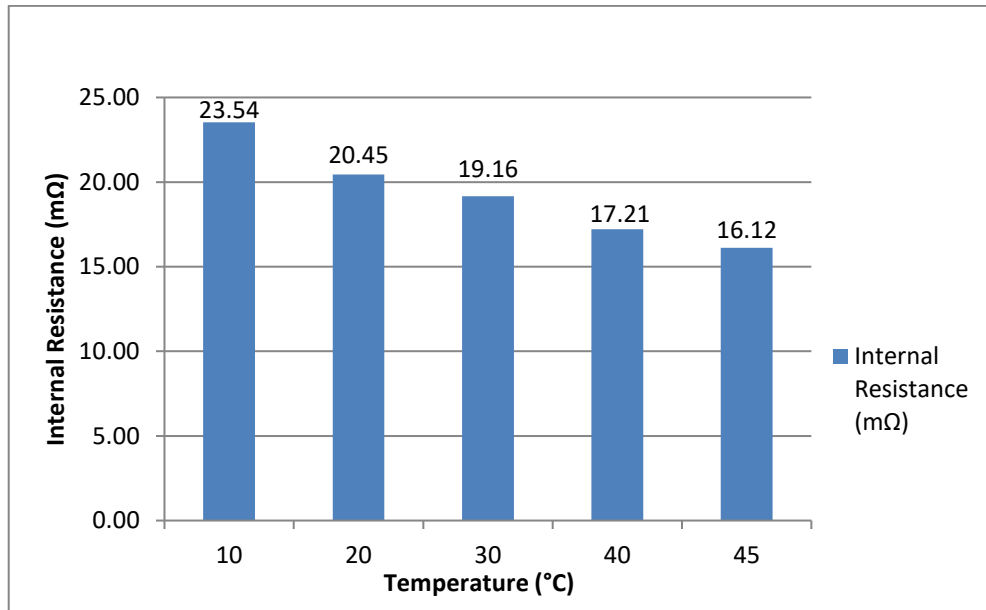


Figure 4.17 Internal resistance of battery at different temperature

The battery's internal resistance is an overall equivalent resistance within the battery that resists charge flow between electrodes. The internal resistance of the battery is caused by a variety of reasons. Internal resistance is mostly determined by the chemical characteristics of the electrodes and electrolytes.

Internal resistance of battery at different temperature is illustrated in Figure 4.17. Temperatures of 10°C and 45°C were found to have the largest and lowest internal resistance, respectively. The plot above clearly indicates that as temperature rises, internal resistance decreases. Electrolytes have a high viscosity at low temperatures and a low viscosity at higher temperatures. The charge transfer between electrodes is restricted by excessive electrolyte viscosity, resulting in a higher temperature internal resistance. At higher temperatures, the rate of a chemical reaction increases and the viscosity of the electrolyte decreases, resulting in a decreased internal resistance.

Conclusions

4.5 Conclusions

Table 4.1 Values of performance parameters of a VRLA battery at different temperatures

	10°C	20°C	30°C	40°C	45°C	Rated Value
Battery Capacity (Ah.)	2.45	3.4	3.64	4.01	4.86	4.1Ah
Discharging Time (min.)	21	29.2	31.2	34.4	41.7	35 min.
Charging Time(Hrs.)	2:24	3:56	4:50	5:16	5:20	5:00 hrs.
Gas generation (ml.)	1.4	5	12.5	15.2	29	
Self Discharge rate (%)		6.7	10.2	11.22		5%
Internal Resistance (mΩ)	23.54	20.45	19.16	17.21	16.12	19.00

The Table 4.1 illustrates the performance parameters of a VRLA battery at five different temperatures. It demonstrates that when temperature rises, capacity, discharging time, charging time, gas generation, and self-discharge rate rise. On the other hand, as temperature rises, battery life and internal resistance decrease.

The capacity and discharge back up are better at higher temperatures, but the battery was run at a higher temperature for an extended period of time, resulting in evaporation of the acid from the AGM separator. Thus, the AGM separator gradually became dry, resulting in decreased battery life. Thus, the AGM separator gradually became dry, resulting in decreased battery life. This indicates that utilizing a VRLA battery at high temperatures is useful for a short period of time but becomes harmful when used for an extended period of time. As a result, prolonged exposure to extreme temperatures reduces battery life.

On the other hand, internal resistance rises at low temperatures, and excessive internal resistance causes a start-up issue in VRLA batteries. So low temperatures are not good for a battery. Finally, it was decided that VRLA batteries should not be used at higher (35°C to 40°C) or lower temperatures (5°C to 10°C). The VRLA battery should be operated between 20°C and 30°C for optimal performance and battery life.

CHAPTER 5. Experimental Studies – 2: Performance assessment of VRLA battery of E-bike in field test

5.1 Introduction

The next step toward developing BTMS for E-bikes is to evaluate the battery performance during the operating condition of E-bikes under various road conditions and ambient temperatures. There are so many factors that affect the performance of the VRLA battery in E-bike during operating conditions. Significant aspects like extreme operating temperatures, variation in discharging rates during accelerating and decelerating the vehicle, driving E-bike in very high or deficient State of Charge (SOC), etc., negatively impact the health and life of VRLA battery.

Ambient temperature is an external parameter responsible for shortening battery life and performance degradation. VRLA batteries have their own optimum operating temperature range. Operating a VRLA battery outside this temperature range affects battery health and life differently. The performance and life of the VRLA battery depend on the operator's driving and charging habits in real-life conditions. Also, various road conditions, climatic changes, etc., have great importance on the thermal and electrical performance of the battery. This is due to the fact that the lab environment differs greatly from the actual working circumstances of the VRLA battery in an E-bike under real-world conditions. Thus, the results of lab experiments may mislead in evaluating the battery's actual thermal and electrical performance. It is necessary to assess various thermal and electrical performance parameters like battery temperature, power, etc., under real-life conditions to evaluate actual thermal and electrical performance of the battery.

In this experiment, the thermal and electrical performance of VRLA batteries is assessed under different driving cycles with various road conditions and climatic conditions. All the driving cycles have been divided according to types of routes, i.e., urban route, gradient route, highway route & rural route, and time duration, i.e., morning, afternoon, and evening. All the experiments have been performed with old and new VRLA battery set for a thorough

Introduction

study of the thermal and electrical performance of battery with different State of Health (SOH). OREVA ALISH E-bike is selected as a test vehicle for the experimental analysis. The OREVA ALISH E-bike is powered by a 500W brushless DC hub motor with a top speed of 40 km/hr. The hub motor is powered by 12V, 25Ah. maintenance-free VRLA battery. Key specifications of the OREVA ALISH E-bike are given as follows,



Figure 5.1 OREVA ALISH E-Bike [148]

Table 5.1 Specification of OREVA ALISH E- BIKE

Parameter	Details
Battery	: VRLA deep discharge batteries
Battery capacity	: 48V, 25 Ah.
No. of batteries	: 4 Nos.
Motor type	: Brushless DC hub motor
Max. output power	: 500 W
Max. speed	: 40 km/hr.
Max. Range	: 45 km./Full charge
Dimensions	: Length: 1820 mm Width : 685 mm Height: 1150 mm
Wheel Size	: Diameter: 406.4 mm Width : 76.2 mm
Vehicle weight with batteries	: 75 kg.
Payload capacity	: Two persons.
Charging time	: 6 to 7 Hrs.

5.2 Experimental setup & Instrumentation

A transportable experimental facility is constructed within the available space of the E-bike for these investigations. Figure 5.2 demonstrate the arrangement of different components of experimental setup in E-bike. The experimental setup consists of a data logger, temperature sensors, voltage and current measurement probes, UPS, GPS unit, etc. There are four nos. of 12V, 25Ah. VRLA batteries have been installed in E-bike. All the batteries are placed below the driver's seat of the E-bike. All VRLA batteries are connected in series to produce 48V to operate the brushless DC hub motor.

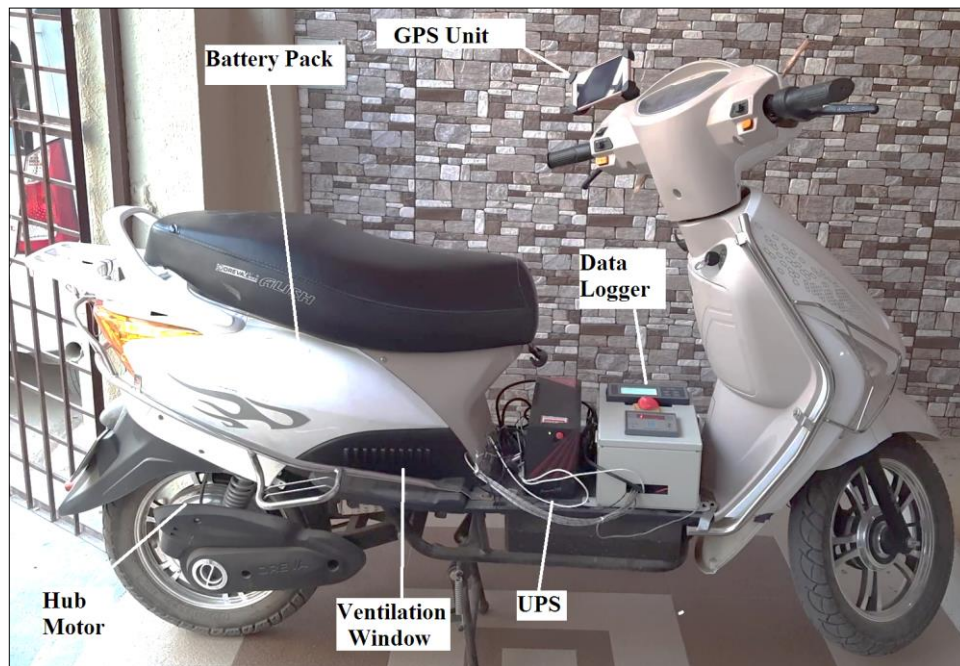


Figure 5.2 Arrangement of different components of experimental Setup in E-bike

The data management system includes a data recorder and a GPS device. In the lag space area of the E-bike, a data logger is installed. The data logger is connected to temperature sensors, voltage and current measurement probes. The data logger is only compatible with 230V, 50 Hz AC power. Hence, the Uninterruptible Power Supply (UPS) unit was employed to power the datalogger during field testing. The UPS unit is installed beside the data logger in the E-leg bike's space. The Global Positioning System (GPS) unit has been positioned on the holder for the left-side mirror to minimise the chance of a poor satellite connection. Track data from the drive bike route has been recorded by the GPS unit. GPS unit-recorded track data can be analysed by using GPX analyzing software.

Experimental setup & Instrumentation

5.2.1 Location of sensors

Four 12V, 25 Ah VRLA batteries are installed inside the E-bike battery pack. All of the batteries are linked in series. All of the batteries are connected in series. Figure 5.3 and Figure 5.4 show the battery arrangement inside battery pack. The brushless DC hub motor is powered by the Battery Management System (BMS).

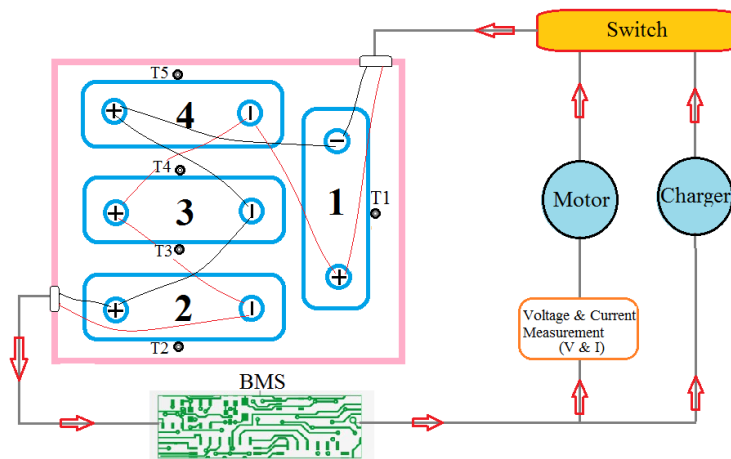


Figure 5.3 Location of temperature sensors and direction of flow of current in E-Bike

The data logger measures and records the surface temperature of the battery as well as the power consumption of the BLDC hub motor during operation. There are five Nos. J - type thermocouples are affixed to the battery's surface. As indicated in Figure 5.4, temperature sensors T1, T2, T3, T4, and T5 are connected with batteries.

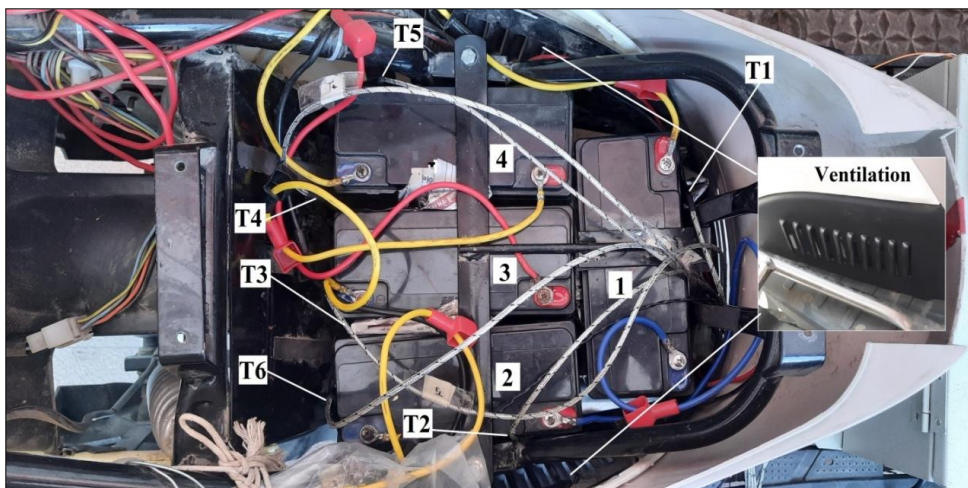


Figure 5.4 Arrangement of temperature sensors in E-Bike battery pack

The front and both sides of the battery pack have air ventilation louvres. Figure 5.4 shows an enlarged view of the air ventilation louvres. The "1", "2", and "4" batteries have direct contact with the ventilated section of the battery pack. The "1", "2", and "4" batteries have direct contact with the ventilated part of the battery pack. Temperature sensors T1, T2, and

Experimental Studies – 2: Performance assessment of VRLA battery of E-bike in field test

T5 are therefore mounted to the exterior surface of the batteries to measure fluctuation in battery surface temperature in the vented area of the battery pack. Battery "3" is surrounded by batteries 1, 2, and 4. Battery "3" is surrounded by batteries 1, 2, and 4. As a result, the air has not circulated adequately around the "3" battery. As a result, temperature sensors T3 and T4 are mounted to the front and rear surfaces of battery "3" to measure the fluctuation in surface temperature in the battery pack's intermediate region. The ambient temperature is measured using the temperature sensor T6. T6 is located below the battery back to prevent it from direct sunlight.

5.2.2 Steps for attachment of temperature sensor

There are the following steps for attachment of temperature sensor on battery surface,

Step – 1



Figure 5.5 Tip of J – type thermocouple

Step – 2

Bottom of thermocouple's tip and top of wired portion pasted on 3 mm thick foam tape.

(Foam tape dimensions: 50 mm x 25 mm x 3 mm)



Figure 5.6 Temperature sensor pasted on foam tape

Step – 3

The temperature sensor with foam tape is attached to Vinyl adhesive tape. Vinyl adhesive tape is selected for better durability and adhesiveness at a higher temperature.

(Vinyl adhesive tape size: 100 mm x 100 mm x 0.12 mm)

Experimental setup & Instrumentation



Figure 5.7 Backside of temperature sensor pasted on Vinyl adhesive tape

Step – 4

Finally, the temperature sensor is attached to the battery surface with vinyl adhesive tape.



Figure 5.8 Temperature sensor pasted on the battery surface

5.2.3 Data logger

As a data acquisition system, the Khoat KH - 208 data recorder is employed. The KH - 208 is an 8-channel paperless data recorder (shown in Figure 5.9) that records readings of various parameters such as battery surface temperature, voltage, and current at specified time intervals.



Figure 5.9 Khoat KH – 208 paperless data recorder

Experimental Studies – 2: Performance assessment of VRLA battery of E-bike in field test

Table 5.2 Data logger channels description

Channel	Identification	Sensor	Application
CH – 1	T1	J – type thermocouple	Battery surface temperature measurement
CH – 2	T2	J – type thermocouple	
CH – 3	T3	J – type thermocouple	
CH – 4	T4	J – type thermocouple	
CH – 5	T5	J – type thermocouple	
CH – 6	T6	J – type thermocouple	Ambient Temperature
CH – 7	V	-	Battery Voltage
CH – 8	A	Electric shunt (30A ~ 70 mV)	Battery Current

5.3 Experimentation

Field tests are carried out in this experiment to assess the thermal and electrical characteristics of the OREVA E-bike. The field testing is being carried out in the city of Junagadh (Gujarat), India. Junagadh is situated at 21.52°N 70.47°E and is 107m above sea level. During the summer, the temperature in Junagadh ranges from 28°C to 40°C.

The performance of an e-bike is affected by factors such as ambient temperature, road condition, velocity, acceleration, journey time, geography of the location, and so on. Thus, the present study began with the selection of routes in Junagadh city, followed by the measurement of thermal and electrical factors. The selection of routes is critical when planning for driving cycle measurement. Based on the region's geography and climate, twenty-four drive cycles have been developed. The Drive route includes both local and arterial streets with varying populations. Studies are carried out at various stages of battery health to undertake a thorough assessment of battery performance. The thermal and electrical parameters of a new and old battery set (shown in Figure 5.10) in an E-bike are examined throughout drive cycles.



(a) New battery Set



(b) Old battery set

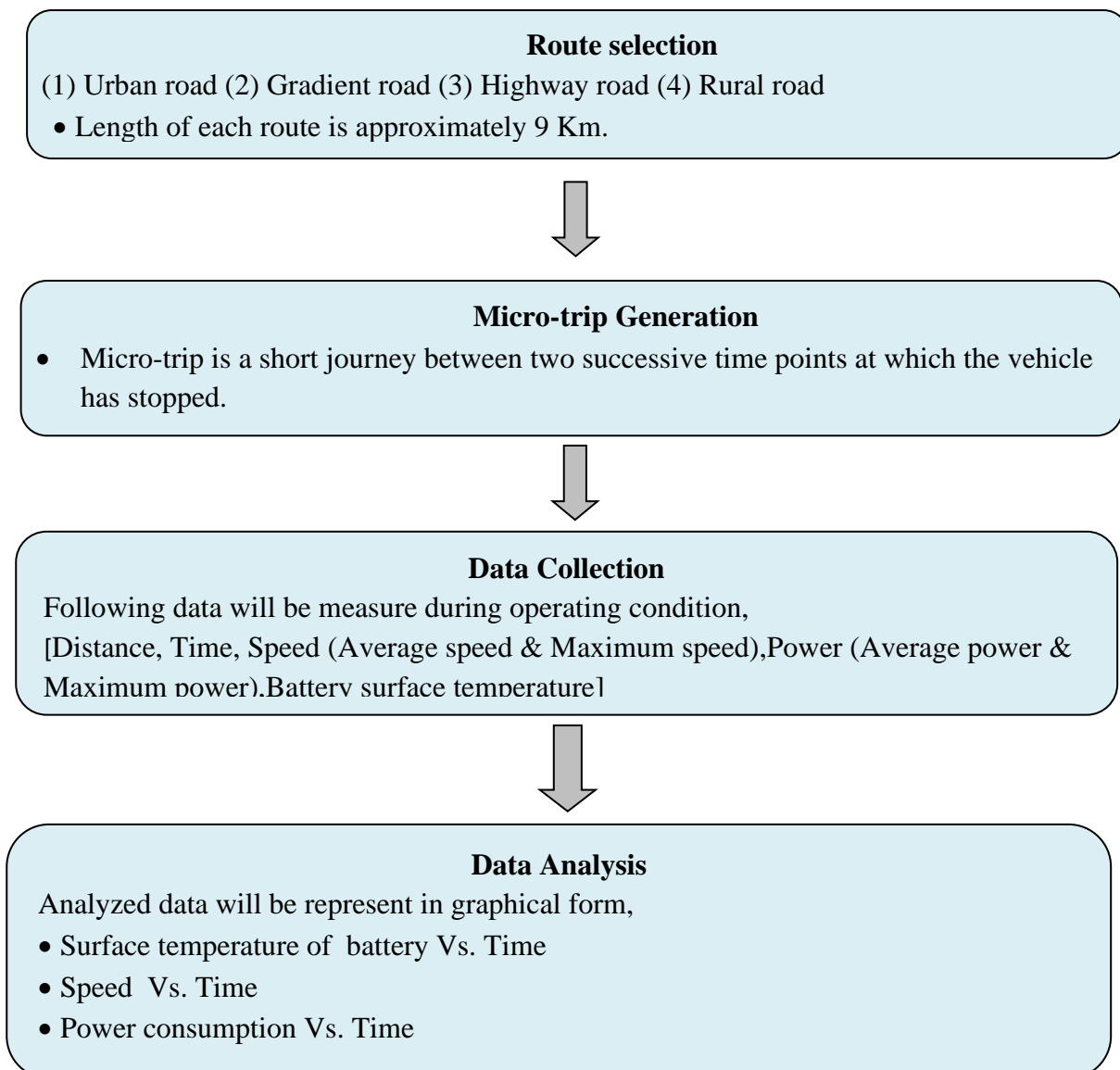
Figure 5.10 OREVA ALISH E-bike battery sets

Experimentation

5.3.1 Development of the driving cycle

The driving cycle includes vehicle operating conditions like idle, acceleration, cruising, and deceleration [149]. A typical driving cycle route includes a collection of varied speeds and accelerations. The route of the driving cycle is classified into four routes based on road conditions: (1) urban route, (2) gradient route, (3) highway route, and (4) country route. [3] The GPS unit measures and records different drive cycle parameters such as distance, time duration, speed and acceleration rates, moving time, and stopping time. The drive cycle parameter changes greatly depending on the type of road.

In experimentation, a process for developing a real-world driving cycle is critical. Route selection, micro-trip production, data collection, and data analysis are all steps in building the driving cycle [150]. The stages involved in developing the driving cycle are detailed below.



Experimental Studies – 2: Performance assessment of VRLA battery of E-bike in field test

5.3.2 Description of Routes

The performance of the VRLA battery in an E-bike was evaluated under various road and climatic circumstances including urban, gradient, highway, and rural roads at distinct periods. The normal route for each road is chosen based on road condition and traffic density. The following are the route details for each road:

Urban Route

The urban route covers all major and minor streets in a densely populated urban area. Figure 5.11 shows the typical route of traveled area of urban route and Figure 5.12 displays the photographs of urban route. The speed of a vehicle on an urban route is determined by traffic density. During pick-up hours, vehicles' operating speeds are influenced by conflicting traffic movements and pedestrians. Therefore, the urban route is plagued by frequent stops because of the high traffic density.

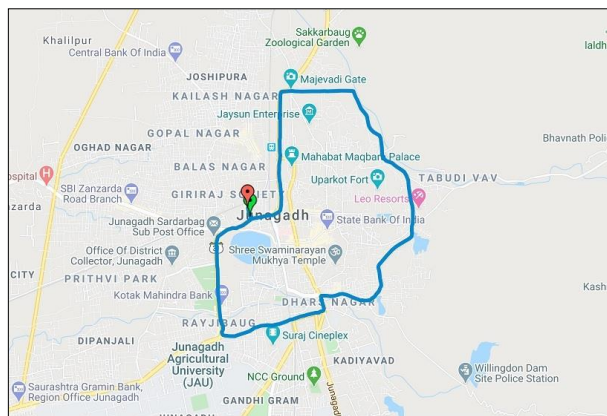


Figure 5.11 Typical route of a traveled area on the urban road with GPS data. Image provided by Google map, map data ©2020



Figure 5.12 Photographs of Urban Road

Experimentation

Gradient route

The gradient route is characterised by the rate of rising and falling throughout the length of the road in relation to the horizontal plane. Figure 5.13 shows the typical route of traveled area of gradient route and Figure 5.14 displays the photographs of gradient route. Length of route is 8 km. The gradient route is chosen to evaluate the E-bike's performance based on its gradeability. The Gradeability of an E-bike varies on a variety of parameters, including as the type of road surface, a hub motor's tractive effort, tyre traction, etc. [151].

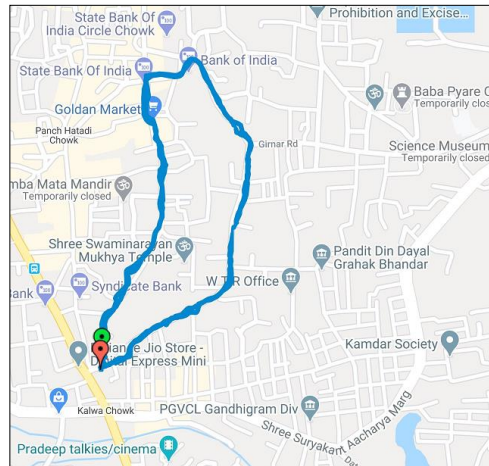


Figure 5.13 Typical route of the traveled area on gradient road with GPS data. Image provided by Google map, map data ©2020



Figure 5.14 Photographs of Gradient road

Highway Route

The highway is an arterial road with at least two lanes of traffic. Highway routes have a flat road surface, allowing for maximum speed on an E-bike. In addition, the performance of an E-bike can be examined with a constant speed over a long distance on the highway. For testing purposes, a two-lane highway route is used. Length of route is 9 km. Figure 5.15 shows the typical route of traveled area of highway route and Figure 5.16 displays the photographs of highway route.

Experimental Studies – 2: Performance assessment of VRLA battery of E-bike in field test

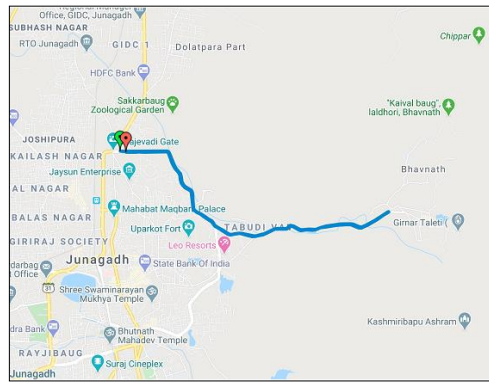


Figure 5.15 Typical route of a traveled area on highway road with GPS data, Image provided by Google map, map data ©2020



Figure 5.16 Photographs of highway road

Rural Route

The rural road is located outside of the city and has a low volume of traffic. The rural road is often a single lane with an earth, dust, and gravel surface. The rural route is mostly utilised by light vehicles. The rural route was chosen to test the capabilities E-bike's on rough and gravelly roads. The Chobari Road, located just outside Junagadh, has been chosen as a rural route for the experiment. Length of route is 7.6 km. Figure 5.17 shows the typical route of traveled area of rural route and Figure 5.18 displays the photographs of rural route.

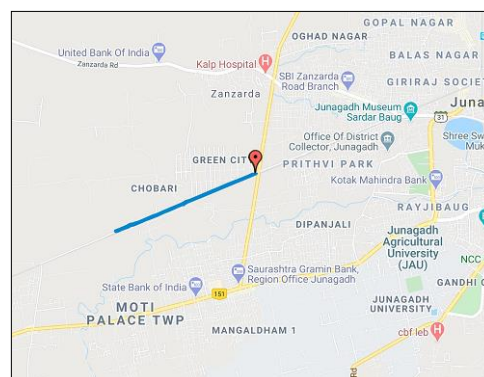


Figure 5.17 Typical route of a traveled area on a rural road with GPS data, Image provided by Google map, map data ©2020

Experimentation



Figure 5.18 Photographs of rural road

Micro – trip Generation

A micro-trip is a short travel between two consecutive time intervals where the vehicle has stopped. The micro-trip-based drive cycle makes it easier to implement a simulated "stop-go" driving pattern. Vehicles consume greater power under "stop-go" conditions due to conflicting traffic movement and pedestrians [152]. As a result, micro-trip based drive cycle construction is a considerably preferable approach for estimating power usage during a "stop-go" driving pattern. The micro-trip mode comprises of acceleration, cruising, and deceleration [150]. Targeted driving cycle parameters have been separately examined for each micro-trip, as required.

5.3.3 Detail of field test

Twenty-four drive cycles have been constructed based on the route type and time period. In the OREVA ALISH E-Bike, twelve drive cycles were performed with a new battery set and the remaining twelve drive cycles with the old battery set. The following are the details of drive cycles, including time periods and route details:

Experimental Studies – 2: Performance assessment of VRLA battery of E-bike in field test

New Battery Set

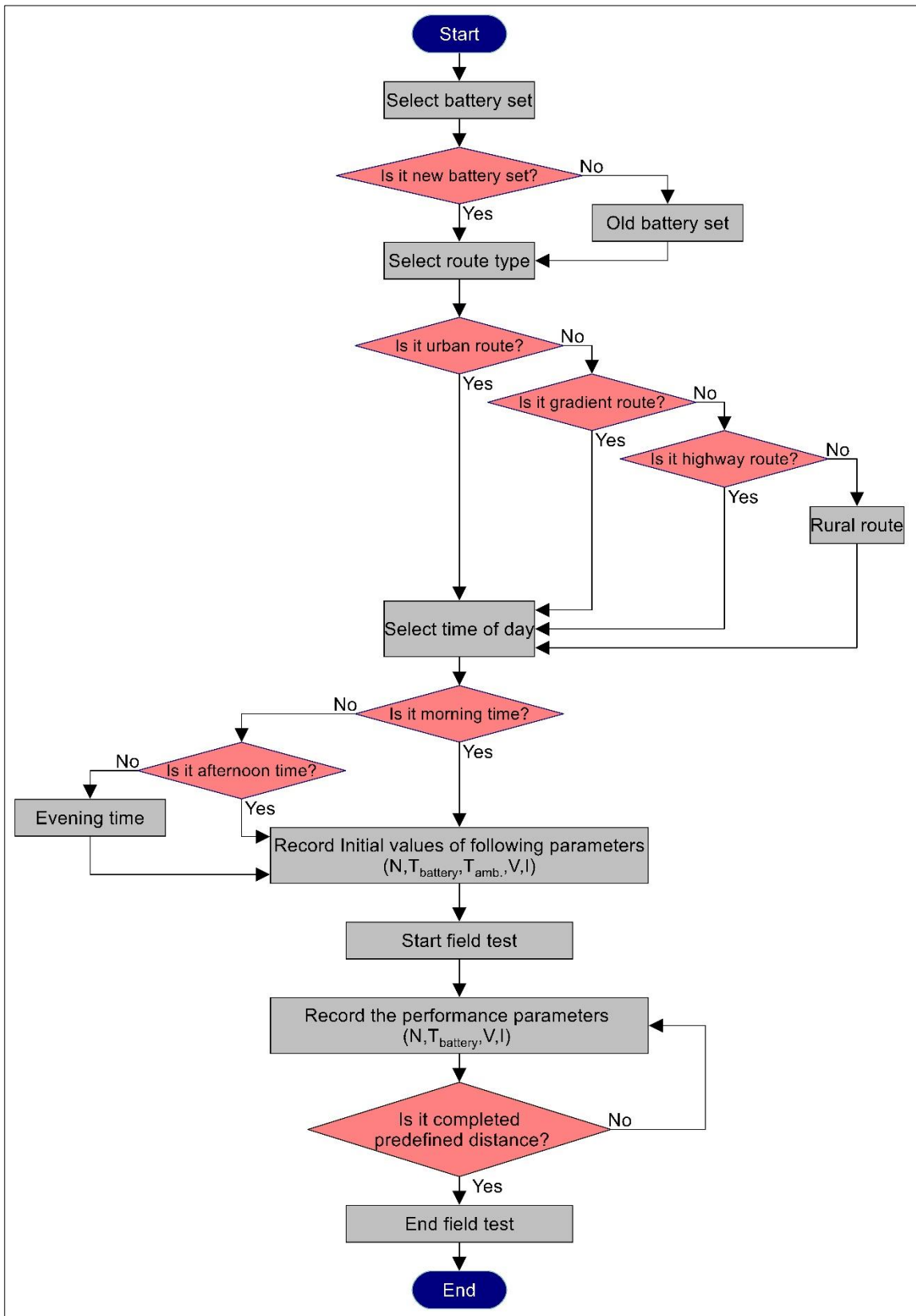
Drive Cycle	Time Period	Route Detail
Urban Route		
Drive Cycle – 1	Morning	GSRTC bus stand → Junagadh Agriculture University → Bahhaudin Science College → Kalva Chowk → Majejadi Gate → Junagadh Railway station → GSRTC bus stand
Drive Cycle – 2	Afternoon	
Drive Cycle – 3	Evening	
Gradient Route		
Drive Cycle – 4	Morning	Kalva Chowk → Diwan Chowk → Old Collector Office → Swaminarayan Temple → Kalva Chowk
Drive Cycle – 5	Afternoon	
Drive Cycle – 6	Evening	
Highway Route		
Drive Cycle – 7	Morning	Majejadi Gate → Girnar Taleti & Back
Drive Cycle – 8	Afternoon	
Drive Cycle – 9	Evening	
Rural Route		
Drive Cycle – 10	Morning	Chobari Road
Drive Cycle – 11	Afternoon	
Drive Cycle – 12	Evening	

Old Battery Set

Drive Cycle	Time Period	Route Detail
Urban Route		
Drive Cycle – 13	Morning	GSRTC bus stand → Junagadh Agriculture University → Bahhaudin Science College → Kalva Chowk → Majejadi Gate → Junagadh Railway station → GSRTC bus stand
Drive Cycle – 14	Afternoon	
Drive Cycle – 15	Evening	
Gradient Route		
Drive Cycle – 16	Morning	Kalva Chowk → Diwan Chowk → Old Collector Office → Swaminarayan Temple → Kalva Chowk
Drive Cycle – 17	Afternoon	
Drive Cycle – 18	Evening	
Highway Route		
Drive Cycle – 19	Morning	Majejadi Gate → Girnar Taleti & Back
Drive Cycle – 20	Afternoon	
Drive Cycle – 21	Evening	
Rural Route		
Drive Cycle – 22	Morning	Chobari Road
Drive Cycle – 23	Afternoon	
Drive Cycle – 24	Evening	

Experimentation

5.3.4 Flow chart of field test experiment



5.3.5 Assessment of field test

An assessment criterion ensures that the created drive cycle accurately represents a driving pattern under real-world situations. The drive cycle was evaluated using distance, time duration, speed and acceleration rates, driving time and stopping time. These drive cycle characteristics vary depending on the type of route and the climate. Analyze the effect of variables such as ambient temperature, road condition, aggressive driving, etc. on E-bike performance based on measured values. The analyzed data is shown graphically in the following section.

Vehicle Speed

The speed-time variation for E-bikes obtained from GPS tracking data for different routes is shown in the Figure 5.19. The average speed of 12 km./h is recorded on the gradient route, which is the minimum average speed compared to the speed of E-bike on other routes. Because the gradient route incorporates an up-down road pattern along the entire length. When E-bike goes uphill, it decelerates and accelerates downhill due to gravity.

The highway route allows for maximum speed on an E-bike for the lengthy run. Thus, as a result, the highway route reached top speeds of 25 to 30 km/h. The rural route is rough and mostly gravelly. On a rural route, the E-bike average speed is 15 kilometres per hour. The E-bike's speed was changed from 10 to 15 km/h up to 26 minutes (1600 sec.) with regular stops along the urban route. The urban route's speed profile reveals frequent stops due to heavy traffic density during the entire field test. During the field test, some micro-trips are seen with all types of routes. These micro-trips are a portion of the speed profile, which begins and finishes with a speed of zero. Micro-trips demonstrate the actual driving pattern, which includes acceleration, idling, and deceleration phases. By comparing the E-bike's average speed, it is easy to see what the fastest and slowest speeds were on highways and grade routes, respectively.

Experimentation

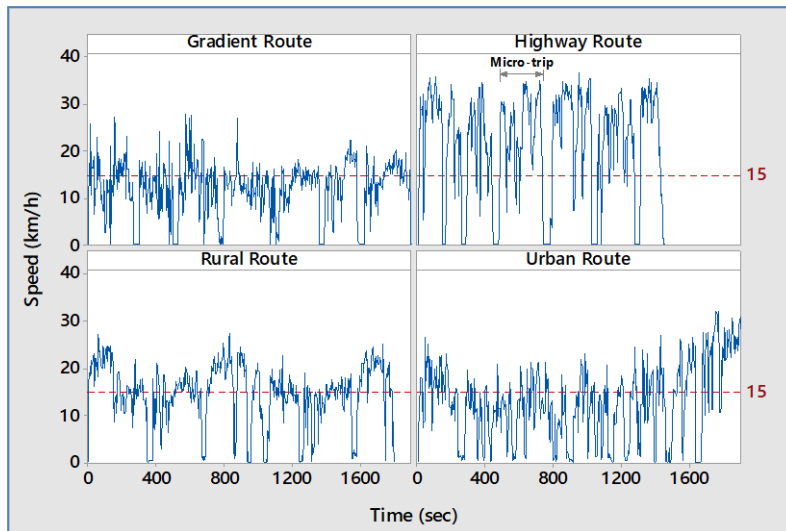


Figure 5.19 Speed – time profile of E – bike on various routes

Power Consumption

The Figure 5.20 represents the power utilized by the E-bike on various routes. The power was calculated using the current drain of the BLDC hub motor and the battery voltage. The BLDC hub motor's current and voltage are adjusted in response to the load. The current drain from the batteries increases as the load on the hub motor increases, and the voltage steadily declines.

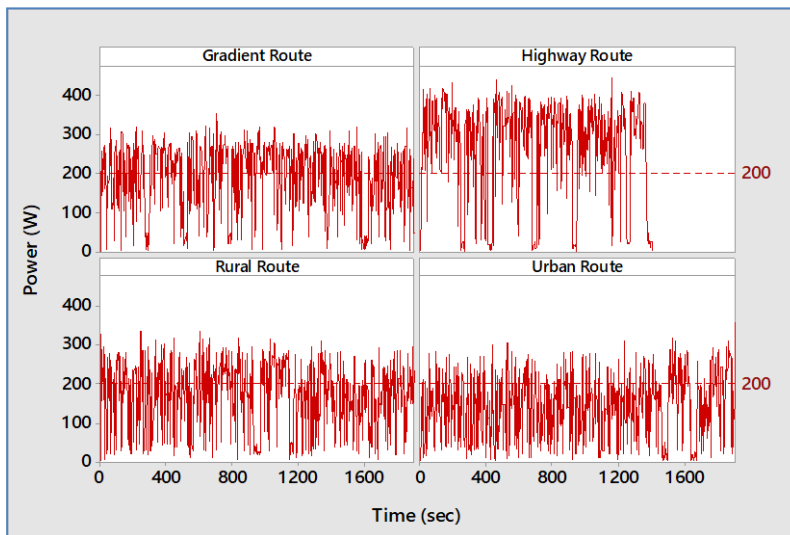


Figure 5.20 power – time profile of E – bike on various routes

E-bikes used an average of 200 W of electricity on gradients, rural, and urban routes, and 300 W of power on highway routes. A comparison of average power consumption reveals that maximum power consumption occurs on the highway route due to the E-bike's higher speed. almost the same average power consumption throughout the gradient and urban route drive cycles.

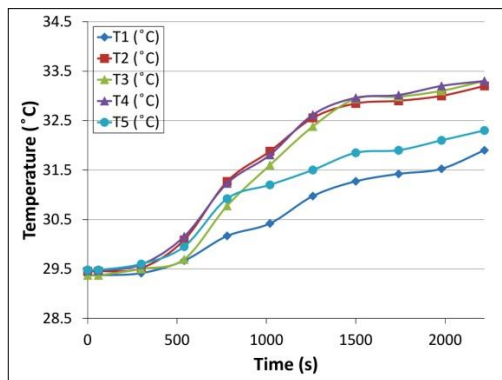
5.4 Results and analysis

The performance of the E-bike in various variables such as road conditions, climatic conditions, and different SOH has been analyzed based on twenty-four trips in a field test. To assess the performance of the VRLA battery during operation, three performance characteristics are measured and analyzed: battery surface temperature, energy consumption, and E-bike speed. This section describes and explains the acquired results.

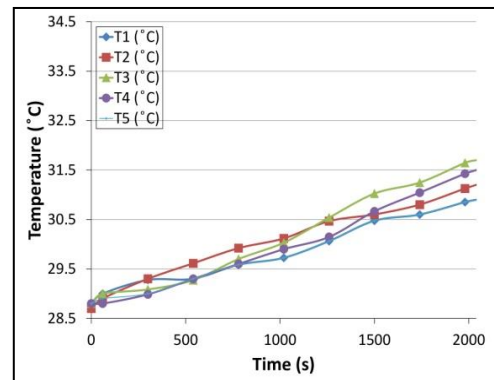
5.4.1 Battery Temperature

The temperature of the battery is a crucial factor in the performance of an E-bike. Every 10°C rise in temperature doubles the reaction rate, and every 8.3°C increase above 25°C halves the battery life [28]. Primarily, the relationship between battery temperature and power consumption rate and ambient temperature is direct. The ambient temperature ranges from 28°C to 43°C throughout the morning, afternoon, and evening phases of the field test.

The temperature profile of new and old batteries during the morning field tests is represented in Figure 5.21. Throughout the morning, the temperature stayed between 28.5 and 31 degrees Celsius. It demonstrates that the temperature profiles T1 and T2 of batteries 1 and 2 are fairly similar. In addition, the temperature T3 of battery no. 3 rises significantly faster than that of another battery. The reason for such a rapid increase in temperature is because this battery is located in the centre of the battery pack, where air circulation and cooling rate are inadequate. During the morning tests, the temperature of both new and used batteries increased by 8.80% and 8.96%, respectively. This indicates that throughout the early hours, the temperature of both new and old batteries rises at a similar rate.

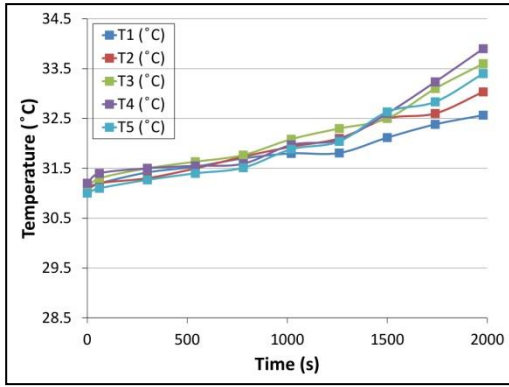


(a) Urban route with new battery set

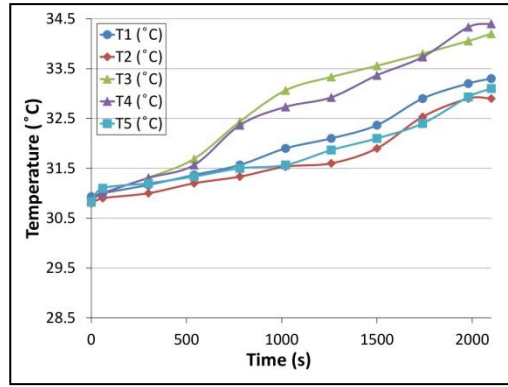


(b) Urban route with old battery set

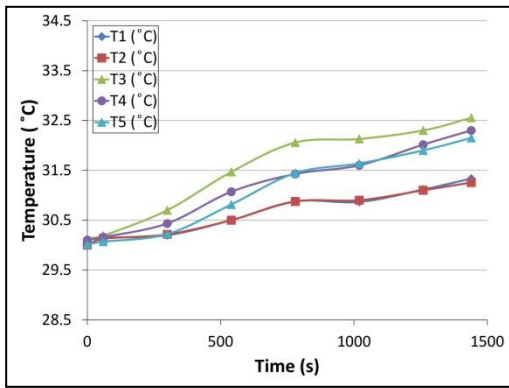
Results and analysis



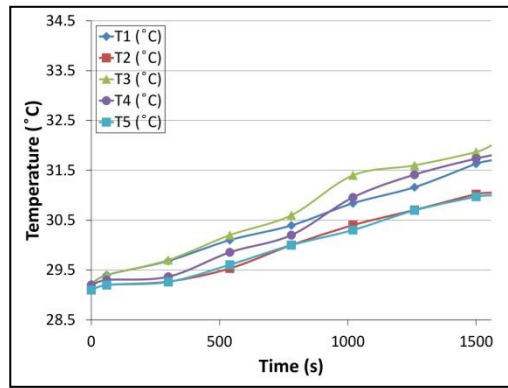
(c) Gradient route with new battery set



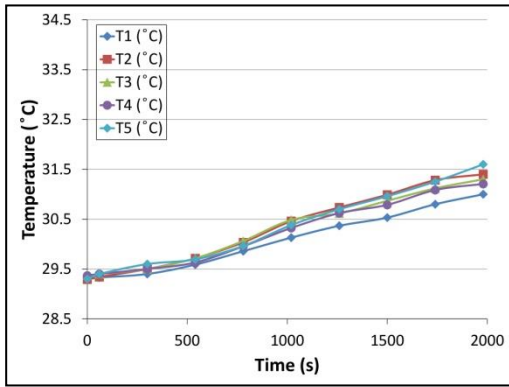
(d) Gradient route with old battery set



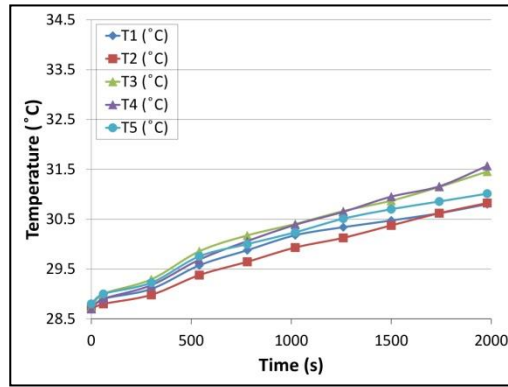
(e) Highway route with new battery set



(f) Highway route with old battery set



(g) Rural route with new battery set



(h) Rural route with new battery set

(A) NEW BATTERY SET

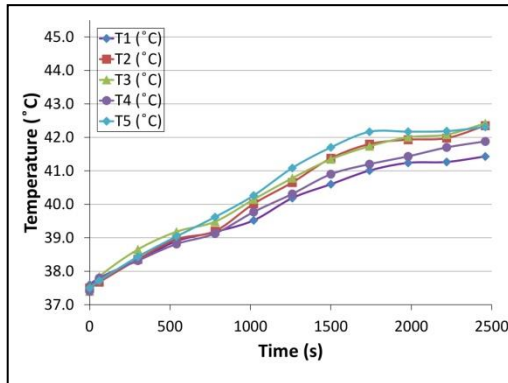
(B) OLD BATTERY SET

Figure 5.21 Battery temperature profiles for new and old batteries during the morning field tests

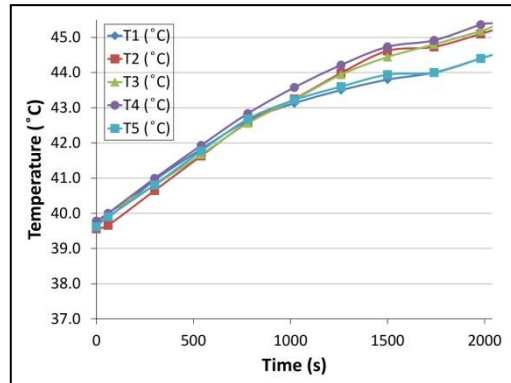
Figure 5.22 shows the temperature profiles of new and old batteries throughout the afternoon field tests. During the afternoon field tests, the ambient temperature was maintained at 37°C and 40°C. The temperatures of all the batteries initially rise uniformly throughout specific afternoon tests. The T2, T3, and T4 temperatures of batteries 2 and 3 increased at a faster rate until the end of the journey. The highest battery temperatures are seen in the afternoon, indicating that E-bike air ventilation is insufficient in the afternoon. Additionally, it is found

Experimental Studies – 2: Performance assessment of VRLA battery of E-bike in field test

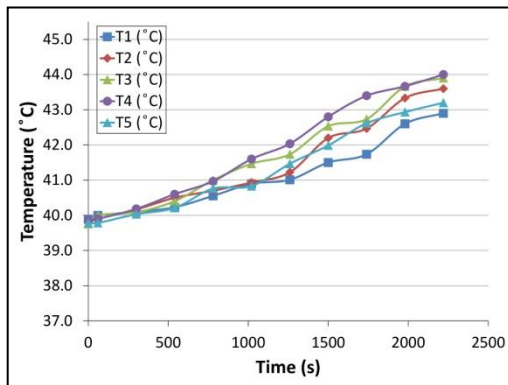
that the temperature of old batteries rises faster than that of new ones. The urban route has an average temperature increase of 5.2°C over the ambient, which is 15.38%, 34.61%, and 40.38% greater than the gradient, highway, and rural routes, respectively.



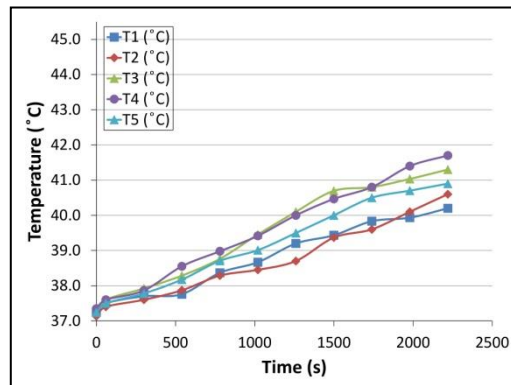
(a) Urban route with new battery set



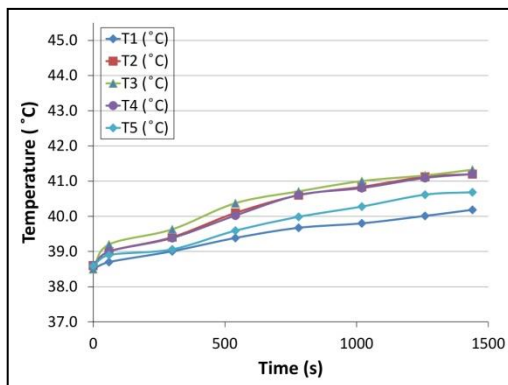
(b) Urban route with old battery set



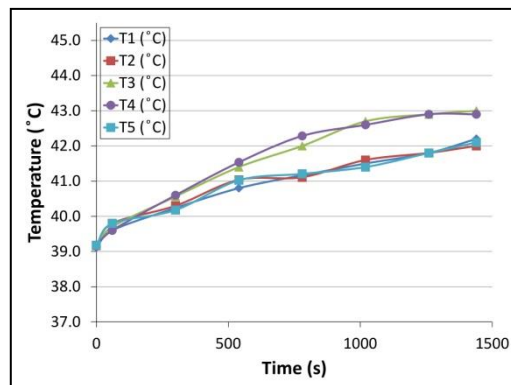
(c) Gradient route with new battery set



(d) Gradient route with old battery set

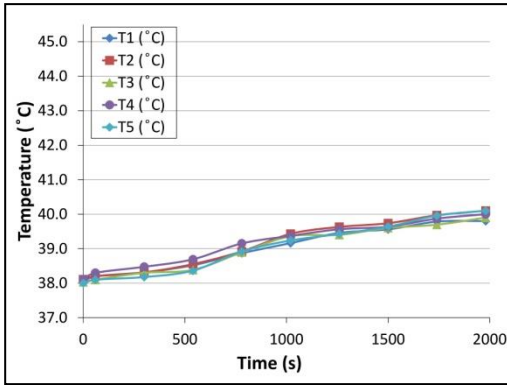


(e) Highway route with new battery set

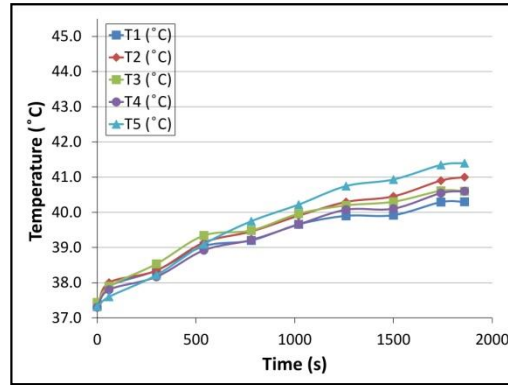


(f) Highway route with old battery set

Results and analysis



(g) Rural route with new battery set



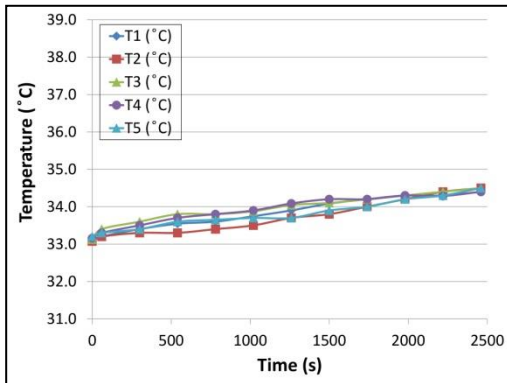
(h) Rural route with new battery set

(A) NEW BATTERY SET

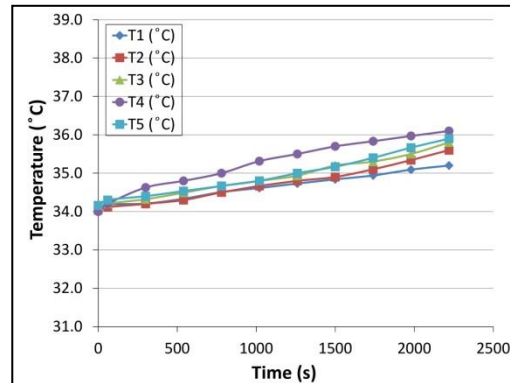
(B) OLD BATTERY SET

Figure 5.22 Battery surface temperature profiles for new and old batteries during the afternoon field tests

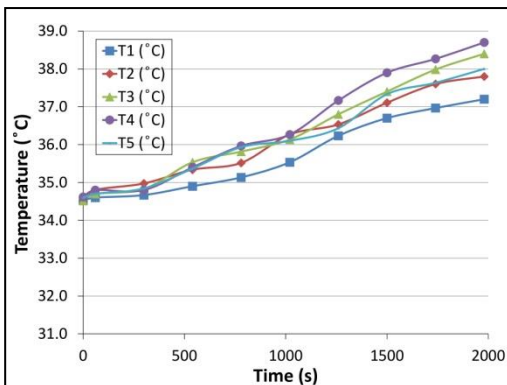
Figure 5.23 illustrates the temperature profiles of new and old batteries during the evening. Temperatures in the evening field tests ranged from 31°C to 34°C. The gradient route has the biggest temperature spike of 4.2°C from the ambient, whereas the other routes have temperature increases of around 2.5°C. The change in temperature between the morning and afternoon is minimal. It is also observed that the evening temperature profiles of new and old batteries are nearly identical.



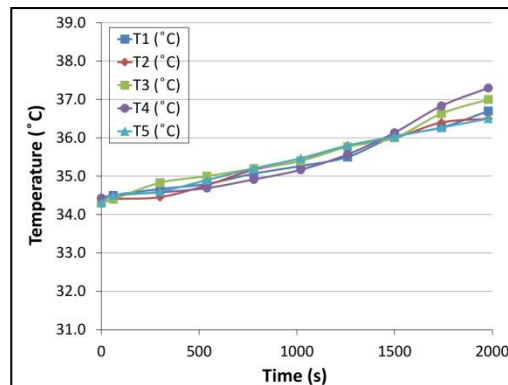
(a) Urban route with new battery set



(b) Urban route with old battery set

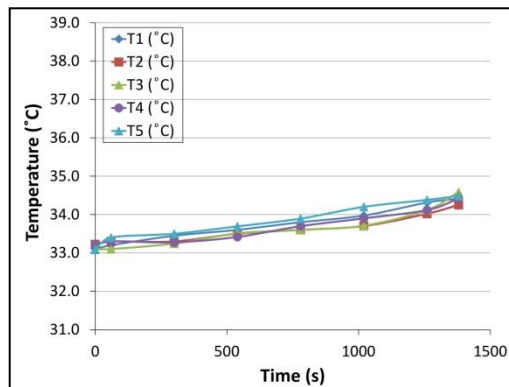


(c) Gradient route with new battery set

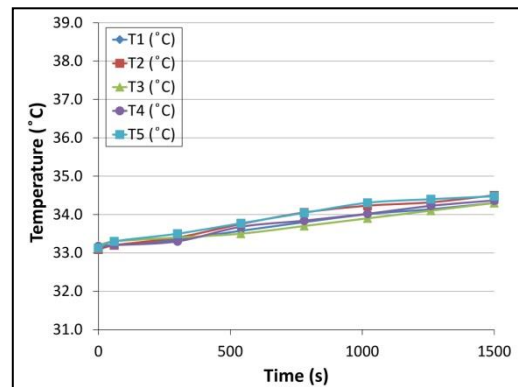


(d) Gradient route with old battery set

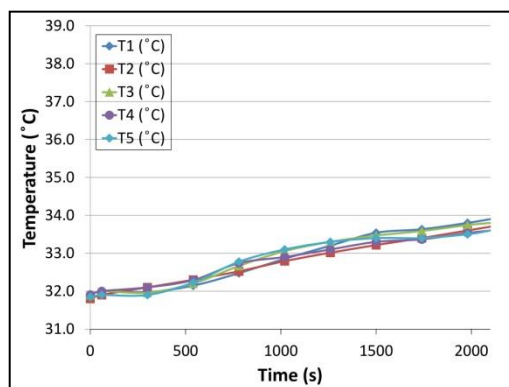
Experimental Studies – 2: Performance assessment of VRLA battery of E-bike in field test



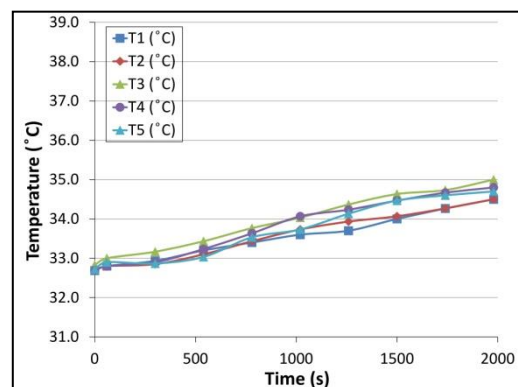
(e) Highway route with new battery set



(f) Highway route with old battery set



(g) Rural route with new battery set



(h) Rural route with new battery set

(A) NEW BATTERY SET

(B) OLD BATTERY SET

Figure 5.23 Battery surface temperature profiles for new and old batteries during the evening field tests

5.4.2 Comparison of battery temperatures

Figure 5.24 compares the highest surface temperature of the batteries to the ambient temperature during various routes with a new battery set in the morning, afternoon, and evening tests. The greatest temperature recorded was 44.0°C during the afternoon gradient route test when the ambient temperature was 39.7°C . Minimum temperature rises (T) were found for all roads in the evening, while minimum battery temperatures were observed during morning tests. According to the Arrhenius equation, the rate of chemical reaction rises with increasing temperature and vice versa [153]. Like a result, when the ambient temperature is high (as in afternoon tests) and the battery is used, the temperature quickly increases above the ambient temperature since the heat generation rate is faster at higher temperatures.

Results and analysis

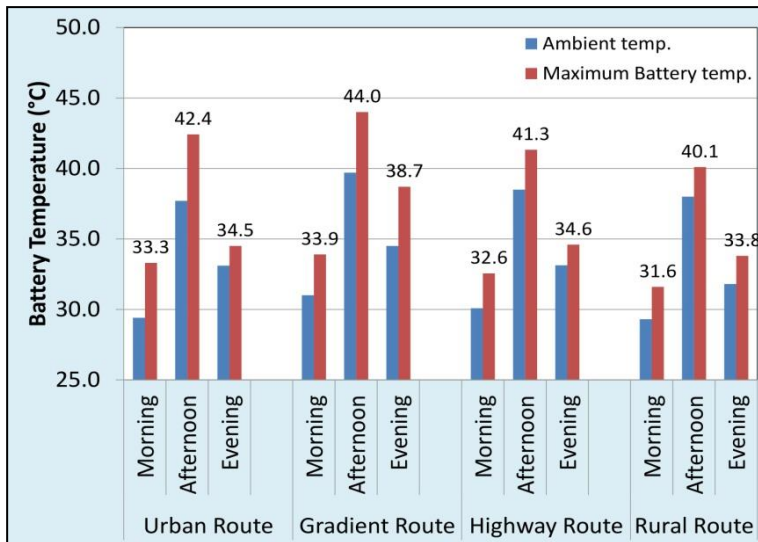


Figure 5.24 Comparison of battery surface temperature during different routes with the new battery set

Figure 5.25 illustrates a comparison of the minimum and highest surface temperatures of the battery during different routes with the old battery arrangement. The highest battery temperature measured in these field testing was 45.4°C in the afternoon test on the urban route while the ambient temperature was 39.7°C. In addition, the lowest temperature rise (T) was seen in the evening on all roadways, while battery temperatures were lower in early field tests.

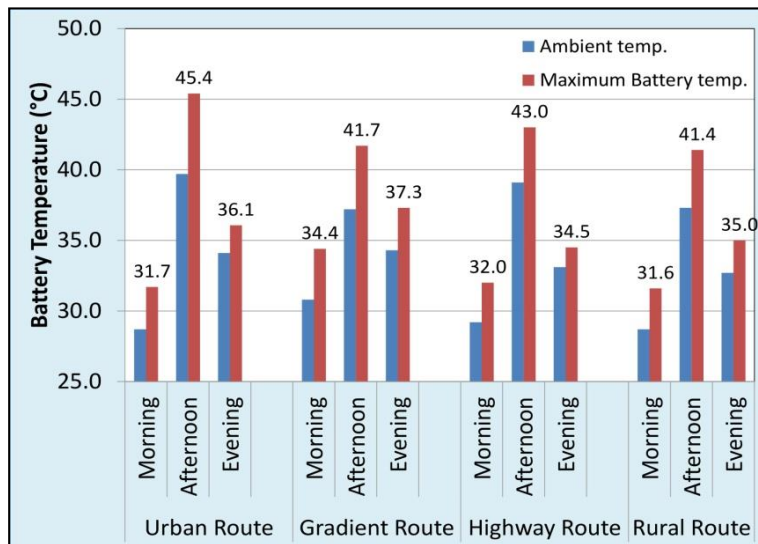


Figure 5.25 Comparison of battery surface temperature during different routes with old battery set

The highest temperature measured in the old battery set during the afternoon time of the urban route is 5.7°C higher than the same value measured in the new battery set. Thus, a higher temperature rise (ΔT) was recorded in the field with an old battery set than with a new one. This is due to the VRLA battery's lead-calcium grid structure, which is extremely

Experimental Studies – 2: Performance assessment of VRLA battery of E-bike in field test

sensitive to battery ageing. The ageing of the battery causes corrosion of the positive plate and grid structure, which rises fast with temperature [28].

5.4.3 Influence of ambient temperature and speed on power consumption

The power consumption of an E-bike is primarily determined by its speed on various routes. However, it also has a noticeable effect on the ambient temperature. The average power consumption for each test versus ambient temperature, as well as the average vehicle speed for that test, are plotted in Figure 5.26. The greatest power, 277.4W, is utilised at an average vehicle speed of 23 km/h with an ambient temperature of 38.5°C, which is nearly the highest value of that parameter recorded. At moderate temperatures (about 30°C), the lowest power consumption has been reported with a low speed. Low power usage at high temperatures may be due to continuous vehicle speed during low traffic.

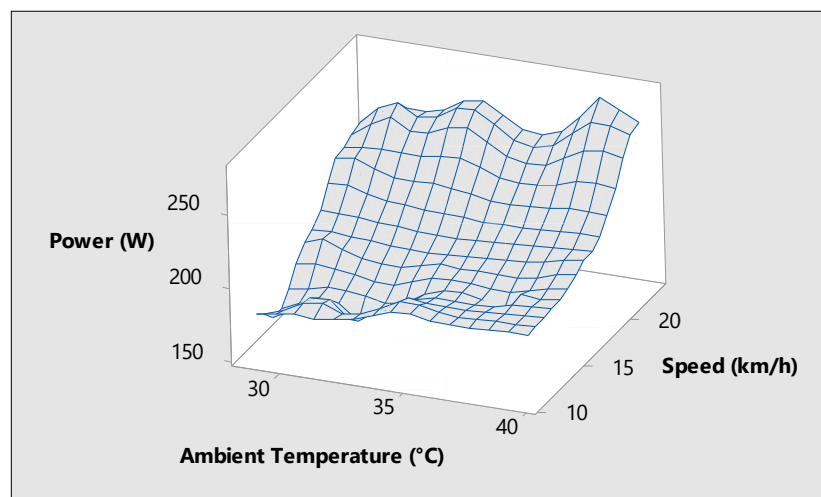


Figure 5.26 Wireframe plot showing the influence of ambient temperature and vehicle speed on power consumption

The combined effect of ambient temperature and power consumption on battery temperature is plotted in Figure 5.27. This Figure shows that battery temperature increases with increase in the ambient temperature and power consumption.

Results and analysis

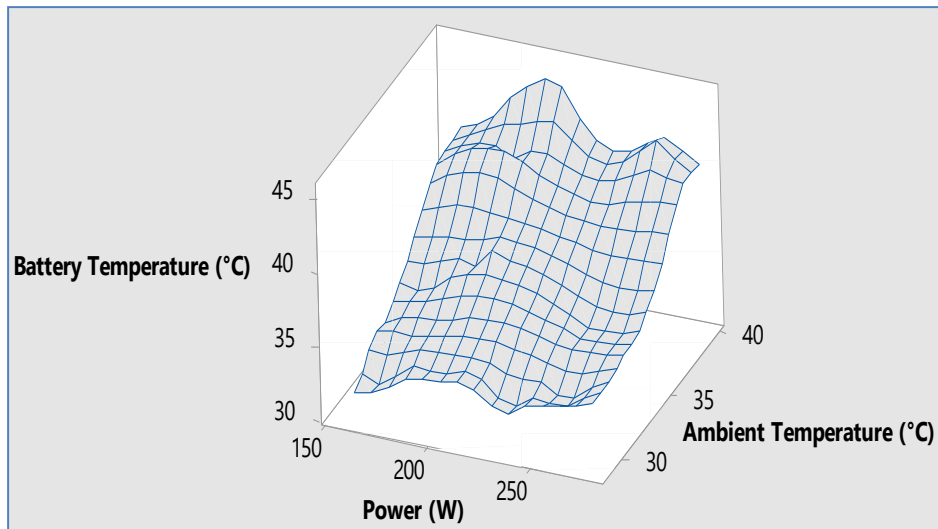


Figure 5.27 Battery temperature as a function of power consumption and ambient temperature

However, ambient temperature is more critical in increasing the battery temperature than power consumption. The fluctuation in power consumption also leads to a rapid increase in battery temperature. E-bike's acceleration and deceleration cycles are responsible for higher power consumption changes. That is one of the reasons behind the higher battery temperatures were recorded during field tests on the urban route because E-bike speed is highly fluctuated due to higher traffic density in urban route.

5.4.4 Influence of route pattern and ambient temperature on energy consumption

The influence of ambient temperature on energy consumption on various routes is shown in Figure 5.28. Each point represents a particular driving cycle, and shape and colors indicate the route type (gradient, highway, rural or urban). The lines represent the linear regression between the corresponding route and energy consumption. The linear regression is used to indicate the relation between the corresponding path and energy consumption. It shows that average energy consumption during various routes is related to ambient temperature and the nature of the way. The highest energy consumption of 15.05 Wh/km is seen on the gradient route, and the rise due to higher ambient temperature is also steeper. On the other than, the energy consumption of 11.20 Wh/km is the lowest on the highway route. The highway route seems to have the most downward effect on ambient temperature, where the range is between 11.20 Wh/km and 12.29 Wh/km.

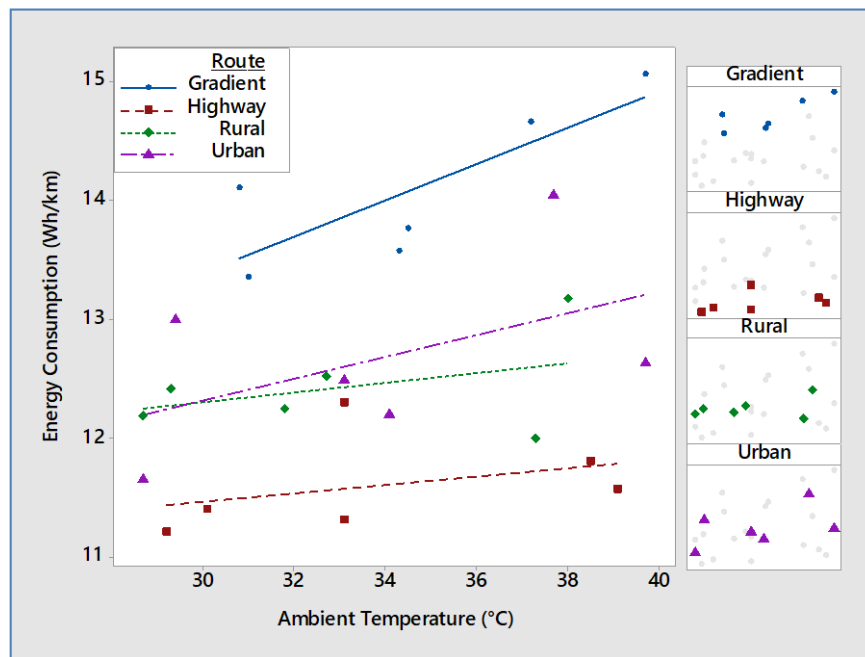


Figure 5.28 Influence of ambient temperature on total energy consumption during a field test.

5.4.5 A mathematical relationship between ambient temperature and energy consumption

A mathematical model has predicted the value of response under different conditions of input parameters. The mathematical model can be derived by regression analysis. Regression analysis is used to determine the change in response values with the value of design parameters change. Regression is a method of determining the conditional expected value of a dependent variable "Y" with the given value of some independent variable "X." regression is represented in a linear algebraic equation known as a regression equation.

The regression equation in the form of,

Response = Constant + coefficient (predictor) + + coefficient (predictor)

$$Y = K + K1(X1) + K2(X2) + + Kn(Xn)$$

The regression analysis can be derived by using MINITAB statistical data analysis software. The parameters to be considered for regression analysis are derived from the Analysis Of Variance (ANOVA). The ANOVA represented in form of table. Table 5.3 shows the estimated values of regression coefficient for battery temperature by MINITAB.

Results and analysis

Table 5.3 Estimated values of regression coefficient for battery temperature by MINITAB

Term	Coef	SE Coef	T-Value	P-Value	VIF
Constant	0.00838	0.00177	4.72	0.000	
Ambient Temperature (°C)	0.000124	0.000052	2.38	0.028	1.02
Gradient	0.001088	0.000332	3.27	0.004	1.52
Highway	-0.000975	0.000330	-2.96	0.008	1.50
Rural	0.000123	0.000333	0.37	0.715	1.53
Urban	-0.001325	0.000540	-2.45	0.024	1.51

Error! Reference source not found. shows the estimated values of the regression coefficient for battery temperature. The P-value of the gradient route is more petite than α – level (0.005). So, gradient routes are significantly affecting energy consumption. The same observation is also noticed in actual field test data, as shown in Figure 5.28. Variance Inflation Factor (VIF) is between 1 and 5. So, predictors are moderately correlated for all predictors.

Regression equation for energy consumption during each route,

$$\text{Gradient : Energy Consumption (kWh/km)} = 0.00946 + 0.000124 \text{ Ambient Temperature (}^\circ\text{C)}$$

$$\text{Highway : Energy Consumption (kWh/km)} = 0.00740 + 0.000124 \text{ Ambient Temperature (}^\circ\text{C)}$$

$$\text{Rural : Energy Consumption (kWh/km)} = 0.00850 + 0.000124 \text{ Ambient Temperature (}^\circ\text{C)}$$

$$\text{Urban : Energy Consumption (kWh/km)} = 0.00814 + 0.000124 \text{ Ambient Temperature (}^\circ\text{C)}$$

The Regression equations are established the mathematical relationship between energy consumption and ambient temperature for various routes. Using the regression equation, energy consumption can be mathematically predicted at a given road's given temperature.

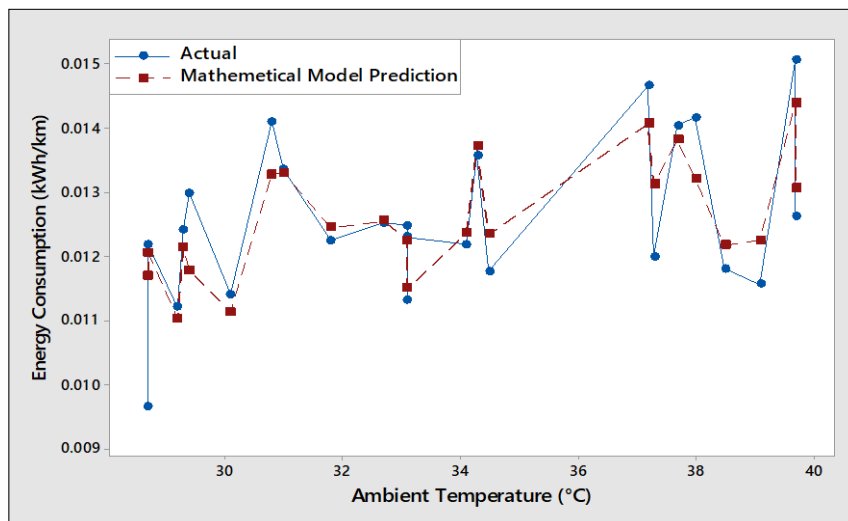


Figure 5.29 Comparison of actual results of energy consumption with mathematically predicted results

Experimental Studies – 2: Performance assessment of VRLA battery of E-bike in field test

Figure 5.29 represents a comparison of mathematically predicted results with actual energy consumption on the various routes. It shows that the mathematical model is well fit to expect the performance parameter with any control parameters.

5.5 Conclusions

This experimental study about the effect of various parameters like road conditions, climatic conditions and SOH on performance parameters such as battery temperature, energy consumption and speed of vehicle for VRLA batteries in E-bike by performing field tests.

It is found from the field tests that ambient temperature plays an essential role in deciding the battery temperature. The battery temperature rises rapidly in afternoon field tests, going up to 45.4°C when the ambient temperature was 39.7°C. Comparing battery temperatures shows that the increase in battery temperature (ΔT) above ambient temperature is up to 3.9°C, 5.7°C and 3.4°C, observed with field tests during the morning, afternoon and evening. This clearly shows that cooling achieved with air ventilation of E-bike is adequate during morning and evening hours but not effective during afternoon hours due to high ambient temperatures. In addition to the above, the route type has an important impact on battery temperature. The highest battery temperature rise (ΔT) of 3.4°C above the ambient is observed in gradient route field tests, which is 8.0%, 33.33% and 30.22% higher than the urban, highway and rural routes, respectively.

It is also found that batteries are heated more rapidly as they age. The field test shows that older batteries are 24.04% more heated than new batteries at higher ambient temperatures. Thus, there is a need for a better thermal management system for batteries, particularly in tropical countries like India, where afternoon temperatures in summer are very high. At lower speeds, the effect of ambient temperature on power consumption by the E-bike was found to be significant. At the same time, it also becomes very substantial at higher rates of fluctuation in speed. In addition to the above, it has been observed that the ambient temperature and route type significantly impact E-bike's energy consumption.

The mathematical relationship was established between ambient temperature and energy consumption for different routes using regression analysis and mathematically predicted results are compared with field test data. It is shown that the energy consumption during various drive cycles is dramatically increased with ambient temperature. The average energy

Conclusions

consumption of E-bike rises by 25.55% when the temperature changes from 29°C to 40°C on a different route, obviously due to consequent battery temperature rise. It is seen that the route patterns have a noticeable impact on energy consumption. The energy consumption during the gradient route is 13.75 Wh/km, 10.35%, 15.66% and 8.47% higher than the urban, highway and rural routes.

This study makes a sound case for a more effective battery thermal management system using techniques like evaporative cooling or refrigeration, as only these can produce cooling temperatures lower than the ambient. Such a system will help maintain the battery temperature in the recommended operating temperature range for geographical regions where summers are long and hot.

CHAPTER 6. Development of Evaporative cooling based BTMS

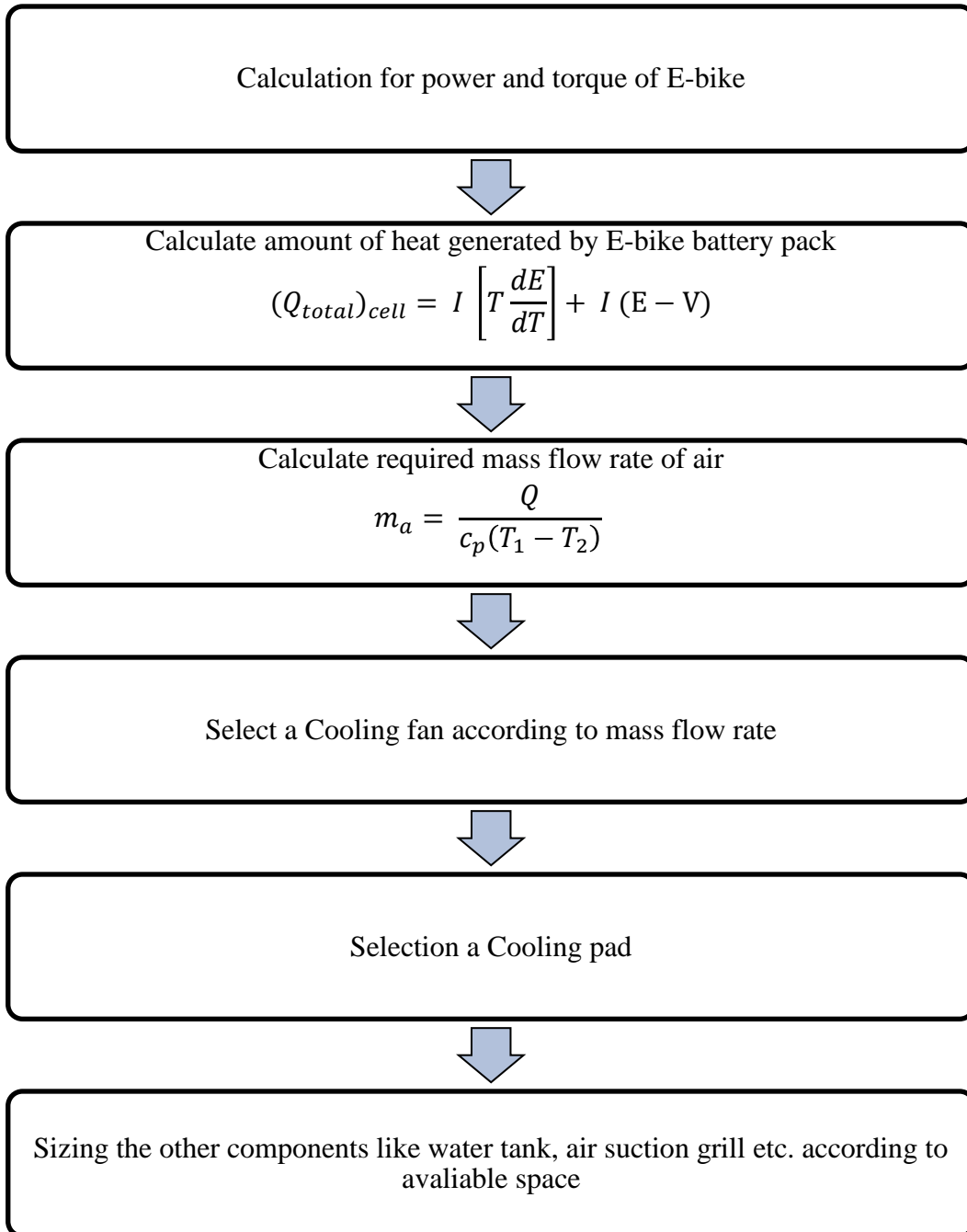
The ideal thermal management system would be small, light, and inexpensive. Battery thermal management system (BTMS) based on air or liquid cooling are commonly utilized in EVs. The energy consumption of various components used in air or liquid cooling, such as pumps, blowers, and so on, directly affects the range of EVs. Because of the fans, pumps, tubing and other equipment in forced air cooling and liquid cooling systems are becomes massive, complicated and costly. Sometimes manufacturers avoid liquid-based thermal management systems due to the leakage [154]. Also, an air or liquid-cooled thermal management system cannot keep the battery temperature below ambient. However, only evaporative cooling or refrigeration can achieve temperatures lower than the ambient.

Furthermore, evaporative cooling is less complicated and expensive than other cooling systems. Thus, an evaporative cooling-based thermal management system is selected and constructed for E-bike. The BTMS with evaporative cooling was designed based on the heat generated at the highest battery temperature in previous field tests.

Design calculations

6.1 Design calculations

The stages for designing an evaporative cooling based BTMS is given as below,



6.2 Uncertainty Analysis

S. J. Kline and F. A. McClintock's [155] technique was utilised to calculate experimental uncertainties. The uncertainty of measuring parameters is as per Table 6.1.

Table 6.1 Possible error in measurement devices

Sr. No.	Device name	Parameter	Symbol	Unit	Max. Value	Error
1	Thermocouple (J-type)	Temperature on Battery	T1 to T5	C	0 to 750	0.1
2	Thermocouple (J-type)	Air Flow Temperature	T6	C	0 to 750	0.1
3	Voltage Measuring Probe (config. through 1K Ω resistor)	Voltage of Battery	V	V	0 to 5	0.2
4	Current measuring probe (using 30A ~ 70 mV shunt)	Current of Battery	I	A	4 to 20	0.01

Calculation of uncertainty in results

The uncertainty of heat generation rate of battery was estimated by,

$$\delta Q_{battery} = \left[\left(\frac{\Delta Q_{battery}}{dI} \times \delta I \right)^2 + \left(\frac{\Delta Q_{battery}}{\Delta T} \times \delta T \right)^2 + \left(\frac{\Delta Q_{battery}}{\Delta E} \times \delta E \right)^2 + \left(\frac{\Delta Q_{battery}}{\Delta V} \times \delta V \right)^2 \right]^{1/2}$$

The uncertainty of Temperature Difference was estimated by,

$$\delta(\Delta T) = \left[\left(\frac{\Delta(\Delta T)}{\Delta T_1} \times \delta T_1 \right)^2 + \left(\frac{\Delta(\Delta T)}{\Delta T_2} \times \delta T_2 \right)^2 \right]^{1/2}$$

The uncertainty of Required Volumetric Flow rate of Air was estimated by,

$$\delta m_a = \left[\left(\frac{dm_a}{dQ_{battery}} \times \delta Q_{battery} \right)^2 + \left(\frac{dm_a}{dT_1} \times \delta T_1 \right)^2 + \left(\frac{dm_a}{dT_2} \times \delta T_2 \right)^2 \right]^{1/2}$$

The calculation steps of uncertainty in results have been presented in Appendix C. The calculated maximum uncertainties in results are 7.37%, 7.06% and 7.43% for heat generation rate, temperature difference and required volumetric flow rate of air respectively.

Design criteria

6.3 Design criteria

The evaporative cooling based BTMS should be fulfil the following requirement,

1. The evaporative cooling-based BTMS should be compact and transportable.
2. The evaporative cooling-based BTMS should be easily implemented in E- bike.
3. The effect of climatic changes should be minimum on batteries in E- bike.
4. The power consumption of evaporative cooling-based BTMS should be minimum.
5. The BTMS based on evaporative cooling should have a modular design that allowing for easy assembly and disassembly of all components.
6. The evaporative cooling-based BTMS should be automatically controlled in accordance with battery temperature.

6.4 Working principle of BTMS

According to the above design criteria, a novel evaporative cooling-based BTMS for VRLA battery pack was developed and implemented in E-bike. The Figure 6.1 depicts the conceptual design of developed evaporative cooling-based Battery Thermal Management System (BTMS). In the current BTMS, cooling is performed through the use of evaporative cooling. The current unique technology employs a cooling module to extract heat from warmer ambient air that is then blown into the enclosed chamber to cool it efficiently.

The evaporative cooling system consists of three units; The battery pack, control unit and cooling unit. The cooling and control units are arranged in mid supported box. The battery pack is placed below the mid-supported box. The battery pack contains four 12V, 25 Ah VRLA batteries' which are connected in series. A 20 W air blower, 2.25 lit. water tank, 3W water pump and a cooling pad make the cooling unit. The air blower and water pump are powered by a 12V, 7Ah VRLA battery housed in a separate control unit. A data logger, temperature control unit and speed regulators for the air blower and pump are arranged inside the control unit. The water level indicator indicates the amount of water in the water tank. The Khoat KH208 paperless data recorder is used as a data management system. The data logger monitors and records the battery's surface temperature and the current delivered to the battery during the operating condition. The cooling system is made fully leakproof. Major components of the cooling unit like the water tank, water collecting channel, cooling pad grill, piping system, etc., are connected through temporary fasteners. So, all the cooling unit components are easily assembled and disassembled. The 2-inch wood–wool cooling pad

Development of Evaporative cooling based BTMS

is used in the cooling unit. The wood–wool cooling pad is arranged inside the L–shaped galvanized perforated iron grill. The L – shape of the grill facilitates air entry from two sides.

The cooling system of BTMS is fully automatically controlled. As shown in Figure 6.1 a temperature controller is provided in the control unit. When the system switches ON, the temperature controller detects the temperature of the battery surface and according to that temperature, a controller operates the cooling blower and water pump. The temperature controller senses the surface temperature of the E-bike battery using a thermocouple and controls the cooling blower and water pump based on that temperature. The air blower and pump are individually regulated through speed regulators provided in a control unit. The temperature controller is configured to set the value of temperature 30°C. When the battery's temperature is higher than the set value, it starts the cooling blower and water pump. When the blower start, The humidified air from the wetted cooling pad is blown into the battery pack. The cooling air has circulated the batteries and extracts the heat from them. Cooling air is extracted from the battery pack through air outlets provided on the left and right sides of the battery pack.

Development of Evaporative cooling based BTMS

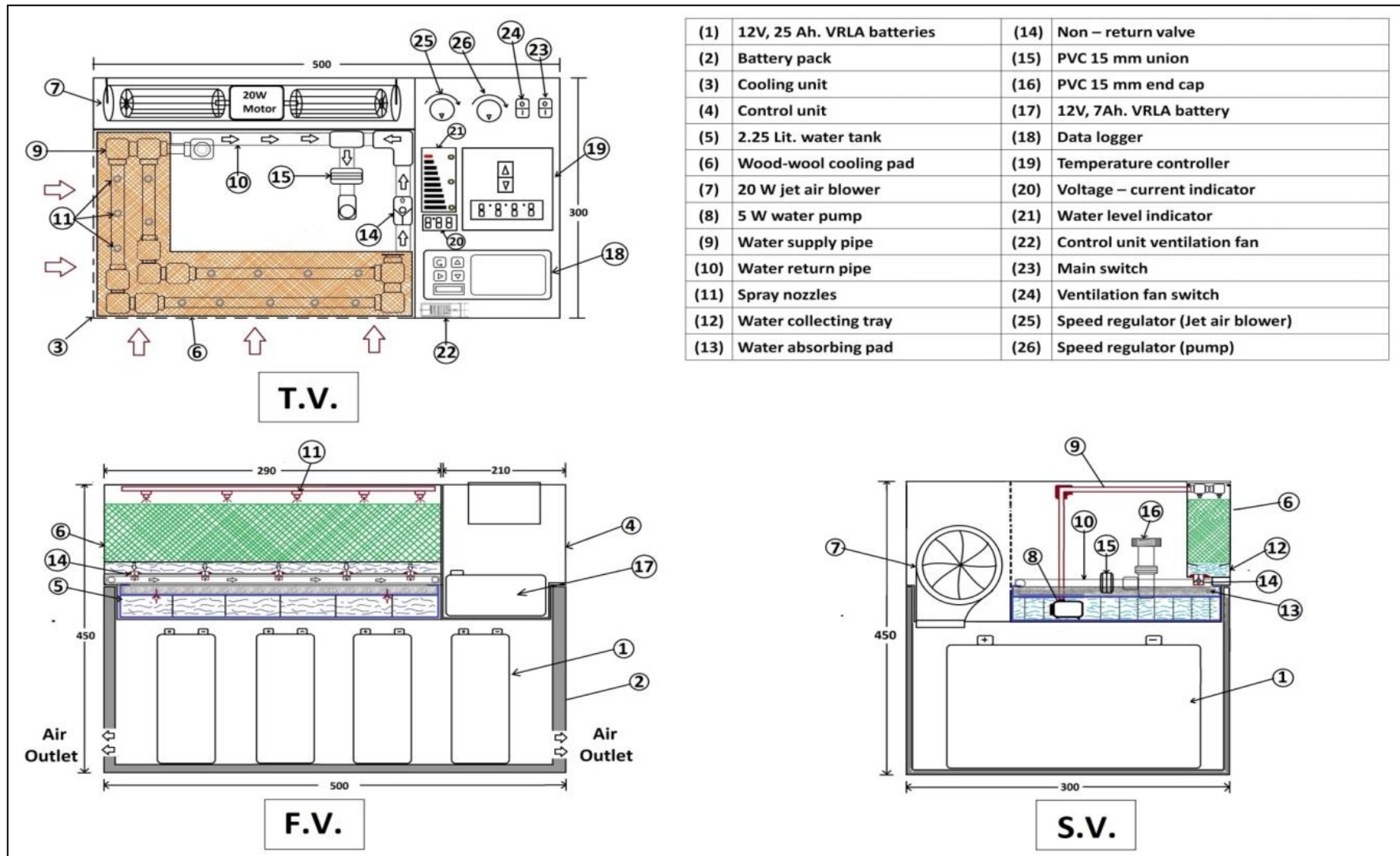


Figure 6.1 Conceptual design of the developed evaporative cooling based Battery Thermal Management System (BTMS)

6.5 Detail of individual components

6.5.1 Battery pack

The battery pack is fabricated using the 20 gauge (0.91 mm) thick galvanized iron sheet. The Figure 6.2 illustrates the detail drawing of battery pack. The battery pack size is 500 mm x 300 mm x 280 mm in the area and the dimensions of the E-bike battery are 180 mm x 175 mm x 80 mm. The battery pack size has been fixed according to the dimensions of the battery used in the E-Bike (12 V, 25 Ah). Four magnets have been located at each end of the outer body. Magnets are used to provide batter strength and facilitate efficiently removing the mid-supported box from the battery pack. Two ventilation windows are provided on both sides of the battery pack to remove the air from the battery pack. The sizes of both ventilation windows are 60 mm in diameter. 25 mm thick glass wool insulation is provided in the battery pack to reduce the effect of heat transfer from the atmosphere. The four battery holders of 185 mm x 85 mm x 50 mm are provided to hold the VRLA batteries. Also, 18 mm gap is provided between each battery holder for proper air circulation.

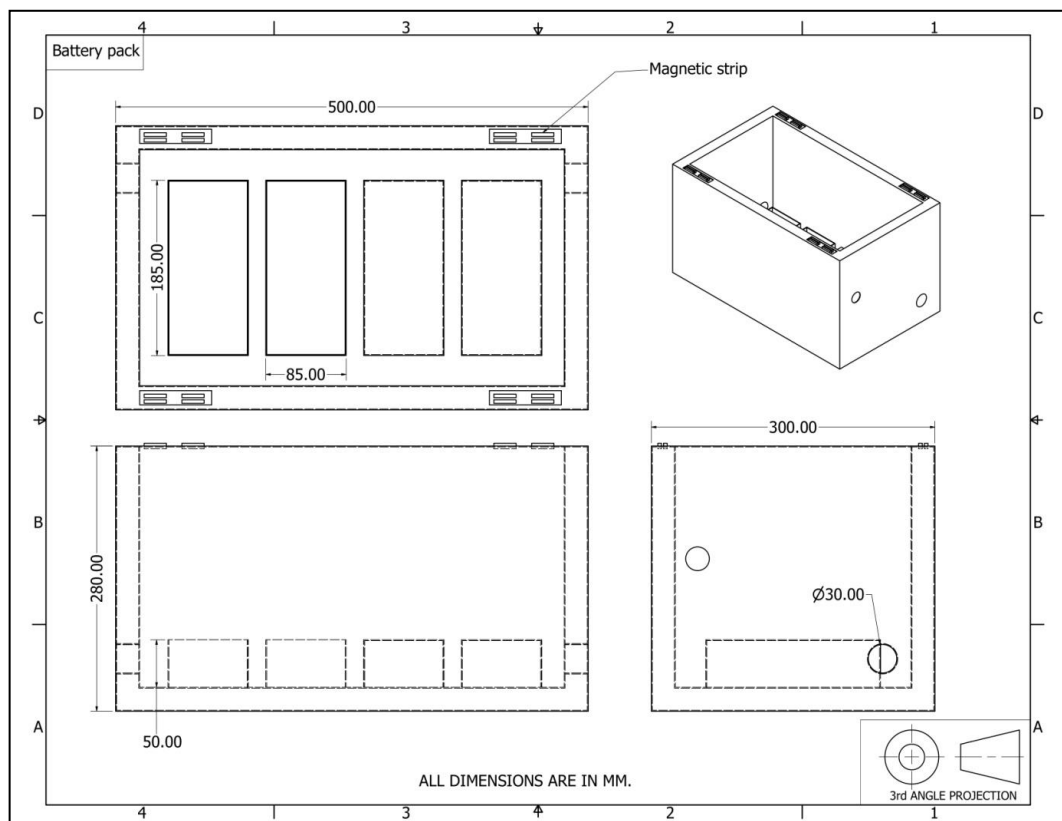


Figure 6.2 Detail drawing of battery pack

Detail of individual components



Figure 6.3 Snapshot of battery pack

6.5.2 Mid supported box

The mid-supported box is arranged between the system's upper and lower portions. Figure 6.4 and Figure 6.5 show the detail drawing of mid supported box and actual mid supported box respectively. The lower part consists of a battery pack, and the upper portion consists of a cooling and control unit. The mid-supported cover is fitted on the top portion of the battery pack using magnets. The mid-supported cover is held by the cooling unit and the control unit at mid of the overall system. Thus it's called a mid-supported box. The dimension of the mid-supported box is 450 mm x 250 mm x 60 mm. accuracy during the fabrication of mid supported box is more important because it is an air-tight cover for a battery pack.

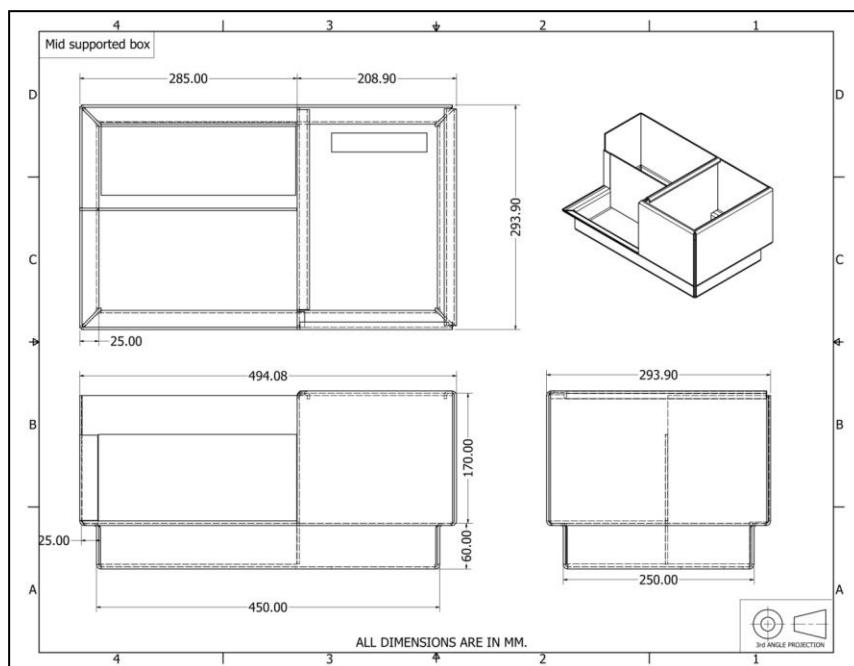


Figure 6.4 Detail drawing of mid supported box



Figure 6.5 Snapshot of mid supported box

6.5.3 Cooling Unit

The cooling unit worked on the principle of an evaporative cooling system. The cooling unit produces the cooling effect by evaporating the water in a wetted cooling pad. The cooling unit consists of a 20W air blower, 2.25 lit. water tank, 3W water pump and a wood-wool cooling pad.

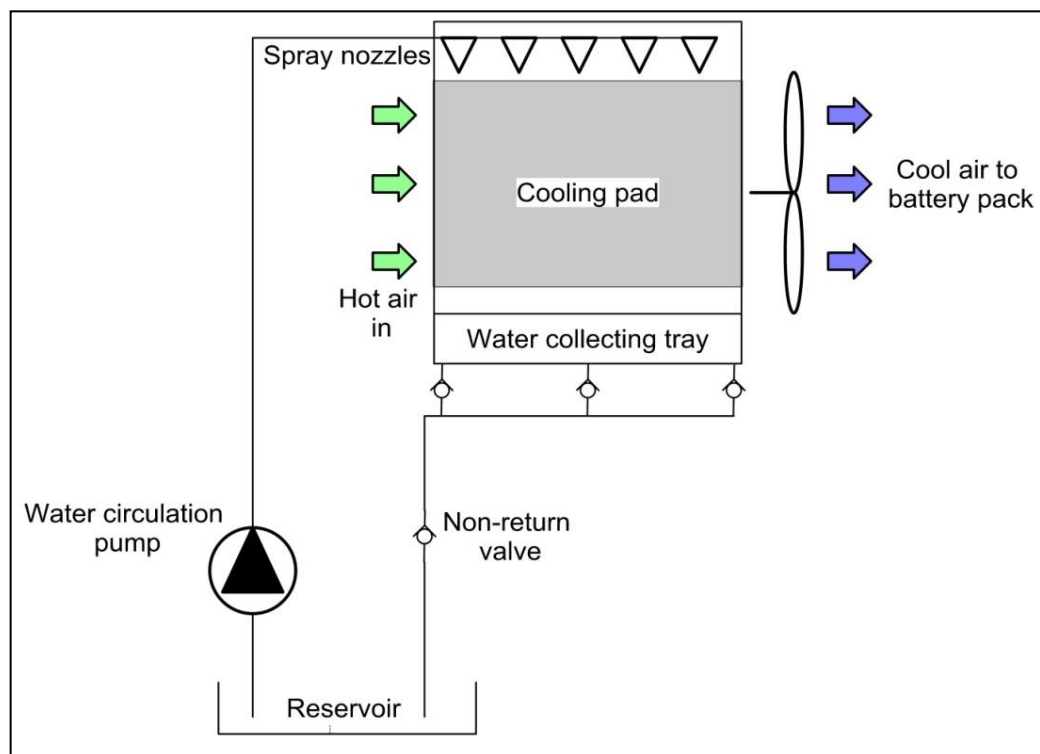


Figure 6.6 Schematic diagram of cooling unit

Detail of individual components

The cooling unit is fully compact and provides a leak-proof operation. The schematic diagram of the cooling unit is shown in Figure 6.6. The working process of the cooling unit is quite simple. A 3W submersible water pump inside the water tanks circulates the water from the tank to the cooling pad. The water in the cooling pad is circulated using 4 mm diameter polyvinyl chloride (PVC) flexible pipes. There are 0.5 mm holes in the pipes for spraying water on the wood wool cooling pad. The water from the holes is sprinkled on a cooling pad, and the place becomes wet. The cooling pad is arranged inside L – shaped metallic grill of size 350 mm x 62 mm x 85 mm. The cooling pad with grill is located on the left side corner of the cooling unit. Especially, L–shaped metallic grill is designed to take advantage of two-side air entry at the corner. The water from the cooling pad is collected inside the water collecting channel, fitted below the grill through screw joints. The inside surface of the water collecting channel is coated with an 8 mm sponge which absorbs the additional water and doesn't allow it to leak from the channel. Water from the channel is back to the tank through a 15 mm PVC piping circuit. PVC piping circuit includes 4 – elbow joints, 2 – tee joints, 1 – non-return valve, 1 – union and 1 – end cap. PVC pipes are connected with the water collecting channel through 8 – non-return valves. These non-return valves are specially designed from 8 mm dia. The copper tube is placed between the water collecting channel and PVC pipe. Non–return valves can flow the water in one direction from channel to pipe. Non–return valves have prevented the backflow of water during the jerky operating condition of e-bikes on the road. One additional non–return valve is provided in the PVC pipe near the endpoint to prevent the backflow of water from the tank to the PVC pipe. The endpoint of PCV pipe is made of a tee joint that is vertically fixed on the tank's cover. One end of the tee joint is connected to a PVC pipe from a water collecting channel through a union. A whole piping circuit connects and disconnects the tank through a union. The end cap is provided on the remaining end of the tee joint. Water can fill the water tank from end cap fitted on tee joint.

The air blower is provided after the water tank, cooling pad grill and piping circuit assembly. The centrifugal air blower is directly fitted in a mid-supported box so that the blower's suction side remains in the cooling unit and the exhaust side in the battery pack. The air blower and water pump are controlled automatically by the temperature controller provided in the control unit. Figure 6.7 and Figure 6.8 show the detail drawing of cooling unit and actual cooling unit respectively.

Development of Evaporative cooling based BTMS

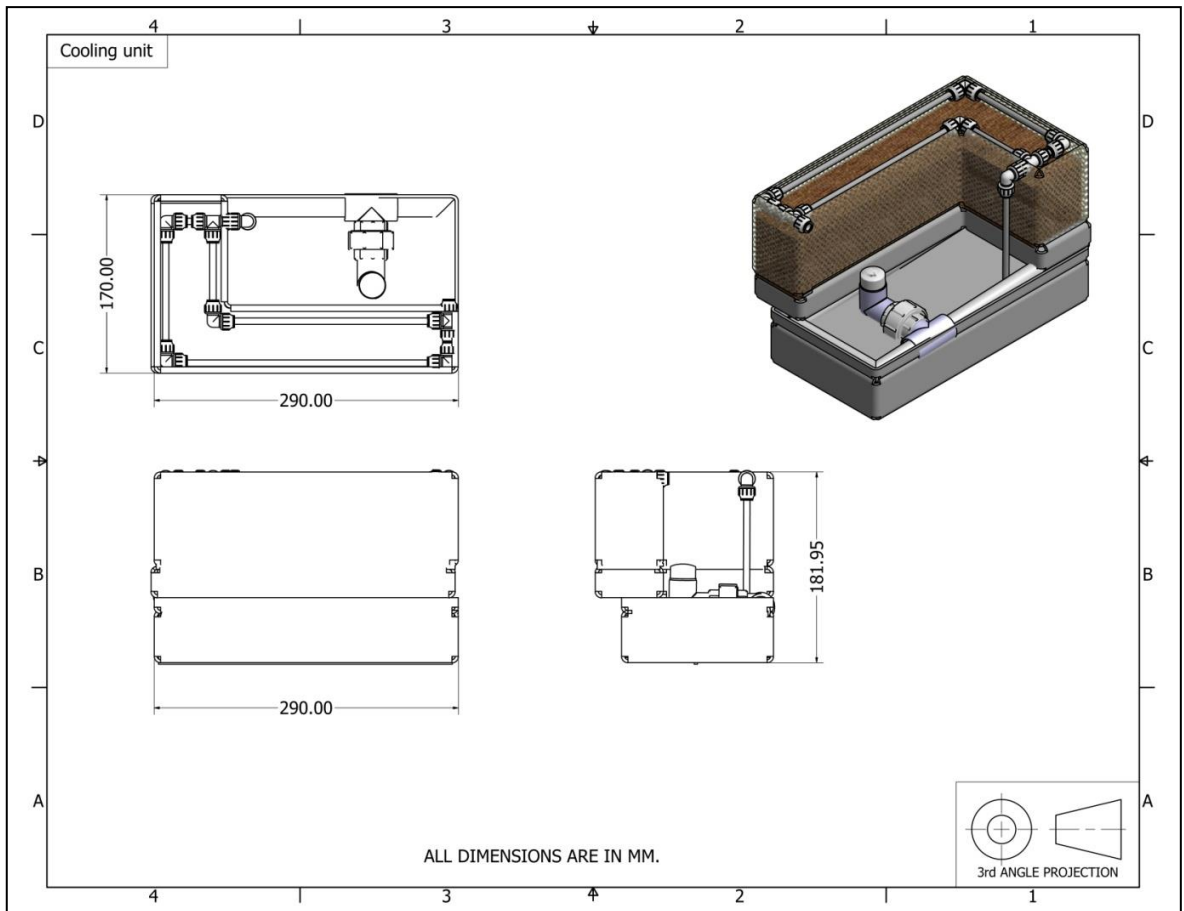


Figure 6.7 Assembly drawing of cooling unit

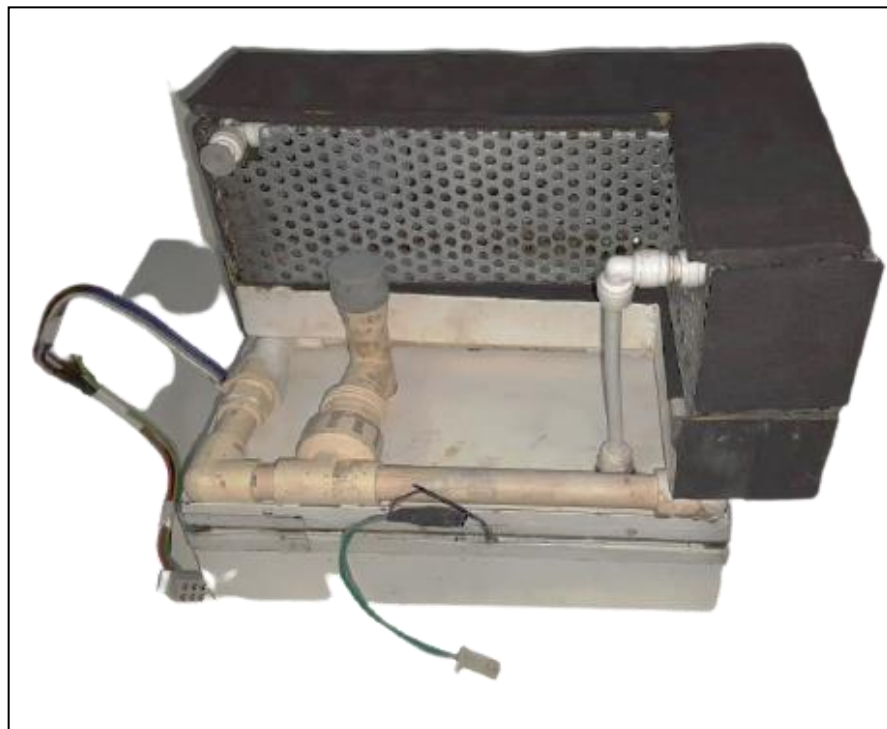


Figure 6.8 Snapshot of cooling unit

Detail of individual components

6.5.4 Control Unit

The Control unit consists of a data logger, temperature controller, water level indicator and speed regulators for the air blower and pump. All the types of equipment in the control unit and cooling unit are powered by 12V, 7Ah. VRLA battery is placed in a lower portion of a control unit. The water pump and air blower are operated on a 12V DC supply, while the data logger and temperature controller are operated with 230V, 50 Hz. AC power supply. Thus, the control unit's circuit is constructed in such a way that all of the components with DC and AC power supplies are powered by a single 12V, 7 Ah. battery. In fully charged condition, this battery can continuously run all types of equipment for up to 2 hours.

The circuit diagram of the control unit is shown in Figure 6.9. The whole circuit is divided into two sections according to the type of power supply. In the first section, the data logger and temperature controller are connected with battery through DC – AC converter. DC – AC converter is converted voltage from 12V DC to 230V AC vice – versa. So, DC – AC converter is also used as a battery charger. The transformer of DC – AC converter generates heat during the operating condition. So, one centrifugal type ventilation fan is provided on the sidewall of the control unit to dissipate the heat from the control unit during the working condition.

In another section, the battery is directly connected to the air blower and water pump in parallel to the temperature controller, as shown in Figure 6.9. Temperature controller is ON/OFF the air blower and water pump according to the surface temperature of E-bike batteries. The temperature controller consists of an electric relay and temperature sensor. The temperature controller is to sense the surface temperature of the E-bike battery by thermocouple and according to surface temperature, it operates the air blower and water pump. The temperature controller facilitates setting the temperature range as per requirement. So, the temperature controller is set with a predefined temperature range according to the optimum temperature range provided by the E-bike battery manufacturer. According to the manufacturer, the optimum battery temperature for E-bike batteries is 27°C. The temperature controller is set from 25°C to 30°C. So, it tries to maintain between 25°C to 30°C temperature of the battery. The water level indicator with 3 LED indicators, i.e., low, medium and high levels, is also provided in a control unit. The water level indicator shows the water level in a water tank with an LED indicator. The snapshot of actual control unit is displayed in Figure 6.10.

Development of Evaporative cooling based BTMS

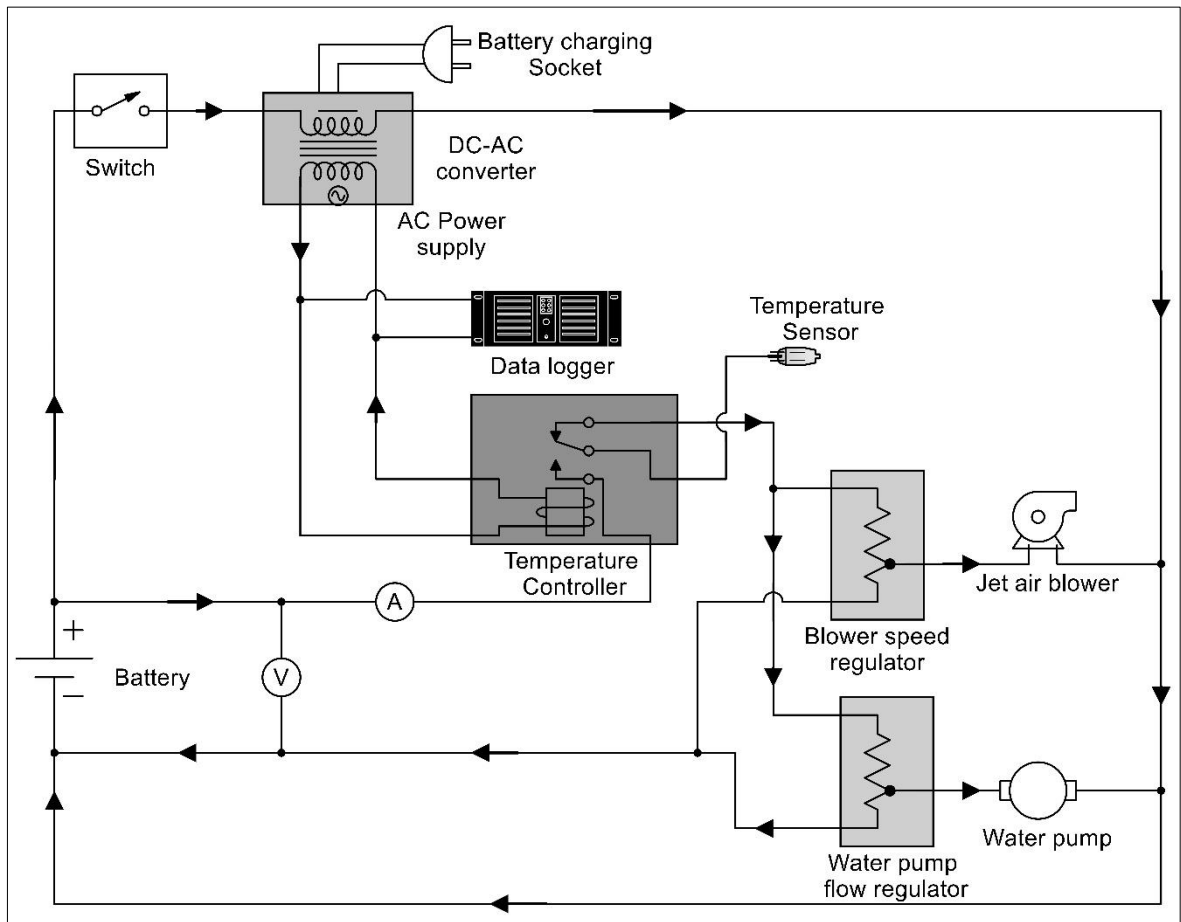


Figure 6.9 Circuit diagram of control unit



Figure 6.10 Snapshot of Control unit

Complete prototype of evaporative cooling based BTMS for E-bike

6.6 Complete prototype of evaporative cooling based BTMS for E-bike

Finally, fabricating the prototype of the battery thermal management system (BTMS) according to the design of every part. The assembly drawing of complete prototype of evaporative cooling based BTMS is shown in Figure 6.11. This BTMS help to maintain the battery temperature in E-bike close the optimum operating temperature ranges (20°C to 30°C). The BTMS operates automatically during the working condition.

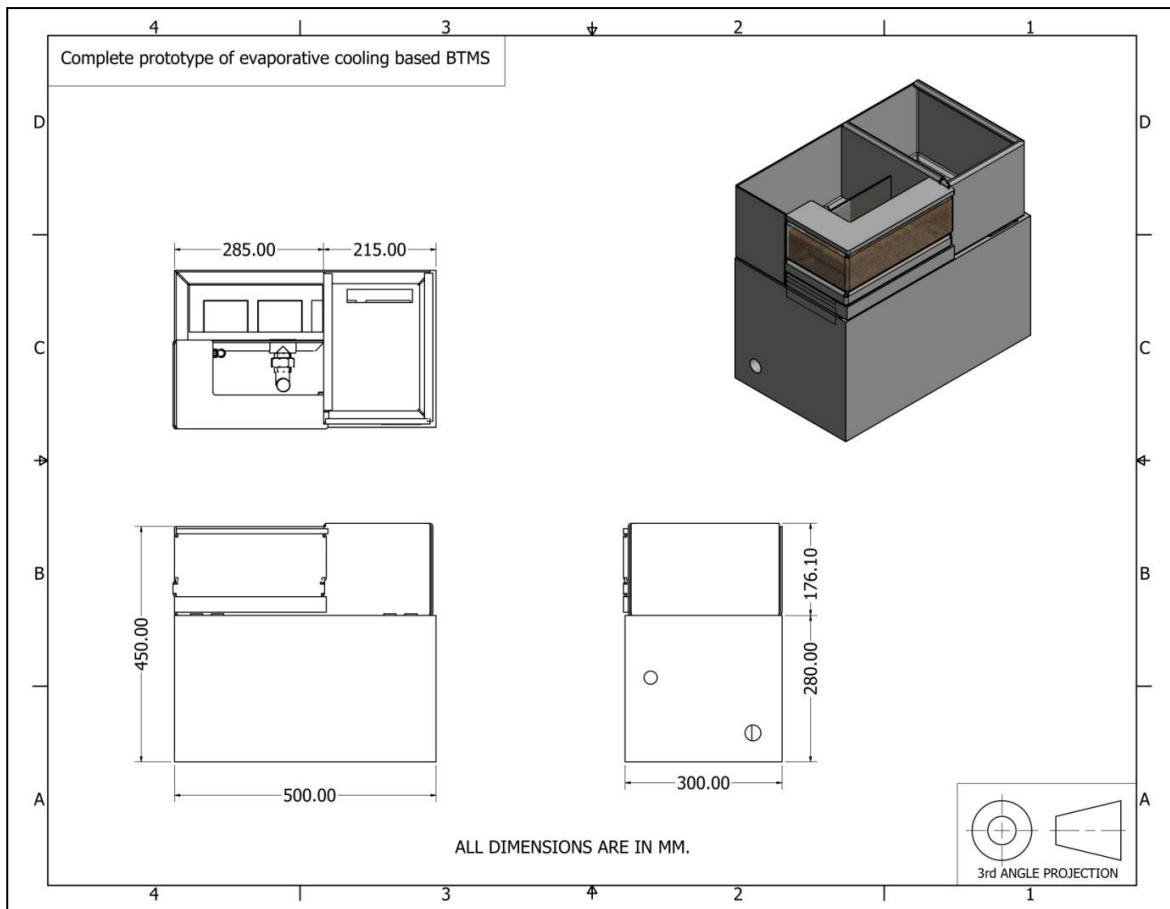


Figure 6.11 Assembly drawing of complete prototype of evaporative cooling based BTMS

Now to fulfil the design aspects, the functional design and fabrication of BTMS is done, as shown in Figure 6.12. All the components are assembled and developed into a complete system. The whole system is separated into two portions; the upper portion includes a cooling system and control unit and the lower part consists of a battery pack. The outer and inner bodies are welded, and glass wool sheets are put in space between the outer and inner bodies. The cooling system and control unit are arranged inside the mid-supported box. And the mid-supported box is air-tight and fitted on a battery pack by magnets. Here high,

Development of Evaporative cooling based BTMS

strength magnets are used for tight-fitting. As a result, the upper and lower pieces were quickly separated with each other. The names of all the fabricated parts are given in the figure. Here, the prototype of BTMS tries to make it more compact with better efficiency.



Figure 6.12 Complete prototype of evaporative cooling based BTMS

CHAPTER 7. Experimental Studies – III: Performance assessment of evaporative cooling based BTMS in field test

The final stage of BTMS development is to conduct an experimental comparison of the VRLA-powered E-bike battery pack combined with the new BTMS to a traditional battery pack. Thus, the thermal behavior of Valve Regulated Lead Acid (VRLA) batteries equipped with an evaporative cooling-based battery thermal management system (BTMS) is investigated experimentally using a field test.

7.1 Experimental setup & Instrumentation

The experimental system is separated into two components: an e-bike and a BTMS with evaporative cooling. The 500W BLDC hub motor and four 12V 25Ah VRLA batteries power the OREVA ALISH E-bike. Batteries are encased in a battery pack beneath the evaporative cooling system to avoid climatic extremes. The evaporative cooling system is adapted to meet the available area on the E-bike. It is mounted in the E-bike's leg-space, as seen in Figure 7.1.

The Khoat KH208 paperless data recorder is employed as a data management system. The data logger continuously monitors and records the surface temperature of the battery and the current supplied to the battery during operation. Figure 7.2 demonstrate the location of measuring elements and current flow direction in VRLA battery pack of E-bike. The battery pack contains four 12V, 25 Ah VRLA batteries. As illustrated in Figure 7.2, all batteries are connected in series. Four J-type thermocouples (T1, T2, T3, and T4) are affixed to the surface of the batteries. Thermocouples T5 and T6 were used to measure the air temperature at the battery pack's entrance and exit. The measurement probs for voltage (V) and current (A) are linked in parallel between battery chargers and battery packs.

Experimental Studies – III: Performance assessment of evaporative cooling based BTMS in field test

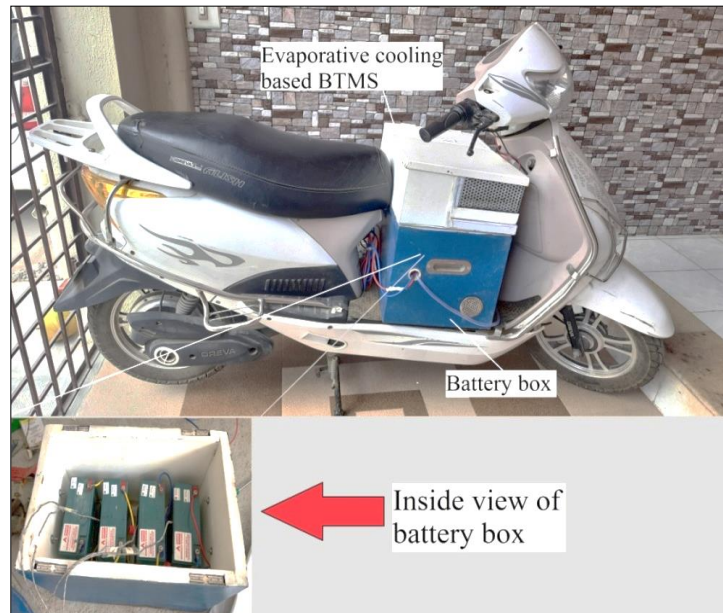


Figure 7.1 Experimental setup

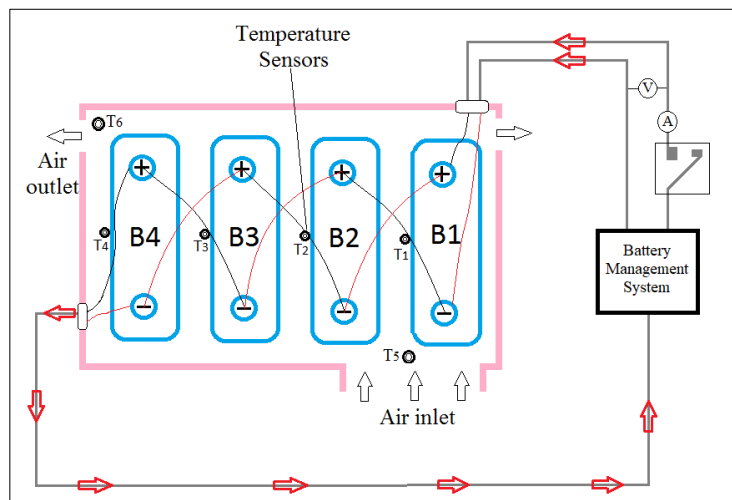


Figure 7.2 Location of measuring elements and current flow direction in VRLA battery pack of E- bike

Table 7.1 Details of instrumentation

Sr. No.	Device Name	Parameter	Symbol	Unit	Range	Accuracy
1.	J – type thermocouple	Battery temperature	T1 to T5	Celsius	0 – 750	0.1
2.	J – type thermocouple	Inlet & outlet air temperature	T6	Celsius	0 – 750	0.1
3.	Voltage measuring probe (config. through 1K Ω resistor)	Battery voltage	V	Volts	0 to 5 V	0.5
4.	Current measuring probe (using 30A ~ 70 mV shunt)	Current	I	Amp.	4 – 20 mA	0.01
5.	Sling Psychrometer	DBT & WBT	T	Celsius	-10 – 50	0.5

Experimental Studies – III: Performance assessment of evaporative cooling based BTMS in field test

7.2 Design of Experiment using full factorial method

Twelve field test-based studies were carried out by three different assessment criteria, including vehicle speed, load condition, and battery pack condition. Detail of different assessment criteria are given below in Table 7.2,

Table 7.2 Assessment criteria for field test

Vehicle Speed Mode	
Eco mode	15 km/h to 20 km/h
Power mode	30 km/h to 35 km/h
Load condition	
Without additional load	70 kg (Person) + 15 kg. (BTMS) = 85 kg.
With additional load	70 kg (Person) + 15 kg. (BTMS) + 30 kg. (Dead weight) = 115 kg.
Battery Pack condition	
With BTMS	Evaporative cooling system will be started at beginning of trip.
Precooling+ With BTMS	E-bike batteries will be precooled by evaporative cooling system for two hours before starting a trip.
Natural Convection	Batteries are allowed to cool by natural convection.

Table 7.3 shows the details of design factors with them levels. Vehicle speed, load condition and battery pack condition are three factors selected for the experimental study. Vehicle speed and load condition factors have two levels, while battery pack condition has three levels. So, the experiments are designed using the multilevel full factorial technique in MINITAB 18 (Statistical data analysis software). The factorial design allows for the investigation of all distinct combinations of factor levels during each trial of an experiment.

Table 7.3 Details of design factors with levels

Factors	Level - 1	Level - 2	Level - 3
Battery pack condition	With BTMS	Precooling + with BTMS	Natural convection
Vehicle Speed Mode	Eco mode	Power mode	--
Load condition	Without Load	With Load	--

Table 7.4 Design summary of full factorial method

Factors	3	Replicates	1
Base runs	12	Total runs	12
Base blocks	1	Total blocks	1

Experimental Studies – III: Performance assessment of evaporative cooling based BTMS in field test

Where,

Factors = 3 (Vehicle speed, load condition and battery pack condition)

Base design = 2 factors and 4 trials

Base Runs = 12 no. of trials

Replicates = 1, Replicates are no. of multiple trials with same factor and level. Increase no. of replicates increase accuracy of results.

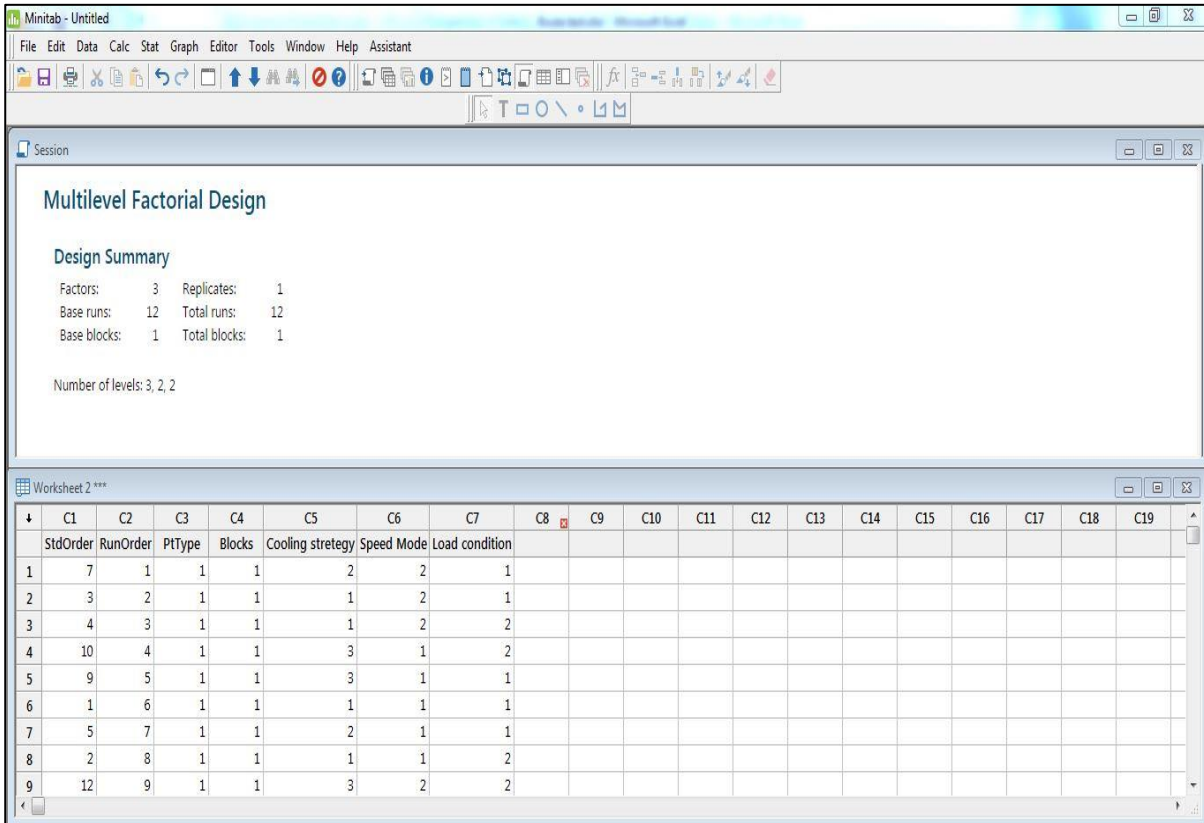


Figure 7.3 Multilevel full factorial design in Minitab with experimental matrix

Figure 7.3 represents the Multilevel full factorial design in Minitab with experimental matrix. The standard order of trials is non-randomized order of trials. Run order is the order of experiments to be performed. The third column represents the Value of a center point. Value “1” indicates the point is a corner point. If a point is “0”, the point represents the center point. Here, the Value of blocks suggests a group of experimental trials performed under relatively homogeneous conditions. Typically, blocks are used in an experimental design to reduce bias and error variance due to uncontrolled factors. The last two columns represent the levels of each factor. The levels of vehicle speed, load condition and battery pack condition are coded in the form of 1,2 and 3. Total of 12 trials are performed with different sets of experimental parameters during the field test. The simplified experimental matrix is shown in Table 7.5.

Experimental Studies – III: Performance assessment of evaporative cooling based BTMS in field test

Table 7.5 Simplified Experimental matrix

Exp. No.	Battery pack condition	Load condition	Vehicle Speed Mode
1	With BTMS	Without load	Eco mode
2	With BTMS	Without load	Power mode
3	With BTMS	With load	Eco mode
4	With BTMS	With load	Power mode
5	Precooling + with BTMS	Without load	Eco mode
6	Precooling + with BTMS	Without load	Power mode
7	Precooling + with BTMS	With load	Eco mode
8	Precooling + with BTMS	With load	Power mode
9	Natural Convection	Without load	Eco mode
10	Natural Convection	Without load	Power mode
11	Natural Convection	With load	Eco mode
12	Natural Convection	With load	Power mode

7.3 Experimentation

7.3.1 Detail of field test

Road tests are performed in the city of Junagadh (Gujarat), India. The trip is approximately 24 kilometers long in total. The field test route (as shown in Figure 7.4) is distinguished by substantial traffic conditions, such as extra-urban (A-B), urban (B-C), and highway (C-D) driving conditions. The detail of route for field test is given in Table 7.6. Extra-urban driving circumstances are chosen, with high traffic density and local streets. The urban driving condition route is selected from with medium traffic density and arterial streets, whereas the highway driving condition route is picked with low traffic density.

Table 7.6 Detail of route for field test

Experimental Studies – III: Performance assessment of evaporative cooling based BTMS in field test

Driving Condition	Route Characteristics	Route	Distance (one side)	Total distance
Extra urban driving	High traffic density & local streets	Giriraj main road to shamaldas gandhi town hall (A to B)	2 km x 2	4 km
Urban driving	Medium traffic density & arterial streets	Shamaldas gandhi town hall to N.R. Vekariya inst. of technology. (B to C)	2.5 km x 2	5 km
Highway driving	Low traffic density & flat road	N.R. Vekariya College to government polytechnic – Junagadh (C to D)	7.5 km x 2	15 km
			Total	24 km

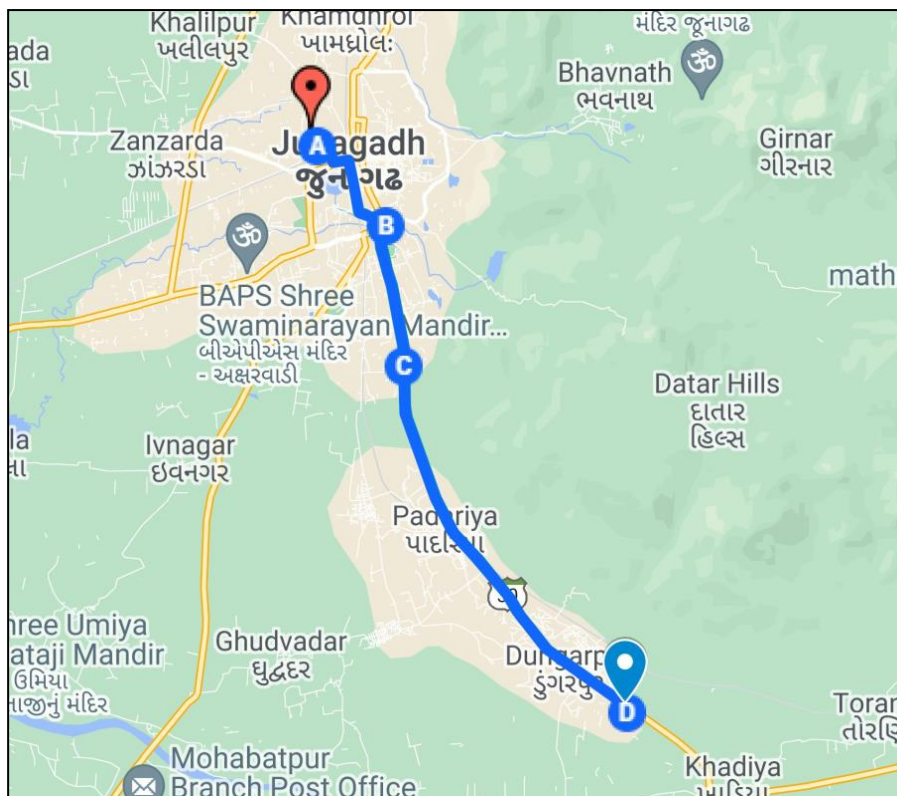


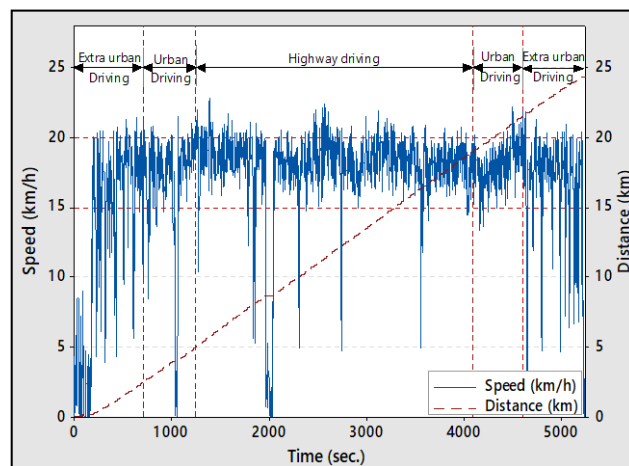
Figure 7.4 Typical route of the travelled area for road test with GPS data

(Image provided by Google map data ©2021)

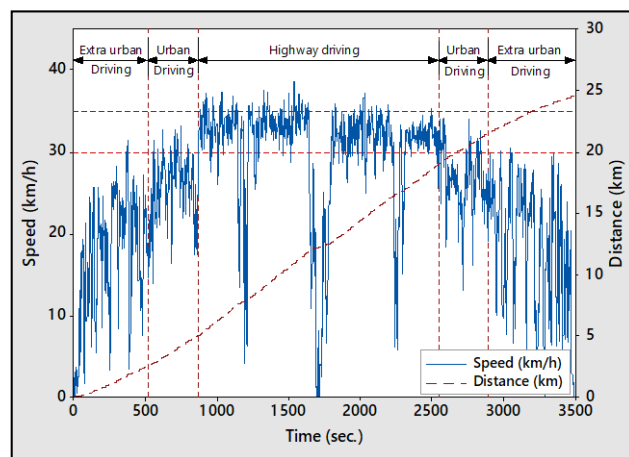
Experimental Studies – III: Performance assessment of evaporative cooling based BTMS in field test

7.3.2 Vehicle speed

Figure 7.5 illustrates the speed-time plot for E-bikes acquired from GPS tracking data in Eco and Power modes. The field test maintains an average speed of 15 to 20 km/h in eco mode. During power mode, the e-bike can reach a top speed of 35 km/h. During the urban trip in power mode, the E-bike's average speed varied between 10 and 15 km/h. Due to the high traffic density, the speed profile of the urban route indicates frequent stops. Due to high traffic density, the E-bike was driven at an average speed of 15 to 20 km/h in extra-urban and urban areas. The highway route allows an E-bike to travel faster for a longer distance. Thus, during a field test, an average speed of 30 to 35 km/h was observed along the highway route.



(a)

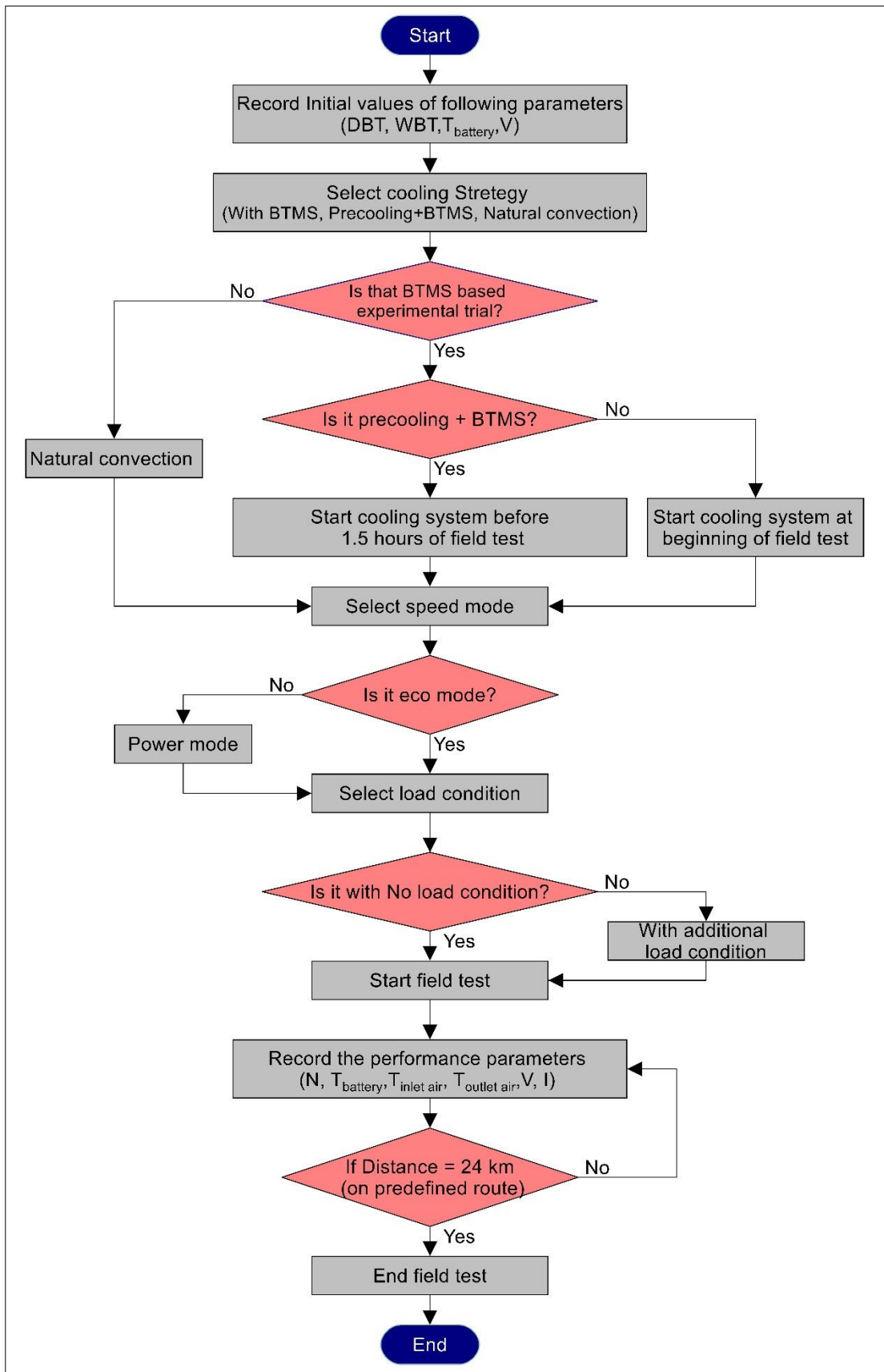


(b)

Figure 7.5 Speed Profile for (a) Eco mode & (b) Power mode

Experimental Studies – III: Performance assessment of evaporative cooling based BTMS in field test

7.4 Flow chart of field test-based experiment



CHAPTER 8. Results and Discussion

The twelve trips with different combinations of vehicle speed, load condition and battery pack condition in a field test are performed to evaluate E-bike performance with newly developed evaporative cooling-based BTMS. The field test were carried out by three different assessment criteria, including battery pack condition (With BTMS, precooling+BTMS and natural convection), vehicle speed (Eco mode and power mode) and load condition (without additional load and with additional load). Mainly, three performance parameters, i.e. battery surface temperature, energy consumption and speed of E-bike, are measured and analysed to assess the performance of the VRLA battery during the operating condition. This section initially presents the variation of battery temperature in different cooling modes, and then comparisons of the summary temperature difference data are followed. Also, results are analysed in MINITAB 18 using the general linear model.

8.1 Battery temperature profile with BTMS cooling mode

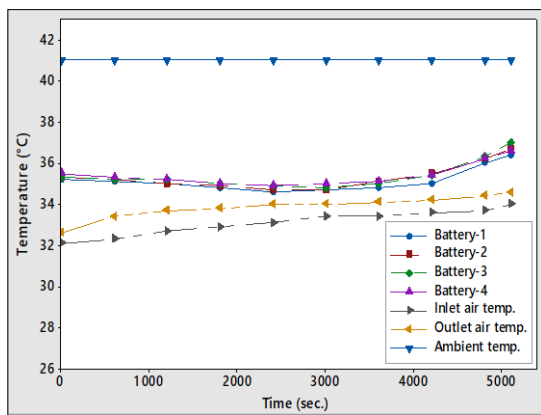
Figure 8.1 illustrates the temperature profile of VRLA batteries with BTMS cooling modes under varying speeds and loads. The individual graph demonstrates the temperature profile of each battery in an E-bike battery pack under various operating conditions. The battery temperature is observed to remain between 34°C and 36.5°C with BTMS cooling mode in eco and power modes, respectively. During each field test, the E-bike is driven approximately 24 kilometres. E-bike operation in power mode and eco mode takes about 1.5 hours and 1.3 hours, respectively. Additionally, it was noted that the battery's initial temperature was 4 to 5 degrees Celsius below the ambient temperature in both the BTMS and precooling + BTMS cooling modes. Because the E-bike batteries are constantly stored within the newly developed BTMS-based battery pack, whether the bike is operating or not. The BTMS-based battery pack wall is insulated with glass wool insulation, isolating the E-bike batteries from the surrounding environment. Due to this, the battery temperature at the beginning of the field test is lower than the ambient temperature. It is assumed that the ambient temperature remains constant throughout the entire field test.

Figure 8.1 (a) and (b) show that the ambient temperature was 41°C and 40°C, respectively, during the field test eco mode and power mode. Up to 3000 seconds, the average battery

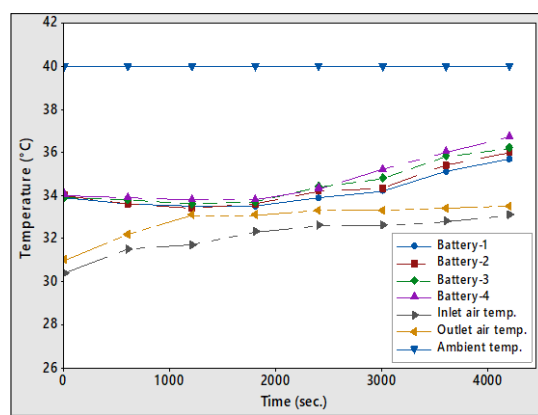
Results and Discussion

temperature gradually decreased from 35.3°C to 34.5°C. During the eco mode, it gradually rises to 36.7°C until the end of the test. During the first 1700 seconds of power mode, the battery temperature dropped slightly from 33.9°C to 33.6°C. After that, it gradually rises to 36.1°C until the test is completed. Compared to the field test in eco mode, the rate of temperature rise in the power mode has been found to be significantly higher.

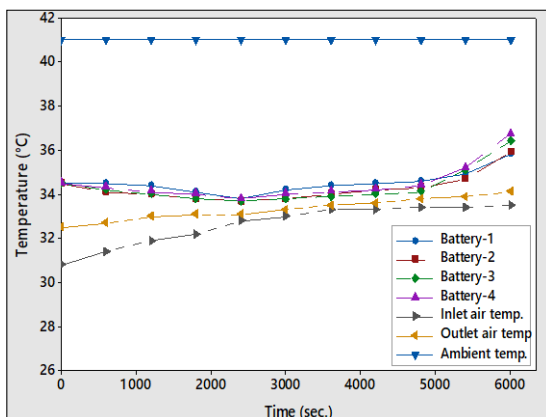
Figure 8.1 (c) and (d) show the temperature profile of the battery in eco and power modes with additional load. During field tests with eco mode and power mode, the ambient temperature was 42°C and 41°C, respectively. Up to 2500 seconds, the average battery temperature gradually decreased from 34.5°C to 33.7°C. After that, it gradually rises to 36.5°C until the end of the test in eco mode. During the first 1300 seconds of power mode, the battery temperature dropped slightly from 34.5°C to 34°C. After that, it gradually rises to 36.1°C until the test is completed. When compared to the eco mode-based field test, the rate of temperature rise in power mode is observed to be faster.



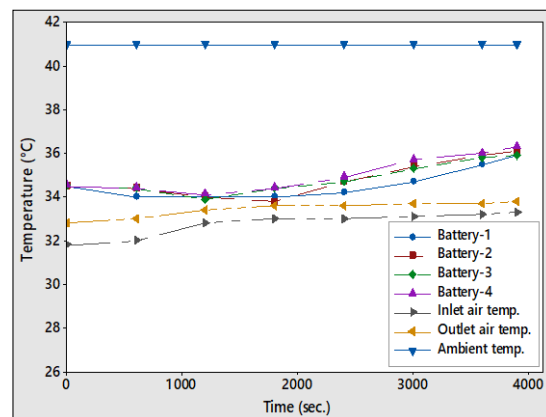
(a) Eco mode and without load



(b) Power mode and without load



(c) Eco mode and with load



(d) Power mode and with load

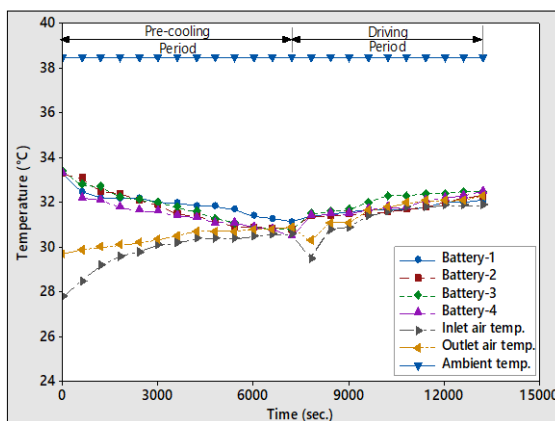
Figure 8.1 Battery temperature profiles during field test with BTMS cooling mode

8.2 Battery temperature profile with precooling+BTMS cooling mode

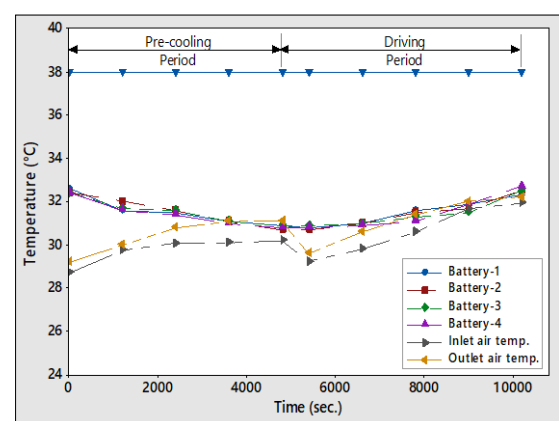
Figure 8.2 depicts the temperature profile of VRLA batteries under various speed and load conditions with precooling + BTMS cooling modes. E-bike batteries are pre-cooled for 1.5 hours before a ride using an evaporative cooling system. Precooling batteries is useful for cooling them down before starting to discharge them. At lower temperatures, the chemical reaction rate of the battery slows slightly. During operation, a slow rate of chemical reaction slows down the rate of heat generation from the battery.

Figure 8.2 (a) and (b) depict the battery temperature profile in eco and power modes and without load. During the pre-cooling period, the average battery temperature dropped from 33.3°C to 30.8°C. The average battery temperature at the start of the field test was 31°C, while the ambient temperature was around 38°C. During the E-bike field test, the battery temperature rose from 31°C to 32.5°C.

The battery temperature profile in eco & power mode and load conditions are shown in Figure 8.2 (c) and (d). The average battery temperature was seen to decrease from 32.2°C to 30.9°C during the precooling phase. The average battery temperature at the start of the field test was 31.6°C, while the outside temperature was about 37°C. During the field test of the E-bike in both the eco and power modes, the battery temperature increased from 31.6°C to 33.5°C. The rate of increase of battery temperature during a field test with precooling + BTMS mode is noted to be slower than with simply BTMS cooling mode. It was demonstrated that when the battery operates at a lower temperature, the heat generation rate is lowered.

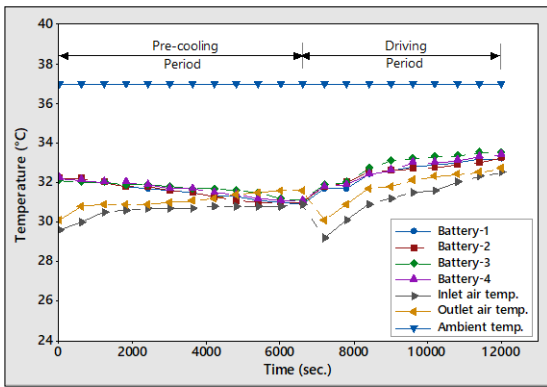


(a) Eco mode and without load

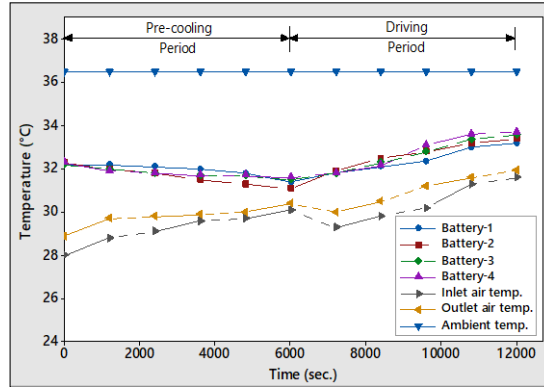


(b) Power mode and without load

Results and Discussion



(c) Eco mode and with load

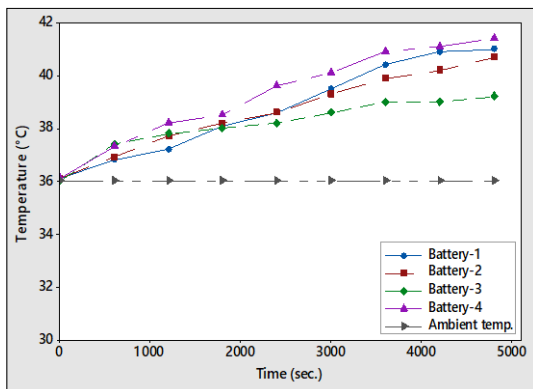


(d) Power mode and with load

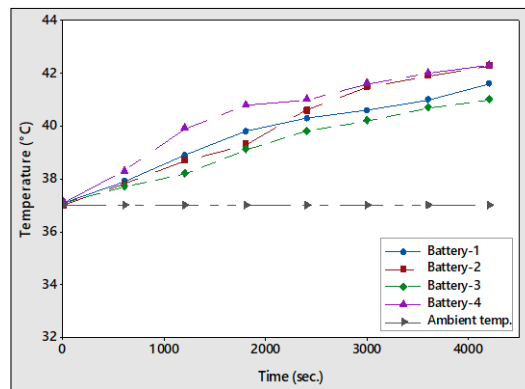
Figure 8.2 Battery temperature profiles during field test with precooling + BTMS cooling mode

8.3 Battery temperature profile with natural convection cooling mode

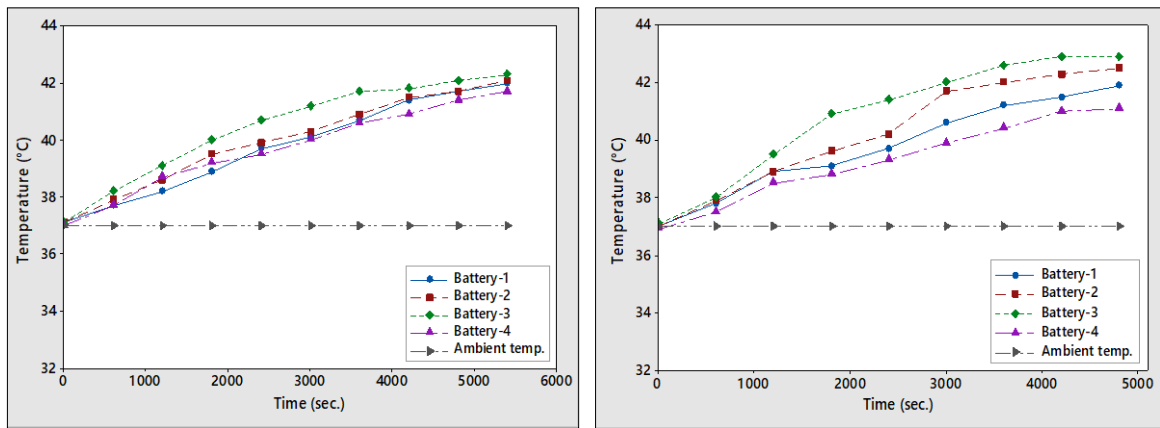
Figure 8.3 illustrates the temperature profile of VRLA batteries with natural convection cooling modes at various speeds and loads. As part of this experiment, the batteries were installed in the standard location below the seat compartment of the E-bike, allowing them to cool naturally by convection. The traditional method for cooling down E-bike batteries during operation is natural convection-based battery cooling. In E-bikes, the battery compartment is surrounded by louvres that allow the battery to be cooled down by convection while in operation. This experiment evaluates battery performance with and without BTMS employing evaporative cooling. As depicted in Figure 8.3, the temperature of battery – 3 has been rapidly growing since the beginning of the field test, whereas the rate of increase for the remaining three batteries has been relatively modest. At the completion of each experiment, the surface temperature of the battery-3 reaches a maximum value. Batteries 3 is kept in the centre of the battery pack, where air circulation and cooling rates are significantly reduced, resulting in a high rate of temperature rise.



(a) Eco mode and without load



(b) Power mode and without load



(c) Eco mode and with load

(d) Power mode and with load

Figure 8.3 Battery temperature profiles during field test with natural convection cooling mode

8.4 Comparison of individual battery temperature ranges

Figure 8.4 illustrates the temperature range for separate batteries with varied cooling mechanisms. The average battery temperature remained between 31.4°C and 33.5°C, 32.7°C and 36.7°C, and 36.1°C and 42.1°C, respectively, throughout pre-cooling + BTMS, with BTMS, and natural convection cooling modes. All batteries used in the pre-cooling + BTMS and With BTMS cooling modes have a temperature range roughly 6°C smaller than the temperature range observed in natural convection cooling mode. The temperature variation is the smallest in the pre-cooling + BTMS cooling mode, at 1.6°C. It demonstrates that pre-cooling combined with BTMS cooling mode provides a more effective cooling effect and temperature uniformity than BTMS alone or natural convection alone.

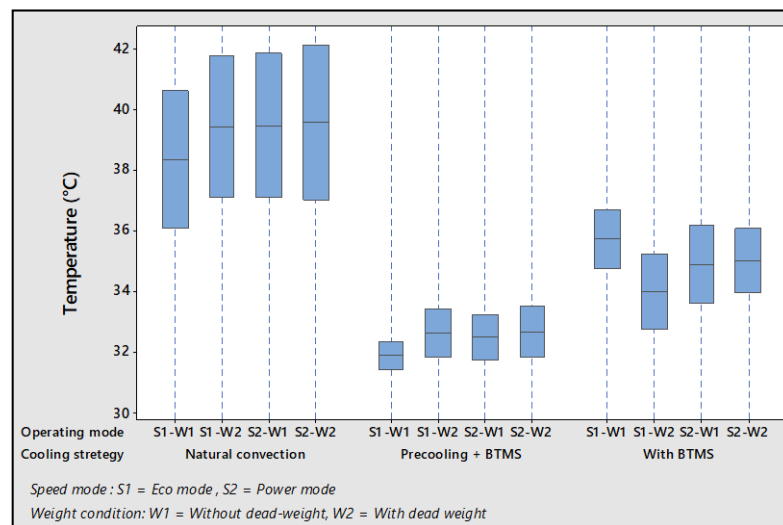


Figure 8.4 Comparison of temperature ranges for individual batteries during field tests with different cooling modes

Results and Discussion

8.5 Comparison of individual battery temperature difference from ambient condition

Figure 8.5 illustrates the average temperature difference from ambient for individual batteries using various cooling strategies. During the road tests with BTMS and pre-cooled + BTMS cooling mode, the average temperature of the batteries remained 5°C and 6°C below the ambient temperature, respectively. During natural convection, the average temperature of the batteries remained 2.5 °C above the ambient temperature. Thus, it has been demonstrated that natural convection alone is insufficient for battery cooling; evaporative cooling-based BTMS provides adequate cooling and keeps the battery temperature below ambient levels during the operating condition.

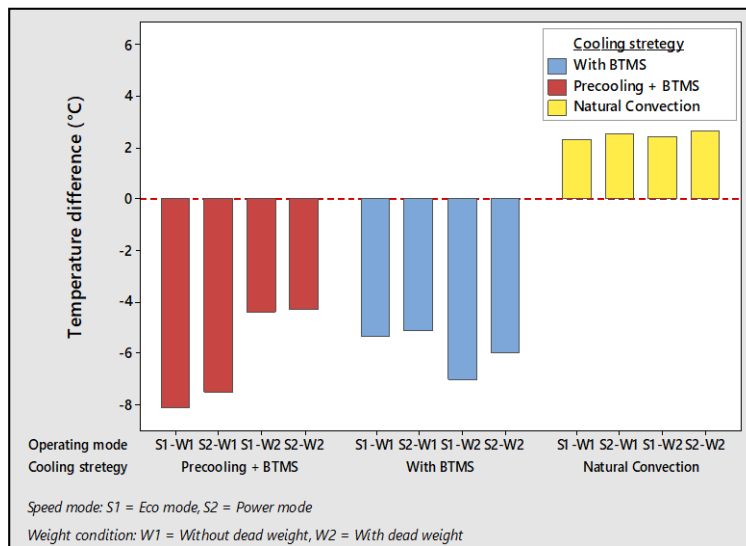


Figure 8.5 Comparison of average temperature difference from ambient condition during charging process with different cooling modes

8.6 Total energy consumption in field test with different cooling mode

Figure 8.6 illustrates the E-bike's energy consumption during a field test with various cooling modes. A box plot is used to demonstrate the graphical analysis of energy consumption during field tests with various cooling techniques. The box plot represents the range of energy consumption along the Y-axis with a maximum, minimum, and mean value. During the field test, the overall energy consumption maintained between 11.3 and 11.9 Wh/km with different cooling methods. In the field test with precooling + BTMS cooling mode, the lowest energy usage of 11.4 Wh/km was observed. At the same time, the field test with natural convection cooling mode reveals the highest total energy usage of 11.8 Wh/km.

Thus, it was evidenced that precooling batteries contributes in reducing total energy consumption under operational conditions.

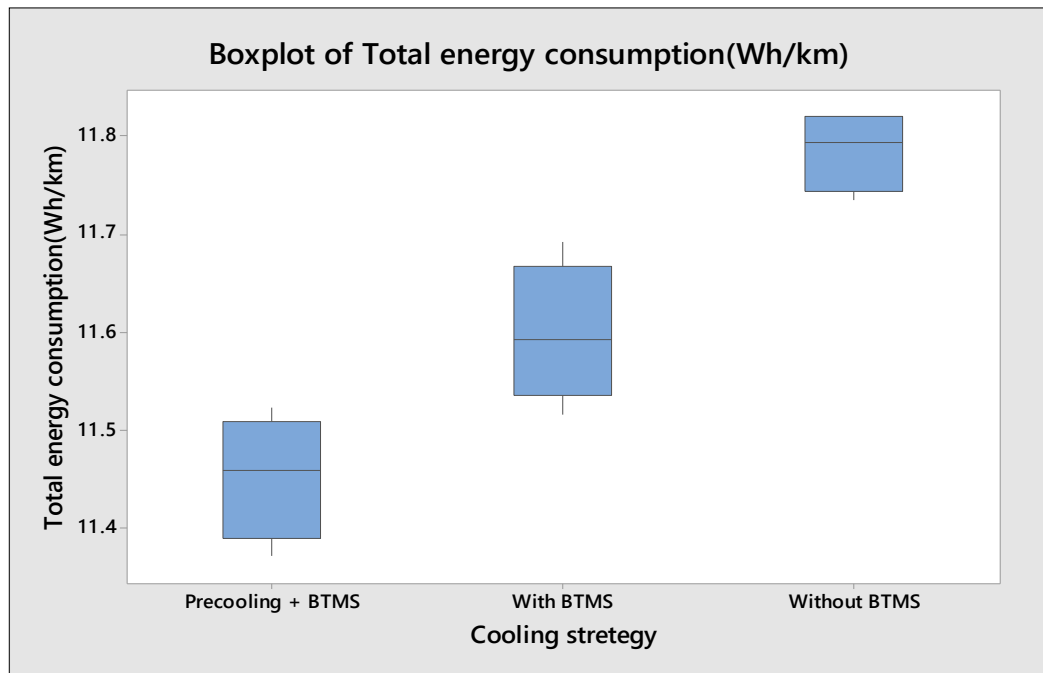


Figure 8.6 Total energy consumption by E-bike with different cooling modes

8.7 Analysis of full factorial design

The Analysis of Variance (ANOVA) is performed to see if the design parameters are statistically correlated to the response values. The general linear model is used to analyse the predictors and response value in this case. The general linear model is an ANOVA method that employs a least squares regression approach to characterize the statistical relationship between a continuous response variable and one or more predictors. The temperature difference is a response value in this case, while the cooling method, speed mode, and load conditions are predictors. The general linear model investigates the impact of Cooling technique, speed mode, and load conditions on battery temperature under operational conditions. Cooling strategy, speed mode, and load condition each have three, two, and two levels. MINITAB 18 Statistical data analysis software is used to perform the ANOVA. The generic linear model for temperature difference vs cooling technique, speed mode, and load condition is shown in Figure 8.7. The ANOVA output is displayed in the form of a table. In ANOVA, the P-Value is utilised to determine whether a difference in means is statistically significant. If the P-value is less than or equal to the α – level (0.005), then design parameters or factors have a significant effect on the response. If the P- value is greater than the α –

Results and Discussion

level, factors have no significant effect on the response. It is evident that the P-value of the cooling approach is lower than the α – level (0.005). Thus, the cooling method has a significant impact on the temperature difference as compared to the speed mode and load condition. The coefficient of determination (R^2) represents the total percentage of variance in response to the parameters specified in the model. The coefficient of determination (R^2) demonstrates that 98.83% of the fluctuation in temperature difference is related to the cooling strategy.

Factor	Type	Levels	Values
Cooling strategy	Fixed	3	1, 2, 3
Speed mode	Fixed	2	1, 2
Load condition	Fixed	2	1, 2

Source	DF	Adj SS	Adj MS	F-Value	P-Value
Cooling strategy	2	23.9860	11.9930	191.61	0.000
Speed mode	1	0.2127	0.2127	3.40	0.108
Load condition	1	0.1639	0.1639	2.62	0.150
Error	7	0.4381	0.0626		
Total	11	24.8008			

S	R-sq	R-sq(adj)	R-sq(pred)
0.250183	98.23%	97.22%	94.81%

Figure 8.7 General Linear Model: ΔT versus Cooling strategy, Speed mode & load condition in MINITAB18

Figure 8.8 shows the residual plots for the difference in temperature based on the predictors cooling strategy, speed mode, and load condition. In ANOVA, residual plots are used to assess the quality of fit. The following figure depicts the normal probability plot, residual versus fits plot, histogram plot, and residual vs order plot. In ANOVA, residual plots are used to assess the quality of fit.

The normal probability plot is used to confirm that the residuals are normally distributed. The residuals in normal probability plot should close to a straight line. The p-values may be

inappropriate if the residuals do not adhere to a normal distribution. The normal probability map forecasts the temperature difference based on the cooling technique, speed mode, and load situation. The residual is plotted on the Y-axis and the fitted values are plotted on the X-axis in a versus fits graph. The versus fits graph is used to validate the assumption that residuals have a random distribution and constant variance. Normally, the points should be scattered at random on both sides of the 0 line. If the point is far from the zero line, it could be an outlier. The residuals histogram plot is used to identify outliers and skewed data. If a large tail in one direction is found in a histogram, the data is skewed. When a histogram shows a large tail in one direction, the data is skewed. A bar in a histogram that is significantly apart from the other bars represents outlier data. The versus order plot demonstrates the residual variation between observation runs. Based on the analysis, it can be seen that the full factorial experiment design is linear.

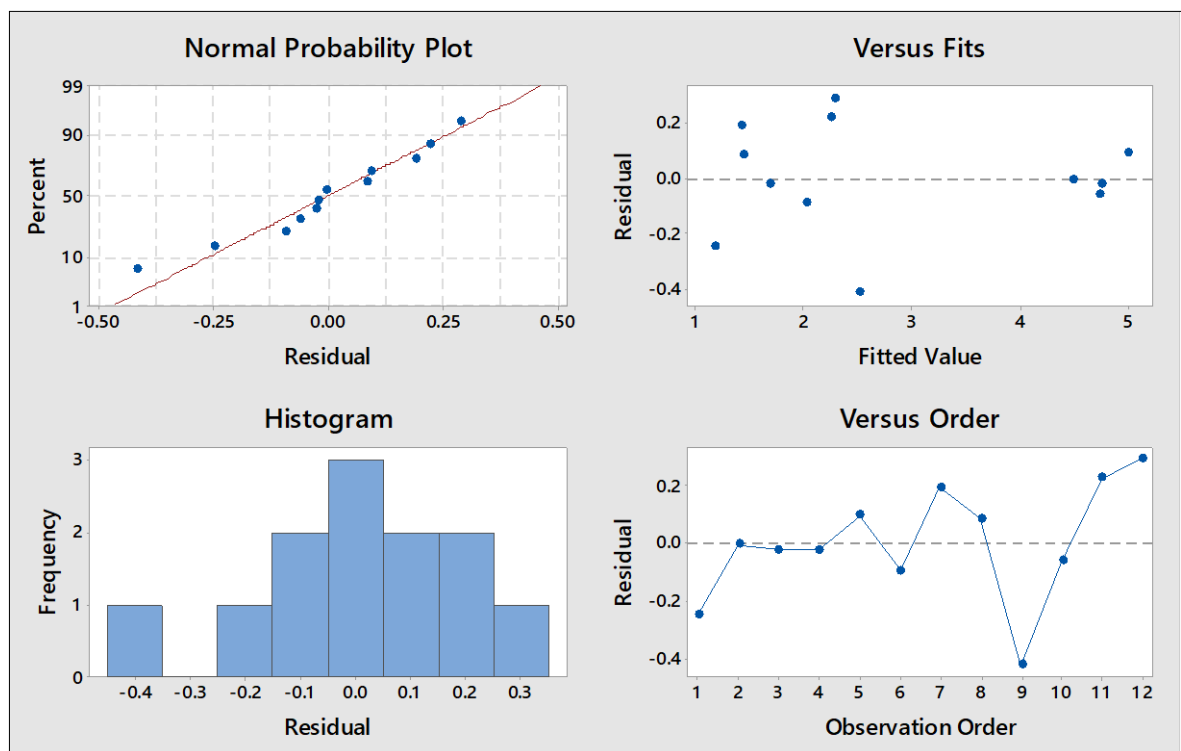


Figure 8.8 Residual plots for temperature difference

CHAPTER 9. Conclusions and Future scope

9.1 Conclusions

In the present research, a Battery Thermal Management System (BTMS) for VRLA batteries used in E-bike is developed step by step using a systematic approach. Initially, an experimental study of the behaviour of VRLA batteries at various operating temperatures was conducted. According to the experimental results, capacity and discharge back up are seen to be greater at higher temperatures, whereas internal resistance is higher at low temperatures. Afterwards, the highest temperature reached by the VRLA batteries was determined when the E - bike is operating under the adverse conditions. The Field tests are performed to assess the performance of valve-regulated lead acid batteries in E-bikes under a variety of road and weather situations. All sets of field tests are classified by route (urban route, gradient route, highway route, and rural route) and time of day (morning, afternoon, and evening). All experiments are carried out with both old and new battery sets in order to conduct a full examination of the performance of batteries in various states of health. According to the results of the field tests.

- The battery temperature rises rapidly in the afternoon. The VRLA battery in the E-bike reached the highest temperature of 45.4°C when the ambient temperature was 39.7°C.
- It was also discovered that the route pattern has a significant impact on the energy consumption of the E-bike. The gradient route has the highest energy consumption of 15.05 Wh/km.

Thus, during warmer seasons, the available cooling scheme in E-bikes is insufficient to keep the VRLA batteries cool. To keep the temperature within the optimal temperature range, an additional battery thermal management device is necessary.

In the following phase, the BTMS was then designed using evaporative cooling based on the heat generated at highest temperature reached by the VRLA batteries in the E-bike during the field test. Finally, experiments were conducted to determine the thermal performance of a VRLA battery pack using three types of operating condition: With BMTS, pre-cooling + BTMS, and without BTMS in field tests. The experimental findings of field tests with

Conclusions and Future scope

various operating condition are compared and analysed. The major conclusions are as follows:

- Significantly lower temperatures and temperature differences were recorded in the VRLA battery when employing the pre-cooling + BTMS cooling mode. During the field tests with pre-cooled + BTMS cooling mode, the average temperature of the batteries remained 5°C below the ambient condition (37°C).
- Temperature rise could be kept limited to 1.6°C during a road test and charging with pre-cooling + BTMS cooling mode.

Thus, it is shown in the current work that pre-cooling + BTMS cooling mode is the most effective technique for cooling of VRLA battery pack and helps to keep battery temperature closer to its optimum temperature range.

9.2 Future scope

Due to limitation and time and resources, the field tests with evaporative cooling system were conducted by keeping the system in foot-rest area. Efforts should be done to design the E-bike and the cooling system such that all components can be integrated inside. Further research may lead to the creation of a battery thermal management system based on evaporative cooling that can be easily implemented in electric cars.

CHAPTER 10. List of References

- [1] “UC Berkeley Earlier Faculty Research Title Transportation in Developing Countries: An Overview of Greenhouse Gas Reduction Strategies.” [Online]. Available: www.pewclimate.org
- [2] S. Ahmad and J. A. Puppim de Oliveira, “Determinants of urban mobility in India: Lessons for promoting sustainable and inclusive urban transportation in developing countries,” *Transp Policy (Oxf)*, vol. 50, 2016, doi: 10.1016/j.tranpol.2016.04.014.
- [3] S. Khalili, E. Rantanen, D. Bogdanov, and C. Breyer, “Global transportation demand development with impacts on the energy demand and greenhouse gas emissions in a climate-constrained world,” *Energies (Basel)*, vol. 12, no. 20, 2019, doi: 10.3390/en12203870.
- [4] U. S. E. I. Administration, “International Energy Outlook 2019 with projections to 2050,” *Choice Reviews Online*, 2019, doi: 10.5860/CHOICE.44-3624.
- [5] World Energy Council (WEC) and Paul Scherrer Institute, “World Energy Scenarios 2019,” *WEC publications*, 2019.
- [6] IPCC, “{Intergovernmental panel on climate change} Fifth Assessment Report: Climate Change 2014 (AR5),” *Climate change 2007: Synthesis report*. 2014.
- [7] K. Pietrzak and O. Pietrzak, “Environmental Effects of Electromobility in a Sustainable Urban Public Transport,” *Sustainability*, vol. 12, no. 3, p. 1052, Feb. 2020, doi: 10.3390/su12031052.
- [8] A. Emadi, “Transportation 2.0,” *IEEE Power and Energy Magazine*, vol. 9, no. 4, pp. 18–29, Jul. 2011, doi: 10.1109/MPE.2011.941320.
- [9] A. Perujo, C. Thiel, and F. Nemry, “Electric Vehicles in an Urban Context: Environmental Benefits and Techno-Economic Barriers,” in *Electric Vehicles â€“ The Benefits and Barriers*, 2011. doi: 10.5772/20760.
- [10] K. Pietrzak and O. Pietrzak, “Environmental effects of electromobility in a sustainable urban public transport,” *Sustainability (Switzerland)*, vol. 12, no. 3, 2020, doi: 10.3390/su12031052.
- [11] P. Andrada, B. Blanqué, E. Martinez, M. Torrent, J. A. Sanchez, and J. I. Perat, “Electric drives for light e-scooters,” *Renewable Energy and Power Quality Journal*, pp. 861–865, Mar. 2013, doi: 10.24084/repq11.471.
- [12] K. Vitols and E. Poiss, “Development of Electric Scooter Battery Pack Management System,” in *2018 IEEE 59th International Scientific Conference on Power and Electrical Engineering of Riga Technical University (RTUCON)*, 2018, pp. 1–5. doi: 10.1109/RTUCON.2018.8659908.

- [13] R. Nocerino, A. Colorni, F. Lia, and A. Luè, “E-bikes and E-scooters for Smart Logistics: Environmental and Economic Sustainability in Pro-E-bike Italian Pilots,” *Transportation Research Procedia*, vol. 14, pp. 2362–2371, 2016, doi: <https://doi.org/10.1016/j.trpro.2016.05.267>.
- [14] “Electric Scooter and Motorcycle Market by Vehicle Type, Battery Type, Distance Covered, Voltage, Technology Region - Global Forecast to 2027,” 2019. [Online]. Available: https://www.reportlinker.com/p05796719/?utm_source=PRN
- [15] “India Electric Scooter and Motorcycle Market 2019-2025,” 2019. [Online]. Available: <https://mobilityforesights.com/product/india-electric-scooter-and-motorcycle-market/>
- [16] P. G. Patil, “Advanced battery technology for electric two-wheelers in the people’s Republic of China.,” *Argonne National Laboratory*, 2009.
- [17] E. Fishman and C. Cherry, “E-bikes in the Mainstream: Reviewing a Decade of Research,” *Transp Rev*, vol. 36, no. 1, 2016, doi: 10.1080/01441647.2015.1069907.
- [18] R. H. Newman, “Advantages and disadvantages of valve-regulated, lead/acid batteries,” *J Power Sources*, vol. 52, no. 1, pp. 149–153, 1994, doi: [https://doi.org/10.1016/0378-7753\(94\)01940-1](https://doi.org/10.1016/0378-7753(94)01940-1).
- [19] D. Berndt, “VRLA batteries, advances and limitations,” *J Power Sources*, vol. 154, no. 2, pp. 509–517, 2006, doi: <https://doi.org/10.1016/j.jpowsour.2005.10.083>.
- [20] P. Casasso, A. Fratta, G. Giraud, P. Guglielmi, F. Villata, and G. Franceschini, “Feasibility, test and novel design of battery packs for EV Scooter,” in *IECON Proceedings (Industrial Electronics Conference)*, 2003, vol. 2. doi: 10.1109/IECON.2003.1280305.
- [21] C. H. Chao and J. J. Shieh, “A extended-range hybrid powered scooter,” in *IET Conference Publications*, 2012, vol. 2012, no. 592 CP. doi: 10.1049/cp.2012.0355.
- [22] V. Jegadeesan, M. P.S., and V. Seetharaman, “PERFORMANCE ANALYSIS OF VRLA BATTERIES UNDER CONTINUOUS OPERATION,” *Int J Res Eng Technol*, vol. 3, pp. 2321–7308, Jul. 2014.
- [23] M. Donald and Devitt John, “Maintenance-free type Lead acid,” US3862861A, 1975
- [24] D. Berndt, “Valve-regulated lead-acid batteries,” *J Power Sources*, vol. 100, no. 1, pp. 29–46, 2001, doi: [https://doi.org/10.1016/S0378-7753\(01\)00881-3](https://doi.org/10.1016/S0378-7753(01)00881-3).
- [25] <http://gpbmindustry.com/en/technologies/sla>, “GPBM industries, Energy storage supplier.”
- [26] Jurgen Garche, “Advanced battery systems—the end of the lead–acid battery?,” *Physical Chemistry Chemical Physics*, pp. 356–367, Jan. 2001.
- [27] “STATIONARY VALVE REGULATED LEAD ACID BATTERIES — SPECIFICATION,” *IS 15549:2005*, Jun. 2005.

- [28] PowerThru, “Lead Acid Battery working – LIFETIME STUDY,” *Technical Paper*. 2012. doi: 10.1109/SOLI.2012.6273526.
- [29] Y. Yang, X. Hu, D. Qing, and F. Chen, “Arrhenius Equation-Based Cell-Health Assessment: Application to Thermal Energy Management Design of a HEV NiMH Battery Pack,” *Energies (Basel)*, vol. 6, no. 5, pp. 2709–2725, 2013, doi: 10.3390/en6052709.
- [30] A. Pesaran, “Battery Thermal Management in EVs and HEVs: Issues and Solutions,” *Battery Man*, vol. 43, Jul. 2001.
- [31] Y. Fan, Y. Bao, C. Ling, Y. Chu, X. Tan, and S. Yang, “Experimental study on the thermal management performance of air cooling for high energy density cylindrical lithium-ion batteries,” *Appl Therm Eng*, vol. 155, 2019, doi: 10.1016/j.applthermaleng.2019.03.157.
- [32] H. Keshan, J. Thornburg, and T. S. Ustun, “Comparison of lead-acid and lithium ion batteries for stationary storage in off-grid energy systems,” Jul. 2016, pp. 30 (7 .)-30 (7 .). doi: 10.1049/cp.2016.1287.
- [33] D. Deng, “Li-ion batteries: basics, progress, and challenges,” *Energy Sci Eng*, vol. 3, Jul. 2015, doi: 10.1002/ese3.95.
- [34] Sarah Fecht, “Article in Popular science: This is what happens inside a battery right before it explodes.,” <https://www.popsci.com/this-is-what-happens-inside-battery-before-it-explodes> .
- [35] E. & systems, S. Chemistry, “Article: Are lithium ion batteries becoming unsafe?,” <https://qnov.com/are-lithium-ion-batteries-becoming-unsafe> , Dec. 2014.
- [36] FAA Office of Security and Hazardous Materials Safety, “Aviation Cargo and Passenger Baggage Events Involving Smoke, Fire , Extreme Heat or Explosion Involving Lithium Batteries or Unknown Battery Types,” May 2017.
- [37] David E. Guberman, “Lead - Mineral Commodity Summaries,” *U.S. Geological Survey*, Jan. 2017.
- [38] Brian W. Jaskula, “Lithium - Mineral Commodity Summaries,” *U.S. Geological Survey*, Jan. 2018.
- [39] J. E. S. A.-H. Greg Albright, “A Comparison of Lead Acid to Lithium-ion in Stationary Storage Applications,” Mar. 2012.
- [40] L. Gaines, “The future of automotive lithium-ion battery recycling: Charting a sustainable course,” *Sustainable Materials and Technologies*, vol. 1–2, pp. 2–7, 2014, doi: <https://doi.org/10.1016/j.susmat.2014.10.001>.
- [41] Battery University, “Article: Battery Recycling as a Business,” http://batteryuniversity.com/learn/article/battery_recycling_as_a_business .
- [42] J. Weinert, A. Burke, and X. Wei, “Lead-acid and lithium-ion batteries for the Chinese electric bike market and implications on future technology advancement,” *Journal of*

- Power Sources - J POWER SOURCES*, vol. 172, pp. 938–945, Jul. 2007, doi: 10.1016/j.jpowsour.2007.05.044.
- [43] “India Electric Two-Wheeler Market, By Vehicle Type, By Battery type, By Voltage, By Technology, By Region; Size and Forecast, 2014-2025,” Noida, U. P. (INDIA), 2018. [Online]. Available: <https://www.blueweaveconsulting.com/india-electric-two-wheeler-market>
- [44] el Dorado Weather, “World climate forecast dictionary,” <http://www.eldoradocountyweather.com/>.
- [45] D. Valkovska, M. Dimitrov, T. Todorov, and D. Pavlov, “Thermal behavior of VRLA battery during closed oxygen cycle operation,” *J Power Sources*, vol. 191, no. 1, 2009, doi: 10.1016/j.jpowsour.2008.10.014.
- [46] C. Hoff and K. Steeves, “NEW INSIGHTS INTO THERMAL RUNAWAY OF VALVE REGULATED LEAD-ACID BATTERIES,” Jul. 2005.
- [47] A. Kirchev and D. Pavlov, “Influence of temperature and electrolyte saturation on rate and efficiency of oxygen cycle in VRLAB,” *J Power Sources*, vol. 162, no. 2 SPEC. ISS., 2006, doi: 10.1016/j.jpowsour.2005.07.008.
- [48] HUTCHINSON RONDA, “TEMPERATURE EFFECTS ON SEALED LEAD ACID BATTERIES AND CHARGING TECHNIQUES TO PROLONG CYCLE LIFE,” California, 2004. [Online]. Available: <https://prod-ng.sandia.gov/techlib-noauth/access-control.cgi/2004/043149.pdf>
- [49] D. Berndt *et al.*, “Characterization of nano-lead-doped active carbon and its application in lead-acid battery,” *J Power Sources*, vol. 195, no. 1, 2015.
- [50] D. Berndt and E. Meissner, “Gas evolution and thermal behaviour of valve regulated lead acid batteries under abnormal operational conditions,” in *12th International Conference on Telecommunications Energy*, 1990, pp. 148–154. doi: 10.1109/INTLEC.1990.171240.
- [51] A. Pesaran, A. Vlahinos, and S. D. Burch, “Thermal Performance of EV and HEV Battery Modules and Packs,” *Fourteenth International Electric Vehicle Symposium*, no. September. 1997.
- [52] M. R. Cosley and M. P. Garcia, “Battery thermal management system,” in *INTELEC 2004. 26th Annual International Telecommunications Energy Conference*, 2004, pp. 38–45. doi: 10.1109/INTLEC.2004.1401442.
- [53] X. Yu, Z. Lu, L. Zhang, L. Wei, X. Cui, and L. Jin, “Experimental study on transient thermal characteristics of stagger-arranged lithium-ion battery pack with air cooling strategy,” *Int J Heat Mass Transf*, vol. 143, 2019, doi: 10.1016/j.ijheatmasstransfer.2019.118576.
- [54] Y. Bao, Y. Fan, Y. Chu, C. Ling, X. Tan, and S. Yang, “Experimental and Numerical Study on Thermal and Energy Management of a Fast-Charging Lithium-Ion Battery Pack

- with Air Cooling,” *Journal of Energy Engineering*, vol. 145, no. 6, 2019, doi: 10.1061/(asce)ey.1943-7897.0000631.
- [55] Z. Qian, Y. Li, and Z. Rao, “Thermal performance of lithium-ion battery thermal management system by using mini-channel cooling,” *Energy Convers Manag*, vol. 126, 2016, doi: 10.1016/j.enconman.2016.08.063.
- [56] Z. Zhang and K. Wei, “Experimental and numerical study of a passive thermal management system using flat heat pipes for lithium-ion batteries,” *Appl Therm Eng*, vol. 166, 2020, doi: 10.1016/j.applthermaleng.2019.114660.
- [57] A. Rahman, H. Ahmed, and M. N. A. Hawlader, “Noble Evaporative Battery Thermal Management System for EVs/HEVs,” 2014.
- [58] H. Behi *et al.*, “Novel thermal management methods to improve the performance of the Li-ion batteries in high discharge current applications,” *Energy*, vol. 224, 2021, doi: 10.1016/j.energy.2021.120165.
- [59] F. Samimi, A. Babapoor, M. Azizi, and G. Karimi, “Thermal management analysis of a Li-ion battery cell using phase change material loaded with carbon fibers,” *Energy*, vol. 96, pp. 355–371, 2016, doi: <https://doi.org/10.1016/j.energy.2015.12.064>.
- [60] Z. Ling, F. Wang, X. Fang, X. Gao, and Z. Zhang, “A hybrid thermal management system for lithium ion batteries combining phase change materials with forced-air cooling,” *Appl Energy*, vol. 148, pp. 403–409, 2015, doi: <https://doi.org/10.1016/j.apenergy.2015.03.080>.
- [61] S. Al-Hallaj, R. Kizilel, A. Lateef, R. Sabbah, M. Farid, and J. R. Selman, “Passive thermal management using phase change material (PCM) for EV and HEV Li-ion batteries,” in *2005 IEEE Vehicle Power and Propulsion Conference*, 2005, pp. 5 pp.-. doi: 10.1109/VPPC.2005.1554585.
- [62] S. Keshavarz Mohammadian, Y.-L. He, and Y. Zhang, “Internal cooling of a lithium-ion battery using electrolyte as coolant through microchannels embedded inside the electrodes,” *J Power Sources*, vol. 293, Jul. 2015, doi: 10.1016/j.jpowsour.2015.05.055.
- [63] Z. Qian, Y. Li, and Z. Rao, “Thermal performance of lithium-ion battery thermal management system by using mini-channel cooling,” *Energy Convers Manag*, vol. 126, pp. 622–631, 2016, doi: <https://doi.org/10.1016/j.enconman.2016.08.063>.
- [64] F. Bai, M. Chen, W. Song, Z. Feng, Y. Li, and Y. Ding, “Thermal management performances of PCM/Water cooling-plate using for lithium-ion battery module based on non-uniform internal heat source,” *Appl Therm Eng*, vol. 126, Jul. 2017, doi: 10.1016/j.applthermaleng.2017.07.141.
- [65] G. Yu, S. W. Chiang, W. Chen, and H. Du, “Thermal Management of a Li-Ion Battery for Electric Vehicles Using PCM and Water-Cooling Board,” *Key Eng Mater*, vol. 814, pp. 307–313, Jul. 2019, doi: 10.4028/www.scientific.net/KEM.814.307.
- [66] Y. Bao, Y. Fan, C. Yanyan, C. Ling, X. Tan, and S. Yang, “Experimental and Numerical Study on Thermal and Energy Management of a Fast-Charging Lithium-Ion Battery Pack

- with Air Cooling,” *Journal of Energy Engineering*, vol. 145, p. 4019030, Jul. 2019, doi: 10.1061/(ASCE)EY.1943-7897.0000631.
- [67] J. Kleiner, R. Singh, M. Schmid, L. Komsiyiska, G. Elger, and C. Endisch, “Influence of Heat Pipe Assisted Terminal Cooling on the Thermal Behavior of a Large Prismatic Lithium-Ion Cell during Fast Charging in Electric Vehicles,” *Appl Therm Eng*, vol. 188, Jul. 2020, doi: 10.1016/j.applthermaleng.2020.116328.
- [68] M. Chen and J. Li, “Nanofluid-based pulsating heat pipe for thermal management of lithium-ion batteries for electric vehicles,” *J Energy Storage*, vol. 32, p. 101715, Jul. 2020, doi: 10.1016/j.est.2020.101715.
- [69] A. El-ladan and O. Haas, “Fan-pad evaporative battery cooling for hybrid electric vehicle thermal management,” Jul. 2015. doi: 10.1049/cp.2015.0901.
- [70] Z. Rao, S. Wang, and G. Zhang, “Simulation and experiment of thermal energy management with phase change material for ageing LiFePO₄ power battery,” *Energy Convers Manag*, vol. 52, no. 12, pp. 3408–3414, 2011, doi: <https://doi.org/10.1016/j.enconman.2011.07.009>.
- [71] X. Yu, Z. Lu, L. Zhang, L. Wei, X. Cui, and L. Jin, “Experimental study on transient thermal characteristics of stagger-arranged lithium-ion battery pack with air cooling strategy,” *Int J Heat Mass Transf*, vol. 143, p. 118576, 2019, doi: <https://doi.org/10.1016/j.ijheatmasstransfer.2019.118576>.
- [72] Y. Fan, Y. Bao, C. Ling, Y. Chu, X. Tan, and S. Yang, “Experimental study on the thermal management performance of air cooling for high energy density cylindrical lithium-ion batteries,” *Appl Therm Eng*, vol. 155, pp. 96–109, 2019, doi: <https://doi.org/10.1016/j.applthermaleng.2019.03.157>.
- [73] Z. Wang, Z. Zhang, and L. Yang, “Paraffin and paraffin/aluminum foam composite phase change material heat storage experimental study based on thermal management of Li-ion battery,” *Appl Therm Eng*, vol. 78, pp. 428–436, Jul. 2015, doi: 10.1016/j.applthermaleng.2015.01.009.
- [74] K. Darcovich, D. D. MacNeil, S. Recoskie, Q. Cadic, and F. Ilinca, “Comparison of cooling plate configurations for automotive battery pack thermal management,” *Appl Therm Eng*, vol. 155, pp. 185–195, 2019, doi: <https://doi.org/10.1016/j.applthermaleng.2019.03.146>.
- [75] H. Behi *et al.*, “Novel thermal management methods to improve the performance of the Li-ion batteries in high discharge current applications,” *Energy*, vol. 224, p. 120165, 2021, doi: <https://doi.org/10.1016/j.energy.2021.120165>.
- [76] R. Zhao, J. Liu, J. Gu, L. Zhai, and F. Ma, “Experimental study of a direct evaporative cooling approach for Li-ion battery thermal management,” *Int J Energy Res*, vol. 44, no. 8, pp. 6660–6673, 2020, doi: <https://doi.org/10.1002/er.5402>.
- [77] M. Mousavi, S. Hoque, S. Rahnamayan, I. Dincer, and G. Naterer, “Optimal design of an air-cooling system for a Li-Ion battery pack in Electric Vehicles with a genetic

- algorithm,” in *2011 IEEE Congress of Evolutionary Computation, CEC 2011*, Jul. 2011, pp. 1848–1855. doi: 10.1109/CEC.2011.5949840.
- [78] D. Solyali and A. H. Akinlabi, “Configuration, design, and optimization of air-cooled battery thermal management system for electric vehicles: A review,” *Renewable and Sustainable Energy Reviews*, vol. 125, Jul. 2020, doi: 10.1016/j.rser.2020.109815.
- [79] K. Chen, S. Wang, M. Song, and L. Chen, “Structure optimization of parallel air-cooled battery thermal management system,” *Int J Heat Mass Transf*, vol. 111, pp. 943–952, Jul. 2017, doi: 10.1016/j.ijheatmasstransfer.2017.04.026.
- [80] X. Wang, M. Li, Y. Liu, W. Sun, and X. Song 宋学官, “Surrogate based multidisciplinary design optimization of lithium-ion battery thermal management system in electric vehicles,” *Structural and Multidisciplinary Optimization*, vol. 56, Jul. 2017, doi: 10.1007/s00158-017-1733-1.
- [81] J. Na and H. Cho, “Analysis on air flow and cooling effect according to number of air guide fins in battery module,” vol. 12, pp. 908–911, Jul. 2017.
- [82] Z. Liu, Y. Wang, J. Zhang, and Z. Liu, “Shortcut computation for the thermal management of a large air-cooled battery pack,” *Appl Therm Eng*, vol. 66, pp. 445–452, Jul. 2014, doi: 10.1016/j.applthermaleng.2014.02.040.
- [83] M. Li, Y. Liu, and X. Wang, “Modeling and optimization of an enhanced battery thermal management system in electric vehicles,” *Frontiers of Mechanical Engineering*, vol. 14, Jul. 2018, doi: 10.1007/s11465-018-0520-z.
- [84] S. Park and L. Thompson, “A Comprehensive Thermal Management System Model for Hybrid Electric Vehicles,” Jul. 2011.
- [85] L. Wickramaratne, “BATTERY THERMAL MANAGEMENT SYSTEM (Formula Student),” 2017. doi: 10.13140/RG.2.2.13379.71203.
- [86] S. M. Hosseini Moghaddam, “Designing battery thermal management systems (BTMS) for cylindrical Lithium-ion battery modules using CFD,” *diva-portal.org*, 2018.
- [87] M. Rahman, H. Rahman, T. M. I. Mahlia, and J. Sheng, “Liquid cooled plate heat exchanger for battery cooling of an electric vehicle (EV),” *IOP Conf Ser Earth Environ Sci*, vol. 32, p. 12053, Jul. 2016, doi: 10.1088/1755-1315/32/1/012053.
- [88] E. Kim and J. Lee, “Real-time battery thermal management for electric vehicles,” in *2014 ACM/IEEE International Conference on Cyber-Physical Systems, ICCPS 2014*, Jul. 2014, pp. 72–83. doi: 10.1109/ICCPS.2014.6843712.
- [89] B. Ye, M. Rubel, and H. Li, “Design and Optimization of Cooling Plate for Battery Module of an Electric Vehicle,” *Applied Sciences*, vol. 9, p. 754, Jul. 2019, doi: 10.3390/app9040754.
- [90] S. Venkatakrisnan, V. Sudhan V.M., S. Kandappan S., S. Vishwanath, S. Saravanan, and P. Pandiyan, “Battery Thermal Management System,” in *2020 6th International Conference on Advanced Computing and Communication Systems (ICACCS)*, 2020, pp. 877–882. doi: 10.1109/ICACCS48705.2020.9074378.

- [91] Q. G. Y. W. T. Z. Ming SHEN, “Design and analysis of battery thermal management system for electric vehicle,” *Journal of ZheJiang University (Engineering Science)*, vol. 53, no. 7, Jun. 2019.
- [92] Ahmad Hilmi bin Khalid, “Development of evaporative cooling battery thermal management system for electric vehicles,” International Islamic University Malaysia, Kuala Lumpur, 2014.
- [93] N. Javani, I. Dincer, G. F. Naterer, and B. Yilbas, “Exergy analysis and optimization of a thermal management system with phase change material for hybrid electric vehicles,” *Appl Therm Eng*, vol. 64, pp. 471–482, Jul. 2014, doi: 10.1016/j.applthermaleng.2013.11.053.
- [94] T. Bandhauer and S. Garimella, “Passive, internal thermal management system for batteries using microscale liquid–vapor phase change,” *Appl Therm Eng*, vol. 61, pp. 756–769, Jul. 2013, doi: 10.1016/j.applthermaleng.2013.08.004.
- [95] Z. Rao, S. Wang, Z. Lin, and F. Li, “Experimental investigation on thermal management of electric vehicle battery with heat pipe,” *Energy Convers Manag*, vol. 65, pp. 92–97, Jul. 2013, doi: 10.1016/j.enconman.2012.08.014.
- [96] X. Li *et al.*, “Experimental Investigation on a Thermoelectric Cooler for Thermal Management of a Lithium-Ion Battery Module,” *International Journal of Photoenergy*, vol. 2019, pp. 1–10, Jul. 2019, doi: 10.1155/2019/3725364.
- [97] Y. Lyu, A. R. M. Siddique, S. Hasibul Majid, M. Biglarbegian, S. Gadsden, and S. Mahmud, “Electric vehicle battery thermal management system with thermoelectric cooling,” *Energy Reports*, vol. 5, pp. 822–827, Jul. 2019, doi: 10.1016/j.egy.2019.06.016.
- [98] H. Park, “A design of air flow configuration for cooling lithium ion battery in hybrid electric vehicles,” *J Power Sources*, vol. 239, pp. 30–36, Jul. 2013, doi: 10.1016/j.jpowsour.2013.03.102.
- [99] Y. Choi and D. Kang, “Prediction of thermal behaviors of an air-cooled lithium-ion battery system for hybrid electric vehicles,” *J Power Sources*, vol. 270, pp. 273–280, Jul. 2014, doi: 10.1016/j.jpowsour.2014.07.120.
- [100] H. Sun and R. Dixon, “Development of cooling strategy for an air cooled lithium-ion battery pack,” *J Power Sources*, vol. 272, pp. 404–414, Jul. 2014, doi: 10.1016/j.jpowsour.2014.08.107.
- [101] X. Tao, “Design, Modeling and Control of a Thermal Management System for Hybrid Electric Vehicles,” 2016.
- [102] F. Merz, A. Sciarretta, J.-C. Dabadie, and L. Serrao, “On the Optimal Thermal Management of Hybrid-Electric Vehicles with Heat Recovery Systems,” *Oil & Gas Science and Technology*, vol. 67, pp. 601–612, Jul. 2012, doi: 10.2516/ogst/2012017.

- [103] B. Mayer, M. Schier, and H. Friedrich, “Stand-Alone Battery Thermal Management for Fast Charging of Electric Two Wheelers—Integrated Busbar Cooling,” *World Electric Vehicle Journal*, vol. 10, p. 37, Jul. 2019, doi: 10.3390/wevj10020037.
- [104] J. Jeffs and T. Q. Dinh, “Thermal Management of a High Performance Electric Motorcycle: Active vs Passive Cooling,” in *2020 3rd International Conference on Power and Energy Applications (ICPEA)*, 2020, pp. 180–185. doi: 10.1109/ICPEA49807.2020.9280126.
- [105] S. A. Khateeb, S. Amiruddin, M. Farid, J. R. Selmán, and S. Al-Hallaj, “Thermal management of Li-ion battery with phase change material for electric scooters: Experimental validation,” *J Power Sources*, 2005, doi: 10.1016/j.jpowsour.2004.09.033.
- [106] T. Wang, K. Tseng, J. Zhao, and Z. Wei, “Thermal investigation of lithium-ion battery module with different cell arrangement structures and forced air-cooling strategies,” *Appl Energy*, vol. 134, pp. 229–238, Jul. 2014, doi: 10.1016/j.apenergy.2014.08.013.
- [107] S. Keshavarz Mohammadian, S. M. Rassoulinejad-Mousavi, and Y. Zhang, “Thermal management improvement of an air-cooled high-power lithium-ion battery by embedding metal foam,” *J Power Sources*, vol. 296, pp. 305–313, Jul. 2015, doi: 10.1016/j.jpowsour.2015.07.056.
- [108] K. Chen, Y. Chen, Y. She, M. Song, S. Wang, and L. Chen, “Construction of effective symmetrical air-cooled system for battery thermal management,” *Appl Therm Eng*, vol. 166, p. 114679, Jul. 2019, doi: 10.1016/j.applthermaleng.2019.114679.
- [109] S. Shahid and M. Agelin-Chaab, “Development and Analysis of a Technique to Improve Air-Cooling and Temperature Uniformity in a Battery Pack for Cylindrical Batteries,” *Thermal Science and Engineering Progress*, vol. 5, Jul. 2018, doi: 10.1016/j.tsep.2018.01.003.
- [110] K. Chen, W. Wu, F. Yuan, L. Chen, and S. Wang, “Cooling efficiency improvement of air-cooled battery thermal management system through designing the flow pattern,” *Energy*, vol. 167, Jul. 2018, doi: 10.1016/j.energy.2018.11.011.
- [111] Y. Liu and J. Zhang, “Design a J-type air-based battery thermal management system through surrogate-based optimization,” *Appl Energy*, vol. 252, p. 113426, 2019, doi: <https://doi.org/10.1016/j.apenergy.2019.113426>.
- [112] Y. Fan, Y. Bao, C. Ling, C. Yanyan, X. Tan, and S. Yang, “Experimental study on the thermal management performance of air cooling for high energy density cylindrical lithium-ion batteries,” *Appl Therm Eng*, vol. 155, pp. 96–109, Jul. 2019, doi: 10.1016/j.applthermaleng.2019.03.157.
- [113] F. He and L. Ma, “Thermal Management in Hybrid Power Systems Using Cylindrical and Prismatic Battery Cells,” *Heat Transfer Engineering*, vol. 37, p. 0, Jul. 2015, doi: 10.1080/01457632.2015.1060776.
- [114] H. Yutao, Z. Rao, X. Liu, and J. Zhao, “Investigation of power battery thermal management by using mini-channel cold plate,” *Energy Convers Manag*, vol. 89, Jul. 2015, doi: 10.1016/j.enconman.2014.10.015.

- [115] R. Sabbah, R. Kizilel, J. R. Selman, and S. Al-Hallaj, “Active (air-cooled) vs. passive (phase change material) thermal management of high power lithium-ion packs: Limitation of temperature rise and uniformity of temperature distribution,” *J Power Sources*, vol. 182, no. 2, 2008, doi: 10.1016/j.jpowsour.2008.03.082.
- [116] M. Li and P. Liang, “Simulation Analysis of Battery Thermal Management System Using Phase Change Material (PCM),” *Applied Mechanics and Materials*, vol. 433–435, pp. 2107–2112, Jul. 2013, doi: 10.4028/www.scientific.net/AMM.433-435.2107.
- [117] W. Q. Li, Z. Qu, Y. L. He, and Y. B. Tao, “Experimental study of a passive thermal management system for high-powered lithium ion batteries using porous metal foam saturated with phase change materials,” *J Power Sources*, vol. 255, pp. 9–15, Jul. 2014, doi: 10.1016/j.jpowsour.2014.01.006.
- [118] Z. Ling, C. Jiajie, Z. Zhang, T. xu, X. Gao, and S. Wang, “Experimental and numerical investigation of the application of phase change materials in a simulative power batteries thermal management system,” *Appl Energy*, vol. 121, pp. 104–113, Jul. 2014, doi: 10.1016/j.apenergy.2014.01.075.
- [119] N. Putra, B. Ariantara, and R. Pamungkas, “Experimental investigation on performance of lithium-ion battery thermal management system using flat plate loop heat pipe for electric vehicle application,” *Appl Therm Eng*, vol. 99, Jul. 2016, doi: 10.1016/j.applthermaleng.2016.01.123.
- [120] Z. Zhechen, Z. Guo, J. Xu, and Z. Xu, “Experimental and Numerical Study of Flat Heat Pipe-Liquid Cooling Battery Thermal Management System.” Jul. 2021. doi: 10.46855/energy-proceedings-7094.
- [121] R. Zhao, S. Zhang, J. Gu, J. Liu, S. Carkner, and E. Lanoue, “An experimental study of lithium ion battery thermal management using flexible hydrogel films,” *J Power Sources*, vol. 255, pp. 29–36, Jul. 2014, doi: 10.1016/j.jpowsour.2013.12.138.
- [122] L. H. Saw *et al.*, “Novel thermal management system using mist cooling for lithium-ion battery packs,” *Appl Energy*, vol. 223, pp. 146–158, 2018, doi: <https://doi.org/10.1016/j.apenergy.2018.04.042>.
- [123] S. K. Mohammadian, Y.-L. He, and Y. Zhang, “Internal cooling of a lithium-ion battery using electrolyte as coolant through microchannels embedded inside the electrodes,” *J Power Sources*, vol. 293, pp. 458–466, 2015, doi: <https://doi.org/10.1016/j.jpowsour.2015.05.055>.
- [124] P. C. Bhatia, “Thermal Analysis of Lithium-Ion Battery Packs and Thermal Management Solutions,” 2013. [Online]. Available: http://rave.ohiolink.edu/etdc/view?acc_num=osu1371144911
- [125] M. Marongiu and R. Clarksean, “Thermal management of battery compartments of outdoor telecommunication cabinets using phase change materials (PCM),” Jul. 1997, pp. 29–34. doi: 10.1109/INTLEC.1997.645861.

- [126] A. Cosentino, “Thermal management of telecommunications batteries using phase change materials (PCM) Jacket™,” Jul. 2000, pp. 237–244. doi: 10.1109/INTLEC.2000.884256.
- [127] A. Chu, Y. Yuan, J. Zhu, X. Lu, and C. Zhou, “The Design and Investigation of a Cooling System for a High Power Ni-MH Battery Pack in Hybrid Electric Vehicles,” *Applied Sciences*, vol. 10, no. 5, 2020, doi: 10.3390/app10051660.
- [128] M. Hu, D. Qin, and X. Ye, “Thermal management method of Ni-MH batteries for hybrid electric vehicle,” *Jiangsu Daxue Xuebao (Ziran Kexue Ban)/Journal of Jiangsu University (Natural Science Edition)*, vol. 32, pp. 148–152, Jul. 2011, doi: 10.3969/j.issn.1671-7775.2011.02.006.
- [129] Z. Rao, H. Yutao, X. Liu, and G. Zhang, “Experimental investigation of battery thermal management system for electric vehicle based on paraffin/copper foam,” *Journal-Energy Institute*, vol. 88, Jul. 2014, doi: 10.1016/j.joei.2014.09.006.
- [130] T. Yuksel, S. Litster, V. Viswanathan, and J. Michalek, “Plug-in hybrid electric vehicle LiFePO₄ battery life implications of thermal management, driving conditions, and regional climate,” *J Power Sources*, vol. 338, Jul. 2017, doi: 10.1016/j.jpowsour.2016.10.104.
- [131] N. Yang, X. Zhang, G. Li, and D. Hua, “Assessment of the forced air-cooling performance for cylindrical lithium-ion battery packs: A comparative analysis between aligned and staggered cell arrangements,” *Appl Therm Eng*, vol. 80, Jul. 2015, doi: 10.1016/j.applthermaleng.2015.01.049.
- [132] L. Hugun Saputra, I. Nashirul Haq, E. Leksono, R. Romadhon, D. Kurniadi, and B. Yulianto, “Development of battery thermal management system for LiFeMnPO₄ module using air cooling method to minimize cell temperature differences and parasitic energy,” Jul. 2017, pp. 87–92. doi: 10.1109/ICEVT.2017.8323540.
- [133] C. Jianhua, D. Gao, L. Jiexun, W. Jieyuan, and L. Qingchun, “Thermal modeling of passive thermal management system with phase change material for LiFePO₄ battery,” in *2012 IEEE Vehicle Power and Propulsion Conference, VPPC 2012*, Jul. 2012, pp. 436–440. doi: 10.1109/VPPC.2012.6422582.
- [134] C.-V. Hémerly, F. Pra, J.-F. Robin, and P. Marty, “Experimental performances of a battery thermal management system using a phase change material,” *J Power Sources*, vol. 270, pp. 349–358, Jul. 2014, doi: 10.1016/j.jpowsour.2014.07.147.
- [135] C. Lin, S. Xu, G. Chang, and J. Liu, “Experiment and simulation of a LiFePO₄ battery pack with a passive thermal management system using composite phase change material and graphite sheets,” *J Power Sources*, vol. 275, Jul. 2015, doi: 10.1016/j.jpowsour.2014.11.068.
- [136] P. T. S. R. Krishnan S. Hariharan, *Mathematical Modeling of Lithium Batteries*. 2018.
- [137] H.A. Kiehne, *Battery Technology Handbook*. CRC Press, 2003.

- [138] D. Berndt and E. Meissner, “Gas evolution and thermal behaviour of valve regulated lead acid batteries under abnormal operational conditions,” in *12th International Conference on Telecommunications Energy*, 1990, pp. 148–154. doi: 10.1109/INTLEC.1990.171240.
- [139] Chemistry libretexts, “The Gibbs Free Energy and Cell Voltage,” [https://chem.libretexts.org/Bookshelves/General_Chemistry/Map%3A_Principles_of_Modern_Chemistry_\(Oxtoby_et_al.\)/Unit_4%3A_Equilibrium_in_Chemical_Reactions/17%3A_Electrochemistry/17.2%3A_The_Gibbs_Free_Energy_and_Cell_Voltage](https://chem.libretexts.org/Bookshelves/General_Chemistry/Map%3A_Principles_of_Modern_Chemistry_(Oxtoby_et_al.)/Unit_4%3A_Equilibrium_in_Chemical_Reactions/17%3A_Electrochemistry/17.2%3A_The_Gibbs_Free_Energy_and_Cell_Voltage).
- [140] A. Bhatia, “Fundamentals of Direct Current Circuits .”
- [141] X. Duan and G. F. Naterer, “Heat transfer in phase change materials for thermal management of electric vehicle battery modules,” *Int J Heat Mass Transf*, vol. 53, no. 23–24, 2010, doi: 10.1016/j.ijheatmasstransfer.2010.07.044.
- [142] D. Bernardi, E. Pawlikowski, and J. Newman, “GENERAL ENERGY BALANCE FOR BATTERY SYSTEMS.,” in *Electrochemical Society Extended Abstracts*, 1984, vol. 84–2. doi: 10.1149/1.2113792.
- [143] A. Pesaran *et al.*, “Thermal Analysis and Performance of a Battery Pack for a Hybrid Electric Vehicle,” *Proceedings of the 15th International Electric Vehicle Symposium, Brussels Belgium*, Jul. 1998.
- [144] D. Berndt and E. Meissner, “Gas evolution and thermal behaviour of valve regulated lead acid batteries under abnormal operational conditions,” Jul. 1990, pp. 148–154. doi: 10.1109/INTLEC.1990.171240.
- [145] D. Berndt, “Valve regulated lead acid batteries-gas and heat management,” in *INTELEC, International Telecommunications Energy Conference (Proceedings)*, Jul. 1988, pp. 89–96. doi: 10.1109/INTLEC.1988.22330.
- [146] Battery University, “Article: Battery Recycling as a Business,” http://batteryuniversity.com/learn/article/battery_recycling_as_a_business .
- [147] Lorenzo Mancini, “Article: China does not want to become the lead-acid battery manufacturer for the whole world,” <https://www.linkedin.com/pulse/china-does-want-become-lead-acid-battery-manufacturer-lorenzo-mancini> .
- [148] “Technical specification of Oreva ALISH E – bike,” <https://oreva.com/product/j-50-plus/>.
- [149] J. Restrepo, J. Rosero, and S. Tellez, “Performance testing of electric vehicles on operating conditions in Bogotá DC, Colombia,” in *2014 IEEE PES Transmission and Distribution Conference and Exposition, PES T and D-LA 2014 - Conference Proceedings*, 2014, vol. 2014-October. doi: 10.1109/TDC-LA.2014.6955276.
- [150] S. H. Kamble, T. v. Mathew, and G. K. Sharma, “Development of real-world driving cycle: Case study of Pune, India,” *Transp Res D Transp Environ*, vol. 14, no. 2, 2009, doi: 10.1016/j.trd.2008.11.008.

List of References

- [151] A. Yamsani, “Gradeability for Automobiles,” *IOSR Journal of Mechanical and Civil Engineering*, vol. 11, no. 2, pp. 35–41, 2014, doi: 10.9790/1684-11273541.
- [152] C. Chen *et al.*, “On-road emission characteristics of heavy-duty diesel vehicles in Shanghai,” *Atmos Environ*, vol. 41, no. 26, pp. 5334–5344, 2007, doi: <https://doi.org/10.1016/j.atmosenv.2007.02.037>.
- [153] W. Diao, Y. Xing, S. Saxena, and M. Pecht, “Evaluation of Present Accelerated Temperature Testing and Modeling of Batteries,” *Applied Sciences*, vol. 8, no. 10, p. 1786, Oct. 2018, doi: 10.3390/app8101786.
- [154] X. Ye, Y. Zhao, and Z. Quan, “Experimental study on heat dissipation for lithium-ion battery based on micro heat pipe array (MHPA),” *Appl Therm Eng*, vol. 130, 2018, doi: 10.1016/j.applthermaleng.2017.10.141.
- [155] A. R. A. T. Upadhyaya Bhanu, “Characteristics and Control of the Motor System in E-bikes,” Blekinge Institute of Technology, SWEDEN, 2014.
- [156] E. E. NPTEL, “Introduction to Hybrid and Electric Vehicles,” <https://archive.nptel.ac.in/courses/108/103/108103009/#>.
- [157] Saurabh Chauhan, “Motor Torque Calculations For Electric Vehicle,” *INTERNATIONAL JOURNAL OF SCIENTIFIC & TECHNOLOGY RESEARCH*, vol. 4, no. 8, Aug. 2015.
- [158] H. A. Kiehne, *Battery Technology Handbook*. 2003. doi: 10.1201/9780203911853.
- [159] A. Samba, “Battery Electrical Vehicles-Analysis of Thermal Modelling and Thermal Management,” 2015.

List of publication

- (1) Jaydeep M. Bhatt, P.V. Ramana, Jignesh R. Mehta, “Performance assessment of valve regulated lead acid battery for E–bike in field test” Materials Today: Proceedings, Volume 49, Part 5, 2022, Pages 2058-2065, ISSN 2214-7853, DOI: <https://doi.org/10.1016/j.matpr.2021.08.305>. (SCOPUS).
- (2) **Jaydeep M Bhatt**, P V Ramana, and Jignesh R Mehta, “Experimental investigation on the impact of evaporative cooling based battery thermal management system on charging process of valve regulated lead acid batteries in E-bike”, Journal of Physics: Conference Series, Volume 2070, November 2021, DOI: <https://doi.org/10.1088/1742-6596/2070/1/012087> (SCOPUS).

Patent


Jaydeep Manojkumar bhatt, Dr. Paladugula Venkataramana, Dr. Jignesh Rajnikant Mehta, “Evaporative Cooling Based Battery Thermal Management System”, Patent journal: 02/2022, Dated: 14/01/2022, No. 202221000095 A

List of Appendices

Appendix A Calibration Certificates

E-mail : anjaney003@yahoo.com

Ph. : (079) 26857696
Mob. : 09869199376
Mob. : 09408280876



ANJANEY THERMOCONTROLS
MFG. OF ALL TYPE OF THERMOCOUPLES & TEMPERATURE CONTROLLER
2/4, AMI APPARTMENT, BHAIKAKANAGAR, THALTEJ, AHMEDABAD - 380 059.

Reference: MS / TS / 17-18 – 0909 09.09.2017

To,
Mr. Jaydeep M Bhatt
Junagadh.

Ref. : As per Our W.O. W17091809

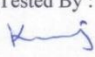
INSTRUMENT UNDER TESTING


Name: Paperless Recorder	Serial No.: 20170724010
Make & Model : Khoat, KH-208B-D-S1-U-N	Supply: 230 V AC @ 50 Hz
Input: 4-20mA	
Temperature Range : 0 to 100	Test Conditions: ROOM TEMP. 36 °C


TEST REPORT

Sr. No.	Actual reading By Chart C° deg.	Reading of AOA-9951/0226 Temp.(in °C)							
		CH#1 4-20 mA	CH#2 4-20 mA	CH#3 4-20 mA	CH#4 4-20 mA	CH#5 4-20 mA	CH#6 4-20 mA	CH#7 4-20 mA	CH#8 4-20 mA
1	0	4	4	4	4	4	4	4	4
2	10	5.5	5.5	5.5	5.5	5.5	5.5	5.5	5.5
3	20	7.1	7.1	7.1	7.1	7.1	7.1	7.1	7.1
4	30	12	12	12	12	12	12	12	12
5	40	16.9	16.9	16.9	16.9	16.9	16.9	16.9	16.9
6	50	20	20	20	20	20	20	20	20

Remarks:
All the errors are found within the accuracy (i.e. 0.5%) specified by the Customer, Unit found ACCEPTED after testing., These results are obtained at the time of testing
DETAILS OF INSTRUMENT USED FOR TESTING
Name: UNIVERSAL CALIBRATOR
Make: G. P. ELECTRONICS
Model: Unical 28531
Serial No.: 0042001

Tested By : 



Checked By : 

E-mail : anjaney03@gmail.com

Ph.:(079) 26857696
Mob. : 9099058140
Mob. : 9099058140



ANJANEY THERMOCONTROLS

MFG. OF ALL TYPE OF THERMOCOUPLES & TEMPERATURE CONTROLLER

No. ANJ/CAL/2019-20/101/1 2/A, ANI APPARTMENT, BHAIKAKANAGAR, THALTEJ, AHMEDABAD-380 059.

Date: 19.03.2020

TEST CERTIFICATE

CUSTOMER NAME : Jaydipbhai Bhatt.
Junagadh.
P.O.No.&DATE : Nil/18.03.2020
SPECIFICATION : Thermocouple Type 'J' Simplex
Sr.No. : J35201 to J35206
CALIBRATED ON : 19th March, 2020
NEXT CALIBRATION DUE ON : 19th March, 2021
CALIBRATION STANDARD : NPL Standard
USED : (1) PRISM CALIBRATION CENTRE, AHMEDABAD
Thermocouple Type : 'S' Calibration Certificate,
No.PCC/T/N/1805069/01 Dt. 22.05.2019
REFERENCE TEMPERATURE : Zero Degree Centigrade
ROOM TEMP. : 24 C
OBSERVATIONS : Temperature VS mV Test

Sr.No.	Measured Temp. on Ref. Standard in (C)	Element	Value Read on UUC in (C)	Expanded uncertainty in (C)
1	50	1	50	0
		2	50	0
		3	50	0
		4	50	0
		5	50	0
		6	50	0
2	75	1	75	0
		2	75	0
		3	75	0
		4	75	0
		5	75	0
		6	75	0
3	100	1	100	0
		2	100	0
		3	100	0
		4	100	0
		5	100	0
		6	100	0



Tested by
(K. Ramanuj)
Engineer Test & Calibration

Appendix B Design Calculations

Calculation of power and torque for E – Bike

OREVA ALISH E-Bike is selected as a test vehicle for experimentation. The OREVA ALISH is an Indian manufacturing electric bike and is the part of Gujarat based two wheeler manufacturer range. The OREVA ALISH is powered by 500W brushless DC hub motor with top speed 40 km/hr. The hub motor is powered by 12V, 25Ah. Maintenance free VRLA battery.

Mathematical analysis based on the following criteria, [155]

- (i) Maximum speed of E-bike is 40 km./hr. The power of the hub motor decreases with an increase in the speed of E-bike.
- (ii) Average speed of E-bike is considered 16 km./hr as per the previous field test-based experiment.
- (iii) The brushless DC hub motor efficiency is 80% to 85%. So, the Actual power of a brushless DC hub motor is less than 500 W.

Now, mathematical equations for the torque, speed and power have been derived to support the experimental analysis of E – bike.

Speed

A 500W brushless DC hub motor is used in OREVA ALISH, which gives the 10 to 40 km./hr. performance speed under various road conditions. Here, As per the previous experiments, 16 km./hr. is an average speed of E – bike under various road condition and traffic. The E – bike speed (km./hr.) and revaluation can be calculated from the following equation,

$$\text{Speed (km./hr.)} = n \text{ (rpm)} \times \text{wheel circumference}$$

Power

Typically, the efficiency of a brushless DC hub motor is 80 to 85%. So, power generation by 500W hub motor is less than 500W in actual condition. Three factors influence the efficiency declination, i.e., rolling resistance, wind resistance and gravity.

So, total power required to E – bike that can be given by sum of power resulting of drag force (P_{drag}), gradient (P_{hill}) and rolling resistance (P_{rc}). [155]

$$P_{\text{total}} = P_{\text{drag}} + P_{\text{rc}} + P_{\text{hill}}$$

Power required to overcome the drag or wind resistance is determined by the frontal area (A) of shape and size of E-Bike, drag coefficient, which depends on the body of E-bike and rider, speed of E-bike and density of air at atmospheric temperature.

Equation for calculate the power resulting of drag force,

$$P_{drag} = \frac{C_d \cdot A \cdot \rho \cdot V^3}{2} \quad (1)$$

Here, Drag coefficient (C_d) = 1 for upright rider, $C_d = 0.7$ for recumbent rider [156]

Speed (V) = 16 km/hr. = 4.44 m/s

Frontal area (A) = $w \times h = 0.68 \times 1.15 = 0.782m^2$

Air density (ρ) = $1.293 \text{ kg}/m^3$ @ 27°C Temp.

Now, put the above values in equation (1),

$$\begin{aligned} P_{drag} &= \frac{C_d \cdot A \cdot \rho \cdot V^3}{2} \\ &= \frac{1 \cdot 0.782 \cdot 1.293 \cdot (4.44)^3}{2} \end{aligned}$$

$$P_{drag} = 44.25 \text{ W}$$

The second parameter, the power required to overcome the rolling resistance, depends on gravity (g) and mass of E-bike and rider (m), rolling coefficient (Rc) and speed of vehicle. The rolling coefficient depends on the frictional force between tires and the road. Typically, rolling resistance for stony and flat asphalt roads is 0.004 and 0.0017, respectively.

Equation for calculate the power resulting of rolling resistance,

$$P_{rc} = g \cdot m \cdot R_c \cdot V \quad (2)$$

Here, Gravitational force (g) = $9.81 \text{ m}/s^2$

Mass of vehicle(m) (self weight + rider weight + BTMS weight) = $75 + 75 + 20 = 170 \text{ kg}$

(Here, BTMS weight is assumed with 20 kg)

Appendix B Design Calculations

Rolling coefficient (R_c) = 0.0017 for flat asphalt road

Speed (V) = 16 km/hr = 4.44 m/s

Now, put the above values in equation (2),

$$\begin{aligned}P_{rc} &= g \cdot m \cdot R_c \cdot V \\ &= 9.81 \cdot 170 \cdot 0.0017 \cdot 4.44\end{aligned}$$

$$P_{rc} = 12.58 \text{ W}$$

The last approximation for power calculation is the power required to drive the E-bike in hilly areas. The gradient or slope of a hilly road (gradient %) is to be considered for determining the required power. The gradient is a ratio of the height of climb to distance. It is described in the form of a percentage. Here, it assumed a 2% gradient to calculate the required power.

$$P_{hill} = \frac{g \cdot m \cdot V \cdot (\text{gradient } \%)}{100} \quad (3)$$

Here, Gravitational force (g) = 9.81 m/s²

Mass of vehicle (m) (self weight + rider weight + BTMS weight) = 75 + 75 + 20 = 170 kg

Gradient or slope = $\frac{\text{Height of climb}}{\text{Distance}} \times 100 = \frac{2}{100} \times 100 = 2\%$ (Assume)

Speed (V) = 16 km/hr = 4.44 m/s

Now, put the above values in equation (3),

$$\begin{aligned}P_{hill} &= \frac{g \cdot m \cdot V \cdot (\text{gradient } \%)}{100} \\ &= \frac{9.81 \cdot 170 \cdot 4.44 \cdot 2}{100}\end{aligned}$$

$$P_{hill} = 148.1 \text{ W}$$

Now, total required power for E – bike can be calculated from summation of P_{drag} , P_{rc} and P_{hill} . So, total power can be calculated from following equation,

$$P_{total} = P_{drag} + P_{rc} + P_{hill}$$

$$P_{total} = 44.25 + 12.58 + 148.1$$

$P_{total} = 204.92 \text{ W}$

Theoretically, the total power required for driving the E-bike is 204.92W at an average speed of 16 km/hr. It is observed that the actual power required to drive E-bike during the field test is 257W. The brushless DC hub motor drives E-bike. So, the power rating for the brushless DC hub motor must be above 204.92. Due to that reason, OREVA ALISH is powered by a 500W brushless DC hub motor.

Torque

Torque is a force to drive the vehicle and set it in motion. Torque is the turning power of the hub motor in E–bike. Hub motor transforms the electrical energy into rotational energy, which drives the wheel. So, the selection of the hub motor depends on the required torque for driving the E-bike. The mechanical power produced by the hub motor depends on the torque (T) and rotational speed of the hub motor (ω) [157].

Total mechanical power which can be produce by the motor is given by,

$$P_{total} = \text{Torque } (T) \times \text{Rotational speed } (\omega)$$

Here, $\text{Rotational speed } (\omega) = \frac{2\pi N}{60}$

So,

$$P_{total} = \frac{2\pi NT}{60}$$

$$T = \frac{P_{total} \times 60}{2\pi N} \tag{4}$$

RPM can be calculated from the equation of linear speed,

$$N \text{ (rpm)} = \frac{\text{Liner Speed (m/min)}}{\text{Wheel circumference (m)}}$$

Here, Liner Speed = 16 km./hr. = $\frac{16000}{60} = 266.6$ m/min.

Wheel circumference = $\pi D = \pi \times 0.406 = 1.275$ m

So, N (rpm) = $\frac{266.6}{1.275} = 209.1$ rpm ≈ 209 rpm

Put the value of N in eq. (4),

$$T = \frac{P_{total} \times 60}{2\pi N}$$

$$T = \frac{204.92 \times 60}{2\pi \times 209}$$

$$Torque (T) = 9.36 \text{ Nm}$$

Current

Current is a flow of electrons from positive to negative electrodes through the hub motor and circuit. The current supply is continuously varied according to the load on the hub motor. A large amount of current is drained from the battery during the start-up of the hub motor and gradually decreases with the increased speed of E-bike. Current can be calculated from the total power and voltage of the battery. The following equation shows the relationship between power, voltage and current.

$$Power (P) = Voltage (V) \times Current (I)$$

$$Current (I) = \frac{Power}{Voltage}$$

Here, 48V, 24 Ah. VRLA maintenance-free battery pack is used as a power source. So, supplied voltage to the Brushless DC hub motor is 48V. The required total power at average speed (12 km./hr.) for E-bike is 210.68W.

$$Current (I) = \frac{Power}{Voltage}$$

$$Current (I) = \frac{204.92}{48}$$

$$Current (I) = 4.26A$$

The current drain by hub motor from the VRLA battery pack is 4.26A at the average speed (16 km./hr.) of E-bike. It is observed that the actual average current drain from the VRLA battery during the field test is 5.35A.

Calculation for heat generation rate

VRLA battery is an electrochemical system. The electrochemical reaction between electrodes in a battery is always connected with the heat effect. There are two sources of heat generation in VRLA battery,

- (1) Heat generation due to reactions between active materials[158][50].
- (2) The joule effect causes by current flow through the battery[158][50].

The summation of heat generation due to reaction and the Joule effect gives the total heat generated by battery cell.

$$Q_{total} = Q_{Rec.} + Q_{Joule}$$

$$(Q_{total})_{cell} = I \left[T \frac{dE}{dT} \right] + I (E - V) \quad \text{----- (1)}$$

The heat generation rate in a cell can be calculated from eq. (1) [51][141][142].

The highest battery temperature recorded during a field test should be used to compute the heat generation rate. The afternoon portion of an urban route field test saw the greatest temperature of 45.4°C, according to earlier experimental data. The field test captured the following variables.

Average power consumption	: 257 W
Battery Temperature(T_b)	: 45.4°C
Ambient temperature (T_a)	: 39.7°C

Now, the total heat generated by battery cell,

$$(Q_{total})_{cell} = I \left[T \frac{dE}{dT} \right] + I (E - V)$$

Where,

Average Current (I)	= 5.35 A
Battery Temperature(T)	= 45.4+273.15 = 318.55 K
Entropy Coefficient (dE/dT)	= 0.4337 mV/K = 0.0004337 V/K [159]
Open circuit voltage (V)	= 54V @4 nos. of batteries= 13.50 V for 1 no. of battery = 2.25 V/cell (6 cells/battery)
Cell voltage (V)	= 48.0 V@4 nos. of batteries= 12 V for 1 no. of battery = 2 V/cell

$$Q = 5.35 [318.55 \times 0.0004337] + 5.35 (2.25 - 2.0)$$

$$Q = 2.077 \text{ W/cell}$$

$$Q_{battery} = 12.46 \text{ W}$$

A battery pack consists of four batteries. Thus, the total heat produced by the battery pack is 49.84W. During the field test, the batteries are discharged with an average power of 257W, at which time a battery pack generates 49.84W of heat.

Calculate required volumetric flow rate of air

The amount of forced air necessary to remove heat from the battery chamber is dependent on the amount of heat generated by the VRLA battery and the required battery temperature surface. The selection of the proper fan for the evaporative cooling system is determined by the desired volumetric flow rate. Air mass flow rate is used to calculate volumetric flow rate.

The mass flow rate of air in forced air cooling can be expressed as,

$$m_a = \frac{Q}{c_p(T_1 - T_2)}$$

Where,

Heat dissipates by battery (Q) = 49.84 W

Specific heat of air (C_p) = 1007 J/kgK

Inlet air temperature (T_1) = 27 + 273.15 = 300.15 K

Outlet air temperature (T_2) = 29 + 273.15 = 302.15 K

Density of air @ 27°C = 1.174 kg/m³

Here, the inlet air temperature is assumed based on the ambient conditions (wet bulb temperature) of the tested region (Junagadh, Gujarat, India) during the summer. In the summer, the average wet bulb temperature in Junagadh is 27°C. Outlet air temperature is assumed according to the battery temperature required to be maintained during operating conditions. According to the manufacturer's recommended temperature range, the VRLA battery temperature should not exceed 30°C during the operating state. The outlet temperature should be slightly lower than the battery temperature. Thus, the outlet air temperature is assumed to be 29°C for evaporative cooling-based BTMS.

Put all the values in above equation

$$m_a = \frac{49.84}{1007(302.15 - 300.15)}$$

Appendix B Design Calculations

$$m_a = 24.75 \times 10^{-3} \text{ kg./sec}$$

$$\text{Volumetric flow rate } (q) = \frac{\text{mass flow rate of air}}{\text{Density of air @27}}$$

$$\text{Volumetric flow rate } (q) = \frac{24.75 \times 10^{-3}}{1.174}$$

$\text{Volumetric flow rate } (q) = 21.08 \times 10^{-3} \text{ m}^3/\text{s} = 44.66 \text{ cfm} \approx 45 \text{ CFM}$

A volumetric flow rate of 45 CFM is required for rejecting the 49.84W heat from the E-bike battery pack.

Appendix C Uncertainty Analysis

(Using Klein's Method)

Step-1 possible error in measurement devices

Sr. No.	Device name	Parameter	Symbol	Unit	Max. Value	Error
1	Thermocouple (J-type)	Temperature on Battery	T1 to T5	C	0 to 750	0.1
2	Thermocouple (J-type)	Air Flow Temperature	T6	C	0 to 750	0.1
3	Voltage Measuring Probe (config. through 1K Ω resistor)	Voltage of Battery	V	V	0 to 5	0.2
4	Current measuring probe (using 30A ~ 70 mV shunt)	Current of Battery	I	A	4 to 20	0.01
5	Sling Psychrometer	DBT & WBT	T	C	-10 to 50	0.5

Step-2 Calculation of uncertainty in results

(1) Heat Generation rate of Battery

$$Q_{battery} = Q_{Rec} + Q_{Joule}$$

$$Q_{battery} = I \left[T \frac{dE}{dT} \right] + I(E - V)$$

$$Q_{battery} = I \left[T \frac{dE}{dT} + (E - V) \right]$$

$$\frac{\Delta Q_{battery}}{\Delta I} = T \frac{dE}{dT} + (E - V) = 750 \times \left(\frac{0.4337}{1000} \right) + \left(\frac{5}{6} - 5 \right) = 0.321$$

$$\frac{\Delta Q_{battery}}{\Delta T} = I \frac{dE}{dT} = 20 \times \left(\frac{0.4337}{1000} \right) = 0.00867$$

$$\frac{\Delta Q_{battery}}{\Delta E} = I = 20$$

$$\frac{\Delta Q_{battery}}{\Delta V} = I = 20$$

$$\delta Q_{battery} = \left[\left(\frac{\Delta Q_{battery}}{dI} \times \delta I \right)^2 + \left(\frac{\Delta Q_{battery}}{\Delta T} \times \delta T \right)^2 + \left(\frac{\Delta Q_{battery}}{\Delta E} \times \delta E \right)^2 + \left(\frac{\Delta Q_{battery}}{\Delta V} \times \delta V \right)^2 \right]^{1/2}$$

$$\delta Q_{battery} = \left[(0.321 \times 0.01)^2 + (0.00867 \times 0.1)^2 + (20 \times 0.2)^2 + (20 \times 0.2)^2 \right]^{1/2} = 5.65$$

$$Q_{battery} = I \left[T \frac{dE}{dT} + (E - V) \right] = 20 \times \left[750 \times \frac{0.4337}{1000} + \frac{5}{6} - 5 \right] = 76.69$$

$$\frac{\delta Q_{battery}}{Q_{battery}} = \frac{5.65}{76.69} \times 100 = 7.37\%$$

(2) Temperature Difference

$$\Delta T = T_1 - T_2$$

$$\frac{\Delta(\Delta T)}{\Delta T_1} = 1 - T_2 = 1 - 750 = -749$$

$$\frac{\Delta(\Delta T)}{\Delta T_2} = T_1 - 1 = 750 - 1 = 749$$

$$\delta(\Delta T) = \left[\left(\frac{\Delta(\Delta T)}{\Delta T_1} \times \delta T_1 \right)^2 + \left(\frac{\Delta(\Delta T)}{\Delta T_2} \times \delta T_2 \right)^2 \right]^{1/2} = \left[(-749 \times 0.1)^2 + (749 \times 0.1)^2 \right]^{1/2} = 105.9$$

$$\Delta T = T_1 - T_2 = 750 + 750 = 1500$$

$$\frac{\delta(\Delta T)}{\Delta T} = \frac{105.9}{1500} \times 100 = 7.06\%$$

(3) Required Volumetric Flow rate of Air

$$m_a = \frac{Q}{C_p (T_1 - T_2)}$$

$$\frac{\Delta m_a}{\Delta Q} = \frac{1}{C_p (T_1 - T_2)} = \frac{1}{1007(750 + 750)} = 6.67 \times 10^{-7}$$

$$\frac{\Delta m_a}{\Delta T_1} = \frac{-Q}{C_p (T_1 - T_2)^2} = \frac{-76.69}{1007(750 + 750)^2} = -3.38 \times 10^{-8}$$

$$\frac{\Delta m_a}{\Delta T_2} = \frac{Q}{C_p (T_1 - T_2)^2} = \frac{76.69}{1007(750 + 750)^2} = 3.38 \times 10^{-8}$$

$$\delta m_a = \left[\left(\frac{dm_a}{dQ_{battery}} \times \delta Q_{battery} \right)^2 + \left(\frac{dm_a}{dT_1} \times \delta T_1 \right)^2 + \left(\frac{dm_a}{dT_2} \times \delta T_2 \right)^2 \right]^{1/2}$$

$$\delta m_a = \left[(6.67 \times 10^{-7} \times 5.65)^2 + (-3.38 \times 10^{-8} \times 0.1)^2 + (3.38 \times 10^{-6} \times 0.1)^2 \right]^{1/2} = 3.77 \times 10^{-6}$$

$$m_a = \frac{Q}{C_p (T_1 - T_2)} = \frac{76.69}{1007(750 + 750)} = 5.075 \times 10^{-5}$$

$$\frac{\delta m_a}{m_a} = \frac{3.377 \times 10^{-6}}{5.075 \times 10^{-5}} \times 100 = 7.43\%$$

Step-3 Uncertainty in results

Sr. No.	Result	Symbol	% Uncertainty	Remarks
1	Heat Generation rate of Battery	$Q_{battery}$	7.37	
2	Temperature difference	ΔT	7.06	
3	Required Volumetric Flow rate of Air	m_a	7.43	

Appendix D Comparison of results of typical field test with new and old battery set

Appendix D Comparison of results of typical field test with new and old battery set

Parameters	Drive cycles (New battery set)											
	1	2	3	4	5	6	7	8	9	10	11	12
Road type	Urban	Urban	Urban	Gradient	Gradient	Gradient	Highway	Highway	Highway	Rural	Rural	Rural
Time slot	Morning	Noon	Evening	Morning	Noon	Evening	Morning	Noon	Evening	Morning	Noon	Evening
Trip distance (km)	9.7	9.78	9.62	7.9	7.9	7.9	9.0	9.01	9.0	7.6	7.6	7.7
Trip duration (min.)	38.0	42.0	42.0	35.0	37.0	33.0	24.0	23.0	23.0	33.0	33.0	35.0
Max. speed (km/h)	32.9	38.9	33.8	27.9	27.6	26.0	36.6	39.4	37.5	28	26.9	26.9
Avg. speed (km/h)	16.23	14	13.8	10.8	10.9	11.5	21.8	23	22.4	13.6	14	13.1
Avg. power (W)	198.95	166.1	171.5	180.8	172.9	169.0	256.5	277.4	265.6	171.5	175.8	161.6
Ambient temperature (°C)	29.4	37.7	33.1	31.0	39.7	34.5	30.1	38.5	33.1	29.3	38.0	31.8
Max. battery surface temperature (°C)	33.3	42.4	34.5	33.9	44.0	38.7	32.6	41.3	34.6	31.6	40.1	33.8
Temperature difference (ΔT) (°C)	3.9	4.7	1.4	2.9	4.3	4.2	2.5	2.8	1.5	2.3	2.1	2.0

Parameters	Drive cycles (Old battery set)											
	13	14	15	16	17	18	19	20	21	22	23	24
Road type	Urban	Urban	Urban	Gradient	Gradient	Gradient	Highway	Highway	Highway	Rural	Rural	Rural
Time slot	Morning	Noon	Evening	Morning	Noon	Evening	Morning	Noon	Evening	Morning	Noon	Evening
Trip distance (km)	9.76	9.8	9.79	7.9	7.9	7.8	9	9.03	9.01	7.6	7.6	7.6
Trip duration (sec.)	35.0	36.0	37.0	35.0	37.0	33.0	26.0	24.0	26.0	34.0	31.0	33.0
Max. speed (km/h)	28.9	32.3	27.6	28.9	33.4	32.0	35.1	38.8	38.1	25.3	27.8	26.9
Avg. speed (km/h)	13.0	17.2	15.9	12.1	13.9	12.4	19.9	22.6	22.1	13.1	14.3	14.2
Avg. power (W)	161.4	206.2	193.5	191.0	187.8	192.5	232.8	261.1	255.7	163.4	176.4	173
Ambient temperature (°C)	28.7	39.7	34.1	30.8	37.2	34.3	29.2	39.1	33.1	28.7	37.3	32.7
Max. battery surface temperature (°C)	31.7	45.4	36.1	34.4	41.7	37.3	32	43.1	34.5	31.6	41.4	35.0
Temperature difference (ΔT) (°C)	3.0	5.7	2.0	3.6	4.5	3.0	2.8	4.0	1.5	2.9	4.1	2.3

Appendix E : Field test data (Experimental study – 3)

Parameters	Trip - 1	Trip - 2	Trip - 3	Trip - 4	Trip - 5	Trip - 6	Trip - 7	Trip - 8	Trip - 9	Trip - 10	Trip - 11	Trip - 12
Cooling strategy	With BTMS	With BTMS	With BTMS	With BTMS	Precooling + BTMS	Precooling + BTMS	Precooling + BTMS	Precooling + BTMS	Natural Convection	Natural Convection	Natural Convection	Natural Convection
Speed mode	Eco	Power	Eco	Power	Eco	Power	Eco	Power	Eco	Power	Eco	Power
load condition	Without load	Without load	With load	With load	Without load	Without load	With load	With load	Without load	Without load	With load	With load
distance(km)	24.5	24.3	24.6	24.6	24.3	24.7	24.3	24.4	24.2	24.7	24.2	24.6
Ambient temperature (°C)	41	41	41	41	39	39	37	36	36	37	37	37
Wet bulb temperature (°C)	29.6	29.1	28.9	28.9	27.1	27.3	25.2	25.8				
Tmin (°C)	34.8	33.6	32.7	34.0	31.4	31.7	31.8	31.8	36.1	37.1	37.1	37.0
Tmax (°C)	36.7	36.2	35.2	36.1	32.4	33.2	33.4	33.5	40.6	41.8	41.8	42.1
Average battery temperature (°C)	35.7	34.9	34.0	35.0	31.9	32.5	32.6	32.7	38.3	39.4	39.4	39.6
Relative humidity(%)	41	39	38	38	39	38	36	40				
Average speed (km/h)	17.1	20.7	15.5	22.0	16.2	27.8	16.7	19.4	17.8	25.2	17.5	21.9
trip duration (Hr.)	1 Hr. 26 min.	1 Hr. 10 min.	1 Hr. 34 min.	1 Hr. 07 min.	1 Hr. 30 min.	1 Hr. 07 min.	1 Hr. 27 min.	1 Hr. 05 min.	1 Hr. 21 min.	0 Hr. 58 min.	1 Hr. 23 min.	1 Hr. 07 min.
Power consumption (W)	192.4	232.5	174.7	247.2	181.9	312.3	187.8	218.7	200.1	283.6	196.5	246.7

